QUANTITATIVE IMAGING OF SEX AND AGE DIFFERENCES IN HUMAN CORTICAL BONE OSTEOCYTE LACUNAE

A Thesis Submitted to the College of
Graduate Studies and Research
In Partial Fulfillment of the Requirements
For the Degree of Doctor of Philosophy
In the Department of Anatomy & Cell Biology
University of Saskatchewan
Saskatoon

By

YASMIN CARTER

Permission To Use

In presenting this thesis in partial fulfilment of the requirements for a Postgraduate degree from the University of Saskatchewan, I agree that the Libraries of this University may make it freely available for inspection. I further agree that permission for copying of this thesis in any manner, in whole or in part, for scholarly purposes may be granted by the professor or professors who supervised my thesis work or, in their absence, by the Head of the Department or the Dean of the College in which my thesis work was done. It is understood that any copying or publication or use of this thesis or parts thereof for financial gain shall not be allowed without my written permission. It is also understood that due recognition shall be given to me and to the University of Saskatchewan in any scholarly use which may be made of any material in my thesis.

Requests for permission to copy or to make other use of material in this thesis in whole or part should be addressed to:

Head of the Department of Anatomy and Cell Biology
University of Saskatchewan
Saskatoon, Saskatchewan, S7N 5E5

Abstract

Osteocytes, the most abundant cell within bone, have been linked to the processes of mechanosensation and transduction. Based upon relatively limited empirical evidence, variations in their abundance and morphology have been linked to sex, age, biomechanics and disease. In order to better elucidate lacunar variation within a healthy cohort, samples from 30 women aged 20-86 and 36 men aged 18-92 were studied utilizing synchrotron radiation micro-CT. Initial studies of normal variation within the femoral proximal shaft cross-section found high variation in lacunar density (up to ~54%) and associated morphological differences linked to biomechanical regions. In women, a non-significant trend in lacunar density reduction was apparent with age; however, a significant reduction in lacunar volume with age (~30%) was observed. Also noted were differences in lacunar morphology, with the lacunae of younger women characterized as flatter and less equant than their older counterparts. The males, who demonstrated lacunar density decline with age and a tendency towards more equant and less elongate lacunae, did not share these characteristics. Intriguingly, the previously noted reductions in lacunar volume were not observed in males. The results of this research indicate that normal variation in osteocyte lacunar parameters is high. To our knowledge the observation that lacunar volume differs in women with age is novel, potentially resulting from preferential surface infilling within the extracellular space. The functional impact of this infilling is unclear but such a change in scale likely impacts the mechanosensing function of the osteocyte network. This hypothesis warrants further investigation as, if confirmed, it would represent a profound negative impact on the osteocyte network and may provide new insights into age-related bone loss.

Acknowledgments

I am grateful for the contributions of numerous individuals and institutions that have made this research possible. I would like to express my deepest thanks to my supervisor, Dr. David Cooper for providing me with an unsurpassed opportunity to conduct research on the cutting-edge of imaging, for teaching me that "real science" is possible and showing me how to do it. I would also like to thank the additional members of my committee, Drs. Dean Chapman, Saija Kontulainen, Angela Lieverse, and Ernie Walker for their advice and assistance over the years.

This research would not have been possible without the kindness and generosity of the donors to the Melbourne Femur Collection and their families. I am deeply indebted to Dr. John Clement and David Thomas of the University of Melbourne for their invaluable assistance and advice. Special thanks go to the staff and Faculty of the Department of Anatomy & Cell Biology and the BioMedical Imaging and Therapy (BMIT) Beamline. Financial resources for this research has come from a number of sources and I would like to acknowledge the Saskatchewan Health Research Foundation (SHRF), CIHR-Training in Health Research Using Synchrotron Techniques (THRUST), the Canadian Light Source (CLS), and the College of Medicine, University of Saskatchewan.

Thank-you to everyone who has been a part of the last five years of my life: some stayed, some didn't, but each gave me a gift and helped make this PhD possible.
Amanda, Andy, Arty, Brian, The Britz Family, Chris, Dean, Dena, Denin, Eric, Isaac, The Jacobi Family, Jessica, Johannes, Keegan, Kit, Kurt, Lindsay, Mark, Nancy, Nikki, Nic, Philip, Robin, Roy, Sam, Spike, Treena, and Virgilio. Special mention goes to Hayley Britz, for her friendship, her support and our breakfast dates, Kim Harrision, who shared caffeine and wobbly pop 'networking' sessions that kept me going and Rhonda Martens, who gave me a family.

"No man is an island" and no person is able to achieve everything I have, and live the incredible, adventurous, wacky and weird life I have done without the love and support of their family. Dad, from the early days of bedtime stories involving the delightful adventures of " the

aerodynamics of rotary wing aircraft" to our late-night skype chats about particle physics, you have always taught me no subject was too scary or impossible to understand. Thank you for showing me a world of wonder, although I bet back then you didn't see this coming…a "research scientist" they never get anything done, right? Leni, the day we met you said you wanted to be my friend; I am blessed to find instead not only a true friend but also family. My love and thanks to you both. Mum, I cannot say enough to thank you for everything you have given me and done for me. I can honestly say I wouldn't be here without you. You made me brave and fearless because what is there to fear when you are part of a team who can do anything. Last but certainly not least, my pack, thank-you to Castiel, who reminded me of the good in the world and Brem, who drove me nuts and kept me sane.

Dedication

This thesis is dedicated to my parents with love and gratitude for giving me the support to succeed, the space to grow and the courage to choose my own path.

“Bite size pieces”

TABLE OF CONTENTS

page

LIST OF TABLES

Page

LIST OF FIGURES

page

LIST OF ABBREVIATIONS

° =	degrees
2D =	two dimensional
3D =	three dimensional
APS =	Advanced Photon Source
BMU =	basic multicellular unit
BMIT =	BioMedical Imaging and Therapy beamline (CLS)
BM =	bending magnet
BMD =	bone mineral density
BsEM =	back-scattered electron microscopy
BSU =	bone structural unit
CLS =	Canadian Light Source
CLSM =	confocal laser scanning microscopy
CT =	computed tomography
EV =	eigenvalue
FIB/SEM =	focused ion beam/SEM
HR-pQCT =	high-resolution peripheral quantitative computed tomography
Hu =	Hounsfield units
keV =	kiloelectronvolt
kVo =	kilovolt
Lc.Φ =	Degree of Orientation
Lc.Eq =	Degree of Equancy
Lc.El =	Degree of Elongation
Lc.Fl =	Degree of Flatness
LCN =	lacuno-canalicular Network
mA =	milliampere
Micro-CT =	micro computed tomography
mm =	millimeter
MRI =	magnetic resonance imaging
Nano-CT =	nano computed tomography
PVA =	partial volume averaging
ROI =	region of interest
SEM =	scanning electron microscopy
SR =	synchrotron radiation
SR micro-CT =	synchrotron radiation micro computed tomography
TEM =	Transmission Electron Microscopy

vs =	versus
μA =	microampere
μCT =	micro-computed tomography
μm =	micron

CHAPTER 1: INTRODUCTION

1.1 Introduction

The fundamental microstructural elements of bone, including the cells and vascular pore systems, remain consistent among many terrestrial vertebrates [1] suggesting they have a strong adaptive relevance; however, a complete picture of the function of this system remains elusive. Bone is a highly complex and dynamic living tissue with the capacity to respond and adapt to many internal and external stimuli including mechanical and chemical signals. Bone forms the rigid yet flexible endoskeleton which provides structural support as well as housing for many important biological functions including red and white blood cell production, and storage for fat, minerals, trace elements, and alkaline salts [2]. Approximately 35% of bone's dry weight consists of organic materials, the majority of which are collagen fibers, which provide the tensile strength of bone. The other 65% largely comprises a calcium-phosphate mineral called hydroxyapatite ($Ca_{10}(PO_4)_6(OH)_2$), which is responsible for the majority of a bone's compressive strength.

1.1.1 Bone Microstructure

Bone can be divided into two macroscopically distinguishable types: cortical bone and trabecular bone. Cortical bone, also known as compact bone, is the outer dense shell of bone which encloses the medullary (marrow) cavity. In long bones, cortical bone is concentrated mainly in the diaphysis, which forms the shaft of skeletal elements such as the femora and humeri. Trabecular bone also known as spongy or cancellous bone forms a honeycomb-like mesh comprised of rod and plate shaped struts found inside bone. In long bones, trabecular bone is concentrated mainly in the epiphyses and metaphyses, which make up the ends of the bone [2]. These two tissue types play different roles in bone strength and together form a synergistic material, which is stronger than the sum of its parts.

Human cortical bone has a complex hierarchical internal microstructure arranged into two tiers of porous spaces and their associated structures. The first, larger, tier of this system forms a network of neurovascular canals which permeate the cortex (Fig.1.1.2). The blood supplied through these canals ultimately allows bones to remain dynamic living organs with the capacity for growth, adaptation and repair. As such, they are commonly referred to as vascular

canals or the vascular porosity. In mature bone, these vascular canals are associated with Bone Structural Units (BSUs) called osteons (Fig.1.1.3). An osteon consists of a central vascular pore surrounded by concentrically arranged layers of mineralized collagen fibers known as lamellae. The incorporation of these canals into cortical bone can occur either during growth, as a 'primary osteon', or subsequently through the process of remodeling, as a 'secondary osteon' [3]. The traditional term Haversian system is synonymous with the term secondary osteon. This process of turnover is discussed further below.

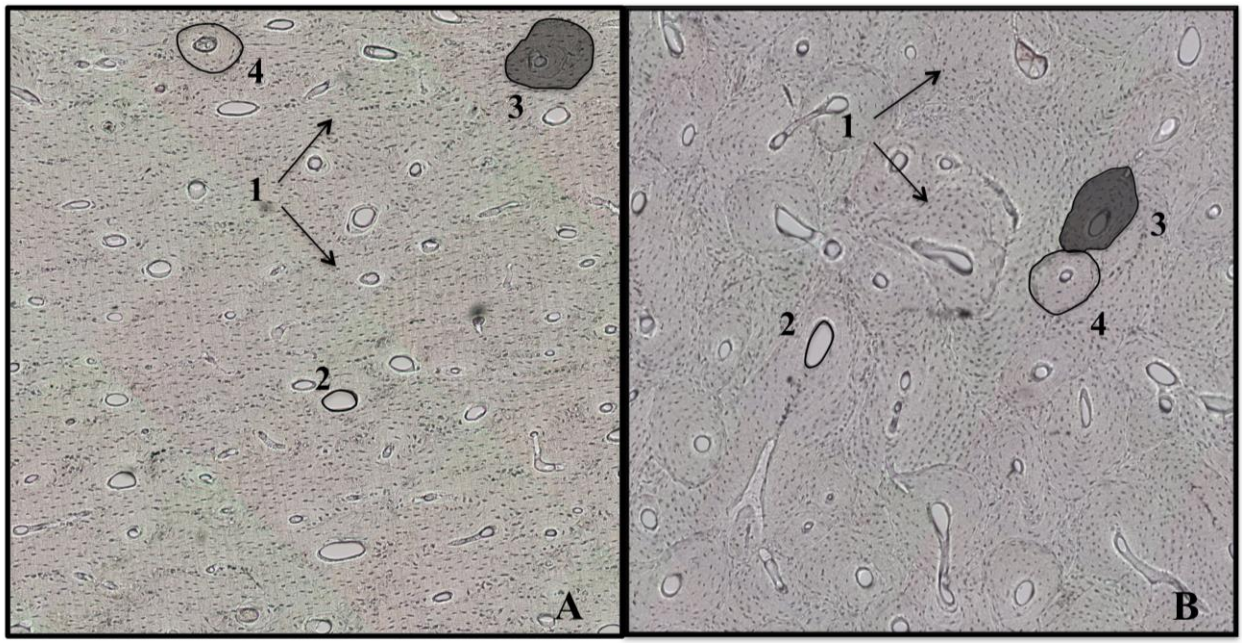

Figure 1.1 Human femoral ground section viewed under plain light microscopy; from 20 year old female consisting of mostly primary bone (A) and 28 year old female demonstrating more secondary bone (B) exhibiting microstructural features: osteocyte lacunae (1), vascular canal (2), osteon (3), osteon boundary (cement line)(4).

The second tier of cortical porosity consists of the osteocyte lacunae and their interconnecting canaliculi, which together form the Lacuno-Canalicular Network (LCN) (Fig. 1.2). The LCN houses the interconnected bone cells, osteocytes, which are encased in the mineralized matrix of bone in spaces called lacunae, and thus require the connectivity of the LCN for nutrient/waste transportation (Fig. 1.2). Beyond cell health, the LCN plays a role in intercellular communication [4] and has been suggested to play a major role in the sensing of

mechanical load, the initiation of remodeling via ion-sensation and regulation for bone matrix maturation and mineralization [5], which will be discussed below. This role is supported by the immense size of the LCN, indeed, the surface area of the LCN is estimated to be 400 times larger than that of the vascular canal system and 130 times greater than the surface area of the trabecular rods and plates [6].

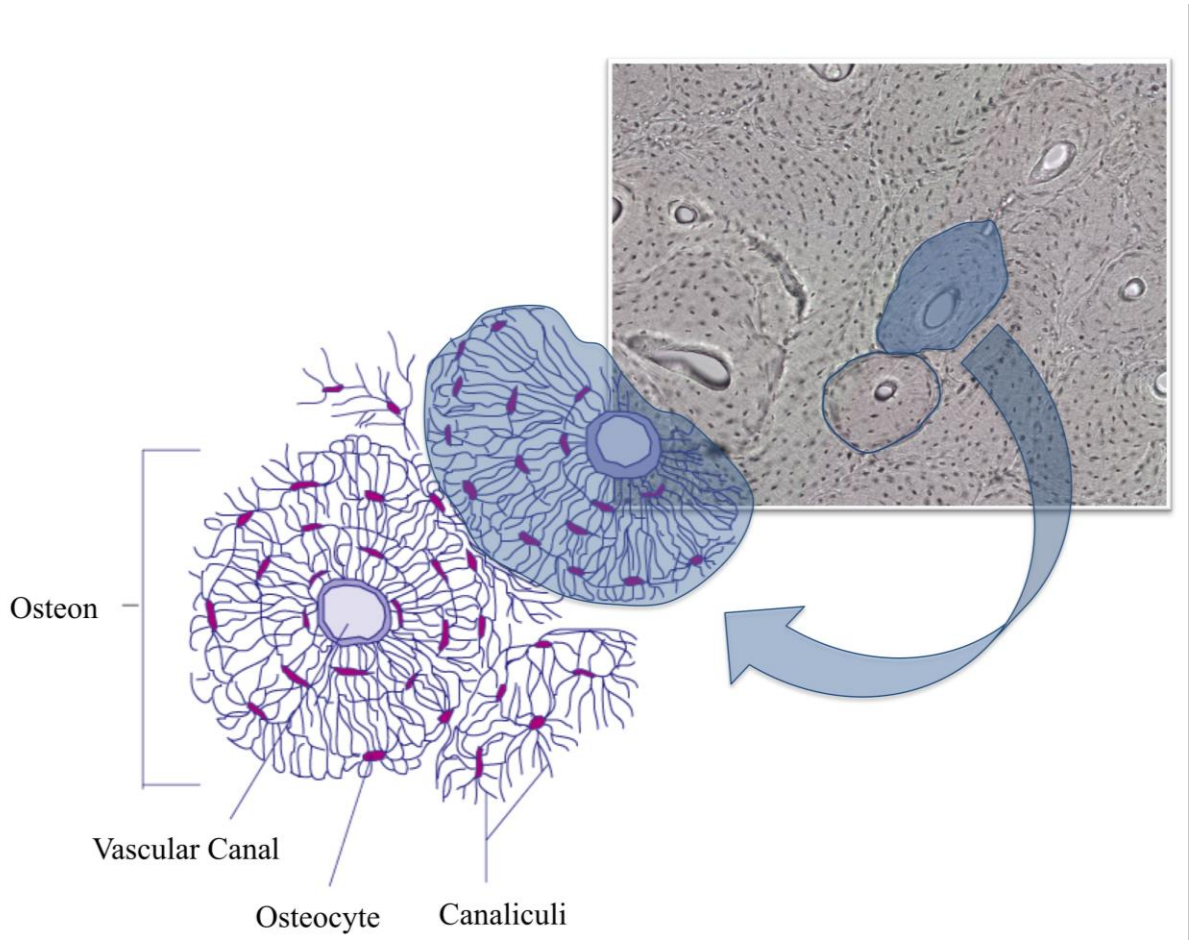

Figure 1.2 Figure demonstrating the elements of the Lacuno-Canalicular Network. Inset adapted from Open Source Wikipedia Image.

1.1.2 Bone Adaptation

Cortical bone has a highly dynamic microstructure that undergoes adaptation and renewal throughout life [7]. Both trabecular and cortical bone undergo similar processes through which bone growth and development occurs: *modeling* and *remodeling* [8].

Modeling is the predominant process of adaptation during bone growth and is responsible for altering the size, shape and position of the bone tissue in space. Bone that is formed by modeling is referred to as primary bone and incorporates primary vascular canals which form the center of primary osteons [9]. Primary bone can be laid down either as woven bone, with irregularly oriented collagen fibers, or as lamellar bone, in concentric layers forming circumferential rings in the diaphysis [2] (Fig. 1.1.A).

While the modeling process is generally restricted to the initial growth period, remodeling is a constant process, adapting the bone over the tissue's lifetime. Remodeling is characterized by the twinned processes of resorption and formation, in which old bone is removed and replaced with new bone [10].

The remodeling process coordinates the removal and replacement of small packets of existing bone through the initiation of Basic Multi-Cellular Units (BMUs). A BMU contains two main cell types: osteoclasts which resorb bone, forming a resorption space, and osteoblasts, which infill in the resorption space with mineralizing osteoid to form new bone [11]. The new packet of bone, its vascular canal and encysted osteocytes are referred to as a secondary osteon. Remodeling is the continual creation of new vascular canals in the tissue and an abundance of these secondary osteons is characteristic of mature bone in humans [12] and variation in this system is closely tied to genetics [13]. In the young, the twinned processes of resorption and formation are balanced; however, with advancing age there comes a net increase in bone resorption and a loss of bone architectural quality leading to fragility and the fractures associated with diseases such as osteoporosis [10].

Both primary and secondary osteons contain a vascular canal and the LCN with its bone cells encircling the canal. While the canal provides blood supply to the cells, osteocytes are thought to play a central role in the adaptive response of this tissue; however, the detailed nature of this response mechanism remains debated. As a consequence, the study of these cells is emerging as an increasingly important area of inquiry within bone biology. Previous studies have described osteocytes and their lacunae in human and non-human animals; however, the quantification of normal osteocyte density has always been problematic due to the relatively small number of osteocyte lacunae which can be visualized using traditional techniques.

1.1.3 Osteocyte Lacunar Density and Normal Variation

The range of variation recorded in the normal LCN is high and largely dependent on location, tissue type and analytical technique, with the research focus generally on the osteocytes and their lacunae. Early numbers for lacunar density from the 1970s were generally low and found human bone to contain between 13,000 and 19,000 lacunae per mm^3 although this was dependent on the sectioning technique used [14, 15]. Later conversions of area densities (mm^{-2}) to volume densities (mm^{-3}) conducted by Metz *et al*. [16] in 2003 found an average of 46,400 mm^{-3} for women of various ages and 70,000 mm^{-3} for elderly women. Differences in methodology may explain this high variance as the majority of these studies extrapolated from a small lacunar count to a per millimeter measure creating a very large margin of error.

Studies of lacunar density in bone have mostly been restricted to counts acquired secondarily often without context, in the pursuit of primary hypotheses regarding disease, aging and biomechanics. Although comprehensive measurements are lacking, the density, arrangement and morphology of lacunae are known to change with the skeletal element [17], bone tissue type [18] and the specific region within the osteon [19]. It has been suggested previously that nutrient burden may play a role in modulating aspects of bone morphology including osteocyte density [20, 21]. Skedros *et al.* [22] note that cortical bone in turkeys is thickest at neutral axis sites and may require an increased cellular population with higher blood and nutrient supply demands. In turn, the allowance for larger bone mass to accrue may come from a greater population of osteocytes [21]. This suggests it is important to study the lacunae within the larger context of the first tier, vascular porosity.

1.1.4 Morphological Osteocyte Lacunae Parameters

Measures of lacunar parameters beyond simple density are rare due to their small size and relative inaccessibility within the mineralized bone matrix. Recent studies of lacunar morphology have focused on disease with varied results. For lacunae of older women with and without osteoporotic fracture, McCreadie *et al*. [23] found no difference in size or shape. Application of high-resolution nano-computed tomography (nano-CT) to the study of osteopenic, osteopetrotic and osteoarthritic tibial samples found morphological differences in lacunae that the authors attributed to their disease state. Osteopenic lacunae were relatively large and round while

osteopetrotic lacunae were small and discoid shaped, and osteoarthritic were large and elongated, although unfortunately no control sample was included [24].

1.1.5 The Role and Importance of Osteocyte Lacunae

Osteocytes have been suggested to play a vital role in bone's ability to adapt to the loading environment it is subjected to [25]. The growing consensus is that the osteocyte syncytium plays a central role in detecting mechanical stimuli, known as mechanosensation, and translating this information into a cellular response, a process known as mechanotransduction [26]. There is no conclusive answer as to how osteocytes sense strains, although the mechanisms have been suggested to include chemical processes of the cells themselves, fluid-flow regulation and matrix deformation [17, 27-34]. Mounting evidence points to flow-induced sheer stress on the osteocyte body and process surfaces as the most probable mechanical signal which is directly detected [35]. Osteocyte lacunae and canaliculi are filled with fluid, which is displaced when the bone deforms under loading. Deformation of the cell induces it to produce prostaglandin and nitric oxide (NO) thereby triggering communication at gap junctions [36-38].

An alternative hypothesis is that small electrical charges, called streaming potentials, are generated by strain-induced fluid flow within the bone matrix. Strain may also be sensed by the plasma membrane of bone cells, which contain stretch-activated ion channels that permit calcium release, which has the potential to initiate other intracellular responses [26]. Thus, the LCN not only provides a means for cell survival and communication, it creates the very microenvironment necessary for the detection of mechanical loading. Concomitantly, this implies that differences in morphology and the relative abundance of osteocytes and their lacunae should affect the efficacy of the system [39]. Large-scale analyses of osteocyte lacunar parameters in 3D will enable further evaluation and clarification of these mechanisms.

Accurate description of the lacunar network is important both in the characterization of normal tissue anatomy and for evaluating the response of bone to aging, loading and pathological conditions [14]. Early studies suggested that lacunae were inconsequential in influencing the mechanical behavior of bone [40]; conversely, recent analyses have suggested the LCN has an important role in mechanical parameters including stiffness [41] and strength [42]. Sugawara and colleagues [43] have found a regular well-organized LCN is required for successful and stable bone maintenance.

1.1.6 The Role of Osteocyte Lacunae in Bone Quality

The traditional measure of fracture potential is related to bone strength. The American National Institutes of Health Consensus Panel on Osteoporosis defined that bone strength is a combination of bone density and bone quality. While bone density is a macroscopic measure, relatively easy to quantify, the question of interest is how do we quantify bone quality, a far more ambiguous term, referring not only to the architecture of the bone but also to the cellular state. Studies examining the relationship between lacunar density and parameters of bone quality have demonstrated inconsistent results. A number of studies [1, 44, 45] found no correlation between lacunar density and bone formation, architecture or resorption. In contrast, Vashishth *et al.* [21] found positive correlations between both cortical and cancellous bone mass accrual and lacunar density. These inconsistent correlations between lacunar density and structural parameters indicate that variation in density may not be a major determinant of bone quality, although further studies are needed to confirm this. It has also been found that changes in loading affect lacunar density; rats subjected to sciatic neurectomy, effectively paralyzing them, experienced a decrease in lacunar density [46]. Transgenic mice selected for improved bending strength demonstrated a significant increase in lacunar density [47]. Rats with increased loading due to exercise have increased lacunar density in the tibial mid-diaphysis, but a decrease in the second metatarsus suggesting local loading and bone specific responses are more important than whole-bone simplified loading dynamics [48]. Interestingly, studies of loading in thoroughbred versus non-athletic horses found no significant difference in lacunar abundance nor any differences related to age [49]. Osteocyte involvement in functional adaptation to loading has been suggested by increased lacunar density in studies of immediate versus delayed loading of human dental implants [50]. Rat ulnae, which have been subjected to a single fatigue-point loading and then allowed to heal, show a reduction in lacunae over time [51]. Studies examining lacunar density in relation to strain, remodeling and metabolic aspects of the local biomechanical environment, found poor correlation, suggesting that lacunar density has little functional relevance to mechanotransduction pathways. Results of a study by Skedros *et al.* [52] indicate that lacunar density has a significant influence on bone's apparent stiffness.

Lacunar density is also relevant to analyses of damage and microcracking. Like all structural materials which undergo repetitive cyclical loading, bone is subject to microdamage

[53] and the relative abundances and morphology of lacunae spaces are likely to affect this. Martin proposed that all remodeling in normal tissue was induced by such microdamage [54] and that remodeling is initiated and steered towards the resultant microcracks, which have caused the death of nearby osteocytes [55]. Although Ma *et al.* [56] determined there was no correlation between lacunar density and microcrack surface density or length, Mori and colleagues [57] found lacunar density inversely correlated with crack density which they suggest supports the hypothesis that the osteocyte network detects microcracks and signals their repair. More recently, a study by Soicher *et al.* [58] found lacunar density correlated positively with the amount of microcracking, a result consistent with the idea that microcracks accumulate more readily in areas with reduced bone mass. Lacunae do not stop microcrack propagation nor do they initiate cracks although evidence does suggest they are able to act as risers, focal points of pressure [59] as well as guiding the path of the crack [60]. Interestingly, fatigue damage occurs more frequently in interstitial bone [61, 62] in which the osteocyte density is lower [63]. Questions of normal variation in lacunar properties add another layer of complexity indicating that the reaction of bone to stress and loading cannot be considered a single homogenous response.

1.1.7 Age-Related Changes in Osteocyte Lacunae Density

Study of age-related changes in osteocyte lacunar properties has focused heavily on lacunar density. It is suggested that lacunar density declines with age in males and females [57, 64-66]. While an age-related reduction in lacunar density is expected, the rate of this decline; however, is still debated. Mori and colleagues [57] found that lacunar density in the trabeculae of the human femoral head did not begin to decline until 70 years of age which was then followed by a sharp decrease, while recent studies have reported the decline to be linear [45] and alternatively, exponential [67]. Reduction in lacunar density can occur through two mechanisms, firstly bone can be remodeled incorporating less osteocytes into the new osteon; secondly ‘infilling’ of existing lacunae can occur. The latter is an age-related process that leads to complete mineralization of the lacunar space, termed ‘micropetrosis’ by Frost [68], which results in a small decline in lacunar density with approximately 15% of lacunae meeting this fate.

Aging cortical bone is characterized by an increase in the heterogeneity of lacunar spatial organization [69]. Two alternative hypotheses have been suggested for these differences. Firstly that with advancing age, specific areas of bone are preferentially resorbed and selectively

repopulated with osteocytes leading to clustering of the lacunae [69]. Alternatively, evidence from *in vitro* studies has suggested that bone abundant in osteocytes is more readily resorbed. Additionally, with age, as bone formation activity declines and or resorption activity increases, osteocyte density will vary [70].

1.1.8 Osteocyte Lacunae Parameters and Osteoporosis

The effect of aging on bone tissue is currently an area of intense interest, in particular with regards to age-related bone diseases such as osteoporosis and osteoarthritis. Osteoporosis, a disease characterized by progressive loss of bone quantity and quality leading to increased risk of fracture [71], represents a growing burden to developed and developing nations around the globe. Tarride and colleagues [72] estimate that in a single year (2007/2008), osteoporosis cost the Canadian health system 2.3-4.1 billion dollars and projected these costs would continue to increase.

While there is general agreement that lacunar density declines with age in humans [57, 64-66], possible links to osteoporotic bone loss have proven elusive. Intriguingly, Knothe-Tate [26] noted that the LCN of late-stage osteoporotic individuals is characterized by severely reduced connectivity and increased heterogeneity of the system. A change in the size and number of lacunae, and interconnectivity of the LCN due to aging and/or disease would have profound functional consequences. As osteocytes are believed to be vital for the sustained health of bone, a decline in their numbers is detrimental and potentially linked to accelerated turnover and bone loss. Metz et al., [16] reported that osteocyte density in sheep is greater in more porous bone. This would suggest that osteoporotic individuals should have elevated osteocyte density. Studies of human vertebral trabecular bone seems to support this concept, as osteocyte density has been reported to be both higher in women than in men and to increase with age [73] and a number of studies report lacunar density to be increased in women with osteoporosis [58, 64, 73]. In contrast to this, a more recent study by Mullender *et al.* [45] found reduced lacunar density in osteoporotic patients. Other research has shown that in some individuals destined to experience an osteoporotic fracture, bone is made with fewer osteocytes than normal [63], suggesting that some individuals may be predisposed to developing an osteoporotic fracture. This is consistent with results by Mori *et al.* [57] and Qiu *et al.* [63] which report an average of 30% lower lacunar densities in patients with a history of osteoporotic fracture and Zarrinkalam *et al.* [74] who found

reduced lacunar density in the lumbar vertebrae of osteoporotic sheep. The conflicting results of Mullender and colleagues [45, 64] led them to deduce that the variation in lacunar density in osteoporosis may be site-specific. Alternative reasons proposed for these differences include issues with sampling autopsy versus *in vivo* specimens and the small number of lacunae able to be analyzed using currently accessible analytical techniques.

Although osteoporosis is known to preferentially affect women, to our knowledge no studies have systematically compared lacunar parameters between men and women over the age span. The importance of this cannot be underestimated, It has been suggested that osteoporosis may be due to a reduction in mechanosensitivity and therefore the ability to initiate mechanotransduction, which would result in a decrease in the bone's capacity to respond to loading [75, 76]. This occurs via an imbalance in the remodeling process, either by an increase in resorption activity or a decrease in the formation of new bone, ultimately leading to decreased bone mass and density, and ultimately osteoporosis [77]. Regardless of the route, the likely mechanism for either of these is through the osteocyte network.

In recent years there has been an increased recognition of the importance of osteocytes as sensors and transducers of mechanical stimuli, initiating and regulating ongoing remodeling [78]. Ultimately, it is an imbalance in remodeling that leads to age-related bone loss and, therefore, understanding osteocyte function is critical. Unfortunately, scientific inquiry in this area of bone biology is fundamentally lacking and no systematic study of age- and sex-related variation in the lacunar parameters of human bone has ever been conducted. Indeed, it has been noted that *"An intriguing but understudied possibility is that the connectivity and structure of the lacunocanalicular system may play a role in bone disease"* [79].

This research aims to make contributions to these areas by utilizing synchrotron radiation-based micro computed-tomography (SR micro-CT) imaging as an innovative tool to analyze normal healthy bone tissue of men and women over the human age span. Within the context of an aging population and the increasing health care burden associated with osteoporosis, the proposed research is both relevant and timely. While there have been numerous hypotheses regarding the interactions and importance of osteocyte density and morphology, this overview demonstrates that further exploration into the variations in lacunar density and its

interactions with aspects of bone material and structure using a larger sample set representing the adult life span is warranted.

1.2 Specific Aims

Many questions are raised by the literature regarding the state of the osteocyte lacunae both in healthy and pathological individuals. If lacunar properties have a role in osteoporotic disease then we would expect to see differences with age and between men and women, as observed in the biased prevalence of the disease. In order to address this, the primary goal of this dissertation will be to investigate two-related research hypotheses:

1. That lacunar density and morphology in cortical bone differs over the adult lifespan.
2. That lacunar density and morphology differs between the sexes.

Innovative aspects that will carry this work forward include the testing of desktop micro-CT to characterize microarchitecture beyond the capabilities previous achieved and the use of synchrotron radiation (SR) micro-CT to characterize osteocyte lacunar density and morphology in 3D.

1.3 Organization of the Thesis

The research described within this dissertation consists of a series of related studies conducted over the past five years (2009-2014). Chapter 2 discusses the benefits of multiple imaging modalities in the quantification of bone microstructural properties. Chapter 3 compares synchrotron-based micro-CT imaging with that of a desktop source, with the intent of validating SR micro-CT for application to human cortical bone lacunae visualization and analysis. Chapter 4 focuses on a new methodology for characterizing osteocyte lacunar density and morphology in 3D and applies this technique to explore intra-element variation in lacunar parameters in a single healthy young male. The content of this chapter has been previously published in *BONE* [80] and has been reprinted with the permission of Elsevier, Inc. (see appendix C). This study involved collaboration with Dr. John Clement and David Thomas of the University Melbourne, Australia, who were involved with the collection of the specimens utilized in this thesis. Based on the results of Chapter 4, Chapter 5 tests the hypothesis that lacunar parameters are different in

normal healthy young males dependent on the anatomical region from which they are examined. The content of this chapter have been previously published in the *Journal of Anatomy* and are reprinted with the permission of Wiley & Sons. (see appendix C). Chapter 6 examines the effect of aging on human lacunar properties in the proximal shaft femoral cortical bone of 30 women over the age span. The content of this chapter has been previously published in the *Journal of Structural Biology* [81] and has been reprinted with the permission of Elsevier, Inc. (see appendix C). Chapter 7 focuses on examining the lacunar parameters of 36 human males across the age range in order to elucidate the effect of sex and age on the human lacunae. Chapter 8 concludes this thesis with an overview of the results from the studies conducted in Chapters 4 through 7 and a discussion of future research directions.

CHAPTER 2: IMAGING AND VISUALIZATION OF BONE MICROSTRUCTURE

2.1 Introduction

Recent developments in high-resolution imaging modalities in combination with increasingly sophisticated computer software have opened up a range of opportunities for quantitative investigation of human bone morphology, particularly with the application of morphometrics in the virtual environment.

2.2 Imaging Modalities for Bone Microstructure

As discussed in the previous chapter, as osteocytes differentiate from osteoblasts they become trapped within the bone matrix as it forms, creating holes or spaces known as lacunae. Preservation and subsequent visualization of the cell bodies is difficult and therefore the lacunae are often used as a proxy for osteocyte properties such as, density and morphology [63]. Recently, growing interest in how these properties potentially relate to bone adaptation, disease and aging has, in part, arisen from the availability of increasingly high-resolution 3D imaging modalities including computed tomography.

2.2.1 Traditional Methods for Studying Bone Microstructure

Early analysis of the LCN was conducted utilizing traditional histology techniques, generally coupled with bright-field, phase contrast or epiflorescence microscopy, at times supplemented with staining protocols to enhance image contrast (Fig. 2.1.A, C) [21, 53, 57, 63, 65, 69, 73, 82, 83]. These setups remain the most accessible and widely employed bone microstructural imaging techniques. Visible light-based microscopy has excellent resolution, limited only by the instrument components and the wavelength of visible light to about 200nm. The use of image enhancements also allows for multiple bone components to be examined together including lacunar density, mineralization, osteon systems and collagen fiber arrangement [84]. The specimens to be imaged must generally be cut into thin sections only a few microns thick and often decalcification is required. The major disadvantage with using traditional light microscopy to quantify lacunar density is the restriction to two-dimensional (2D) planes of view [84]. Comprehensive studies of lacunar abundance require sufficient numbers to be counted which in turn requires quantification of a larger region of interest. Utilizing

traditional techniques, samples over 1 mm^3 can only be examined using mechanical serial sectioning, an approach which is both destructive and time consuming. Decalcification and subsequent sectioning by microtome also requires precise alignment of possibly deformed sections. Sequential sectioning of undecalcified specimens by saw can affect the accuracy of density counts due to a loss of bone matrix between sections [85]. Analyses of lacunar descriptors beyond density counts, particularly morphology, are inherently difficult with these techniques due to the three-dimensional nature of the spaces.

2.2.2 Three-Dimensional (3D) Imaging Techniques

More recent imaging developments have enabled the collection of 3D data. Confocal microscopy, for example, allows for a change in the depth of the focal plane resulting in a relatively short stack of serial 2D images, which are then combined to form a 3D data volume (Fig. 2.1.B) [21, 39, 63, 65, 67, 69, 73, 82, 86]. When a laser is used for illumination of the sample, the technique is called Confocal Laser Scanning Microscopy (CLSM) [17, 24]. As image information is obtained from multiple planes, 3D reconstruction of the bone can be performed without superimposition of the structures. Unfortunately confocal microscopy has a limited penetration depth, for example less than 100 microns for untreated bone. By utilizing a beam of electrons to illuminate the sample, resolution can be further improved. Two techniques using this setup have been extensively used in bone analyses, Transmission Electron Microscopy (TEM) [87] and Scanning or Back-Scattered Electron Imaging (S/BsEM) (Fig. 2.1.D) [22, 47, 52, 88, 89]. Compared to optical microscopy these systems require extensive sample preparation, including, for TEM, sectioning into ultra-thin slices of 10-100nm [90]. Additionally, electron microscopy is relatively difficult and expensive to utilize [84]; however, electron microscopy allows for excellent resolution of individual lacunae and their canaliculi [87]. BsEM also enables the examination of relative differences in the mineralization of bone matrix, permitting the analysis of the lacunae and haversian system concomitantly [91]. Alternative 3D visualization methods less commonly applied include Confocal Scanning Optical Microscopy (CSOM) [86], pytchographic CT [92], transmission x-ray microscopy-CT [34], and serial Focused Ion Beam/SEM (FIB/SEM) [93].

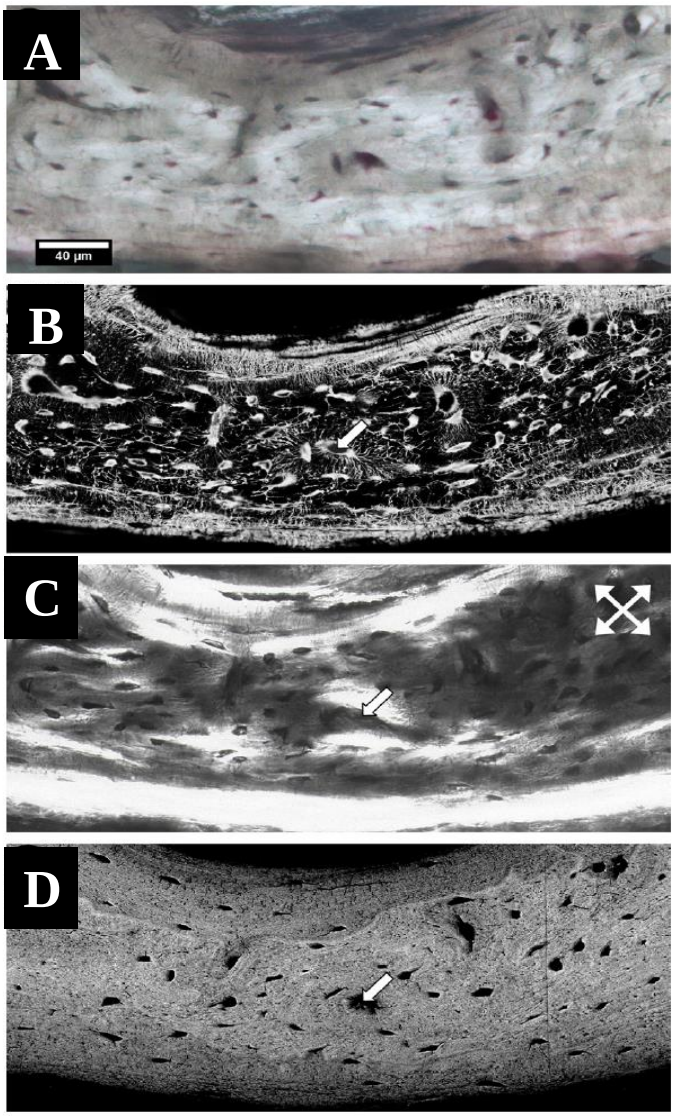

Figure 2.1 Figure demonstrating traditional imaging techniques in murine bone. Light microscopy (A), confocal microscopy (B), polarized light microscopy (C) and back-scattered electron microscopy (D) Adapted from Kershnitzki *et al.* 2011.

The majority of these techniques provide excellent resolution and are able to examine the nanostructure of the osteocytes and their lacunae, down to the canaliculi and even beyond. These techniques; however, are inherently restricted in that they survey a very limited volume of interest; this restricts analysis to only a few to a few hundred lacunae. These techniques, for the most part also require intensive, time consuming and often destructive preparation of the samples

prior to imaging and in the case of FIB/SEM the sample is destroyed as part of the imaging process [93]. Human bone is difficult to collect and ethics requires us to consider the use of the least destructive methods which allow for analysis.

2.2.3 X-Ray Based Imaging Techniques

The 3D nature of bone's microstructural network makes using a 3D technique to study it preferable. X-ray based computed tomography (CT) systems entered the market in 1973 [94]. Utilizing the principles of basic radiography, CT relies on the differential x-ray absorption of differing tissues, creating a visual distinction with materials denser to x-rays appearing more opaque. CT utilizes the collection of a series of projection images; from these projections a 3D image of the object can be reconstructed. In medical CT scanners, such as those found in hospitals, the x-ray source and detector array rotate around the sample measuring fan-beam attenuation (absorbance) within the confines of a single projection image (Fig. 2.2). Digital cross-sectional images are calculated from these attenuation measured projection data and are represented in inverted grey-scale with black representing the lowest and white the highest density. This attenuation is measured in Hounsfield units (Hu), the Hounsfield scale is defined by values that represent the attenuation of the x-ray beam through air (–1000Hu) and water (0Hu) [95].

The major drawback to any use of penetrating x-rays is radiation dose, whereby the tissue absorbs some of the energy from the x-rays. While dose is not a significant issue in plain film radiography, when multiple images are taken in sequence, this dose can reach unsafe levels. Since its development, CT scanning has superseded conventional radiography as the preferred imaging modality for the investigation of bone structure. The production of cross-sectional 3D image stacks in CT overcomes the issue of structural superimposition typical of conventional radiography. Important to note is that CT is more pertinent to the study of bone due to its high contrast and differential x-ray attenuation; soft tissues are better visualized using magnetic resonance imaging (MRI) modalities [95].

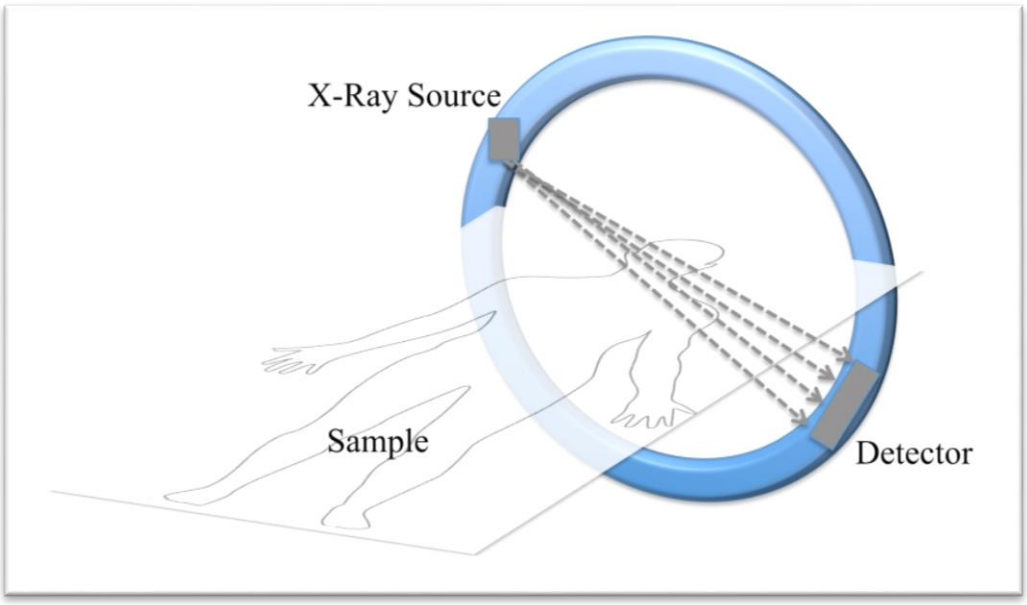

Figure 2.2 Figure demonstrating the components of medical CT. Adapted from Webb (2002).

Like any digital image, each CT scan slice consists of a specific number of picture elements or pixels. Different to a photo; however, each slice has a third dimension, thickness. Therefore each element is actually a volume element known as a voxel. The voxel size is limited by the scan machine's capabilities and operational selections. The 'spatial resolution', or ability to visualize small details separately is not as good in CT as in traditional radiography. The contrast resolution; however, is superior in CT so that small density differences can be visualized such as those between similar structures of differing thicknesses [95, 96]. Unlike medical CT scanners, dedicated industrial and research high-resolution micro-CT scanners have been developed which provide images with thinner slices and significantly higher spatial resolution allowing much smaller structures to be visualized [97].

2.2.4 In Vivo X-ray Imaging Techniques: High-Resolution peripheral Quantitative Computed Tomography

While *in vivo* visualization techniques are best for studying a dynamic living tissue such as bone, they are hampered by limits in resolution when aiming to examine small structures. High-Resolution peripheral Quantitative Computed Tomography (HR-pQCT) allows for study of bone mineral density (BMD), mechanical parameters and cross sectional morphology in 3D but

is restricted to distal limb segments such as the forearm and lower leg [98, 99]. While clinical work has focused on the application of HR-pQCT to macroscopic measures of the shape and relative abundance of trabecular and cortical compartments, examination of cortical porosity is possible. The traditional segmentation techniques used to examine HR-pQCT scans are coarse, precluding the possibility of studying the intra-cortical porosity [100]. Utilizing special segmentation algorithms; however, examination of the cortical porosity safely *in vivo* is achievable at ~80μm pixel size [101]. This approach has been subsequently refined and extended, and successfully applied to the intra-cortical porosity of humans regarding questions of age, sex and health (see for example: [102-105]). This technique is restricted; however, in that the resolution in living humans is restricted to larger pores and cannot visualize or quantify the LCN (Fig. 2.4) [98, 99].

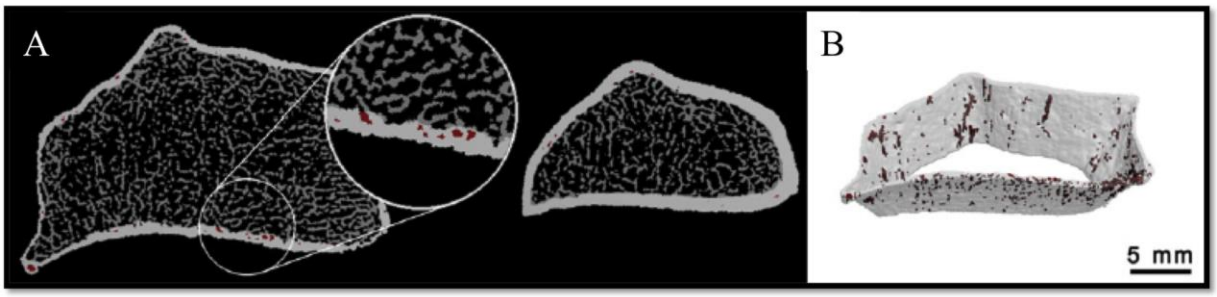

Figure 2.3 Figure demonstrating the potential of HR-pQCT showing the cortical compartment of the radius (A) and subsequent 3D segmentation of the cortical porosity (red) (B). Adapted from Burghardt *et al.* 2010.

2.2.5 In Vivo X-ray Imaging Techniques: In Vivo Synchrotron Radiation Micro-CT

In the late 1990s synchrotron radiation based x-ray sources were applied to high-resolution *in vivo* micro-CT imaging of trabecular bone of animal models [106, 107]. Synchrotron radiation offers a number of advantages over conventional x-ray sources including high spatial resolution, small beam divergence and monochromaticity [108]. Kinney and colleagues [106], were the first to utilize SR micro-CT *in vivo*, with subsequent studies expanding on the techniques and applying them to questions of age, sex, genetics, biomechanics and disease (e.g: [107, 109-115]). The use of *in vivo* SR micro-CT is generally limited to

trabecular bone by the radiation dose imparted on the animal by the x-ray beam. Recent work has expanded the use of *in vivo* SR micro-CT into high-resolution imaging, achieving scans of the cortical porosity of adult rats through the use of propagation phase contrast [116]; however, examination of the cellular level microstructure of bone remains unachievable.

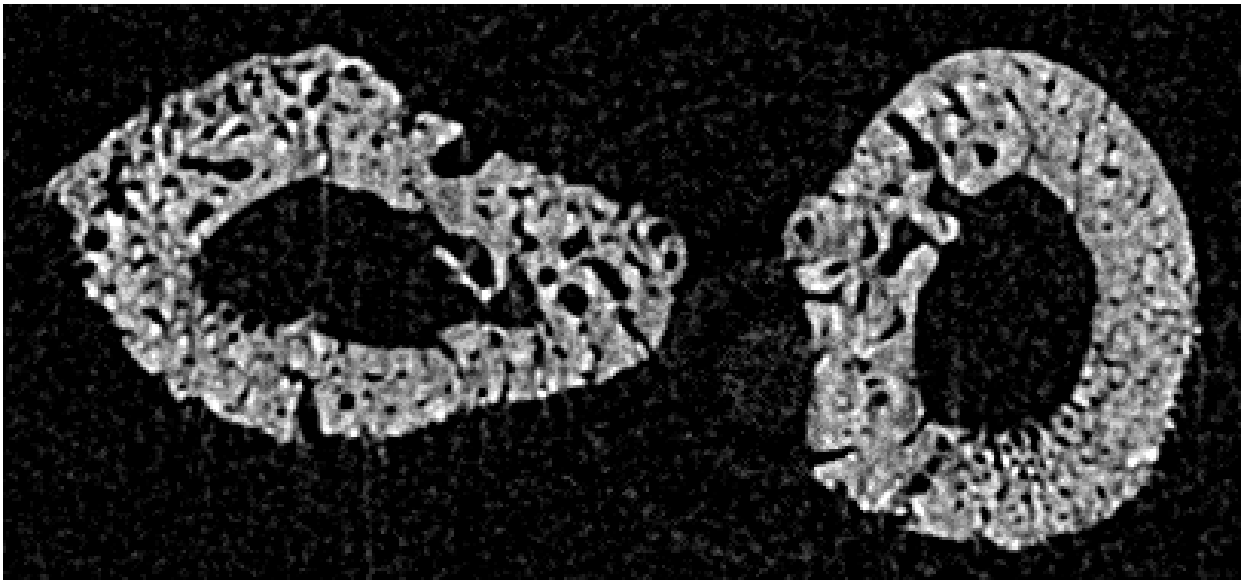

Figure 2.4 Figure demonstrating cortical porosity in a rat tibia visualized using *in vivo* synchrotron radiation Micro-CT. Adapted from Pratt, 2013.

2.2.6 In Vivo X-ray Imaging Techniques: In Vivo Desktop Micro-CT

An alternative method for examining bone architecture in living animals is through the use of commercially developed "desktop *in vivo* micro-CT" scanners [117, 118]. Developed out of early synchrotron monochromatic x-ray source-based *in vivo* imaging, desktop *in vivo* micro-CT utilizing polychromatic x-ray sources began to appear in the early 2000s [117, 118]. Allowing for dynamic data collection over time, this technique is not applicable to human bone, although it can be applied to animal models [119, 120]. The main limitation of *in vivo* micro-CT, is the resolution the setup is capable of achieving while keeping the x-ray radiation dose low enough for the animals' health [7]. Additionally, any movement by the animal will cause artifacts in the scan. The dose absorbed by the animal is essentially inversely proportional to the resolution, so that increase in resolution has a high corresponding increase in dose. Hence, this technique is limited to the study of trabecular morphology, with resolution insufficient to

elucidate the cortical porosity or osteocyte lacunar network [117, 118]. Since its development, *in vivo* micro-CT technology has advanced allowing safe, smaller resolutions and shorter scan times. Additionally, the novel use of contrast agents is also being pursued in an attempt to visualize the vascular network [121].

2.2.7 Ex Vivo X-ray Imaging Techniques: Desktop Micro-CT

With the current technology, visualization of the LCN is limited to *ex vivo* methodologies. While medical CT scanners are calibrated to the dimensions and material properties of the human body, i.e. the inclusion of soft tissues with scan times in the order of seconds per slice to reduce *in vivo* radiation exposure, typically in research *ex vivo* micro-CT radiation intensity and exposure is less of a concern, allowing for longer scan times and concurrently higher signal-to-noise ratios.

A number of commercial small-unit micro-CT scanners are available, commonly called laboratory or desktop micro-CT. These machines use the same principles as the medical CT scanners just on a smaller scale. One major difference is, in the case of desktop micro-CT, the specimen rotates on a stage between the source and detector rather than the source-detector apparatus rotating (Fig. 2.5). These scanners employ a polychromatic micro-focus x-ray tube as the source, producing a cone-shaped beam, which is used to create the geometric magnification that allows high-resolution imaging. The resolution of these systems is typically limited by the spot size of the x-ray tube, producing pixel sizes in the micron range.For bone research applications, this setup allows for smaller detector apertures, adaptable source-detector geometry and longer sampling intervals, which can improve spatial and contrast resolution. Importantly, micro-CT does not generally require extensive specimen preparation although this depends largely on gantry size and field of view, a significant limiting factor for volume of interest [96]. Desktop micro-CT systems have been used extensively to examine human bone microarchitecture [9, 122-124]. Their resolution is considered to be in the tens of microns [125], with the osteocyte lacunae currently inaccessible [126]. Experiments aiming to push these limits and the applicability of this to the analysis of osteocyte lacunae will be discussed in Chapter 3.

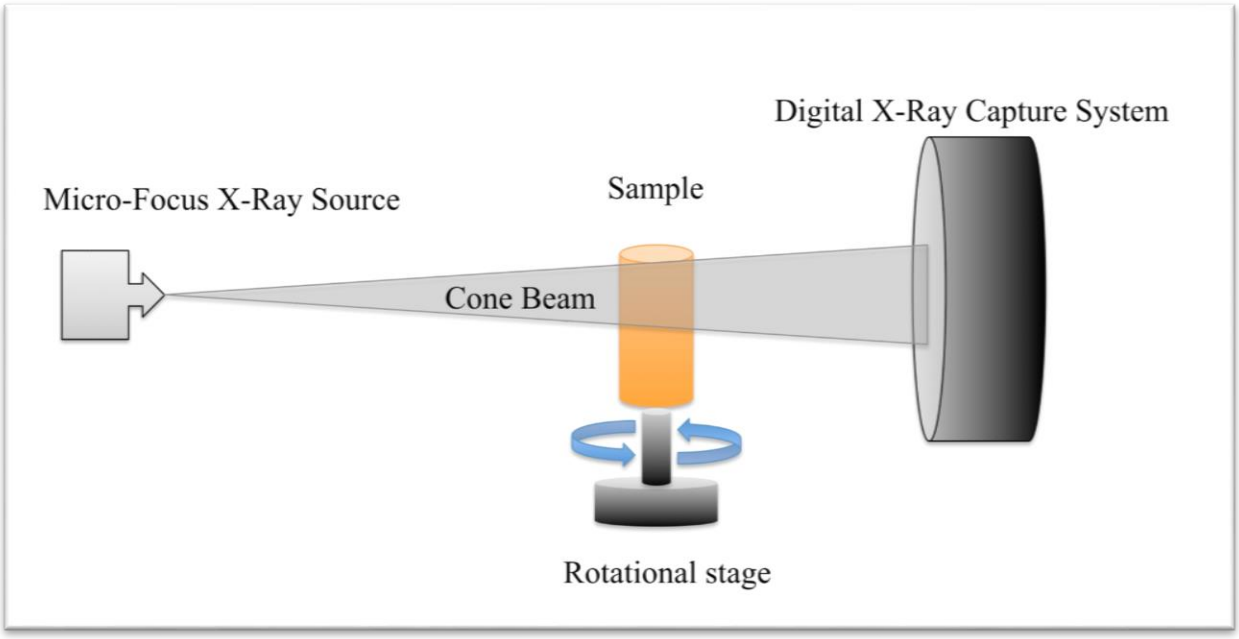

Figure 2.5 Figure demonstrating the setup for scanning in a desktop micro-CT. Adapted from SkyScan 1172 manual.

2.2.8 Ex Vivo X-ray Imaging Techniques: Desktop Nano-CT

Analysis of the LCN has been achieved on ultra-high resolution desktop systems often termed 'nano-CT' [17, 24]. Nano-CT utilizes a setup similar to micro-CT but with a focused x-ray source with a nanometer spot size allowing pixel sizes in the range of 400-700nm (Skyscan Bruker). These systems, however, have limited fields of view allowing for the quantification of fewer than 100 lacunae in any one scan and are more useful for analyzing the morphology of a single lacuna (Fig. 2.5) [17, 24]. Ideally a technique is required which is non-destructive, has the 3D capabilities of confocal microscopy, combined with sufficient resolution to analyze morphology with a large enough volume of interest to accurately determine lacunar density.

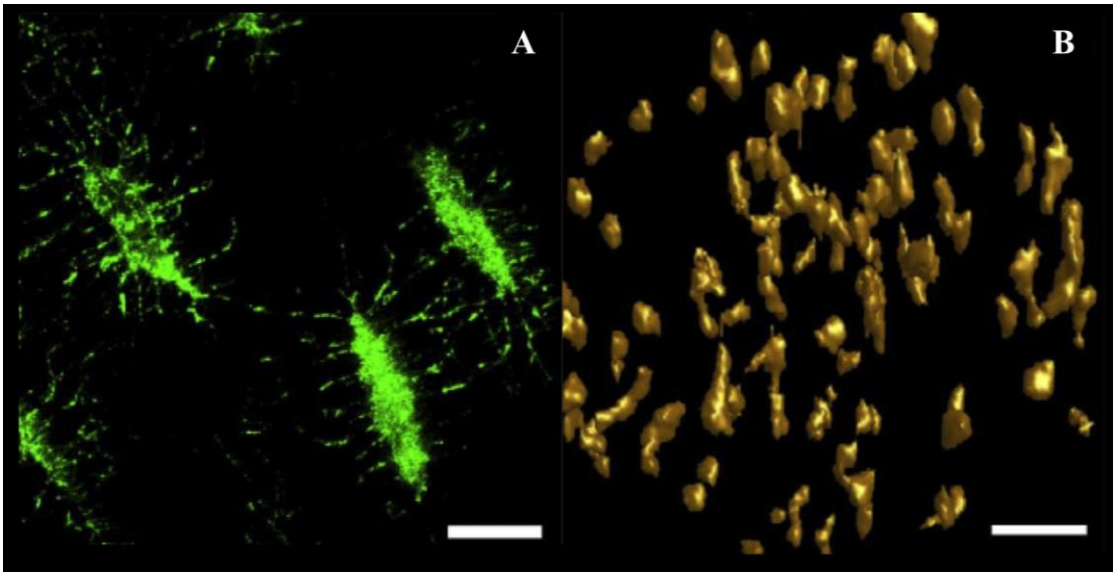

Figure 2.6 3D reconstructions of human osteocyte lacunae utilizing confocal microscopy (A) and nano-CT (B). Scale bar = 15um. Adapted from Van Hove *et al.* 2009.

2.2.9 Synchrotron Imaging Techniques

Synchrotron radiation-based micro-CT (SR micro-CT) has sufficient penetration and resolution to visualize the osteocyte lacunae and has increasingly proven to be a useful tool for lacunar density quantification in larger volumes of interest [84]. A synchrotron is a circularly arranged particle accelerator that is used to generate an exceptionally intense beam of radiation (light), which is manipulated to produce a specific wavelength of light including high-intensity x-rays which end in an experimental endstation setup known as a beamline (Fig. 2.7). Synchrotron radiation is the electromagnetic radiation emitted by electrons or positrons moving at relativistic velocities along a curved trajectory with a large radius of curvature [108]. The curved trajectory of the electrons or 'beam' is maintained by the use of magnets within booster and storage 'rings'. (For an excellent primer on synchrotron radiation, its properties and application see Margaritondo et al. 1988 [108]).

Visible synchrotron radiation was first noted in 1947 and research utilizing it began parasitically at storage rings designed and operated for high-energy physics experiments. Once dedicated synchrotron radiation facilities began to be built in the 1970s, their use as a light

source in research expanded rapidly [127]. While there are a number of synchrotrons in the world, many with dedicated micro-CT or biomedical beamlines, determining which to use is a balance of finding a facility with the setup required for specific analyses and availability of beamtime (for more information see [128] www.lightsources.org). Synchrotron radiation offers a number of enhancements over conventional x-ray sources including high intensity in broad spectral range, high brightness (the higher the brightness, the higher the photon count), small angular divergence, small source size, temporal coherence, tunable wavelength (by monochromator), spatial coherence, pulsed time structure, and polarization [127]. It is the high intensity and brightness which allow high-resolution studies of small samples.

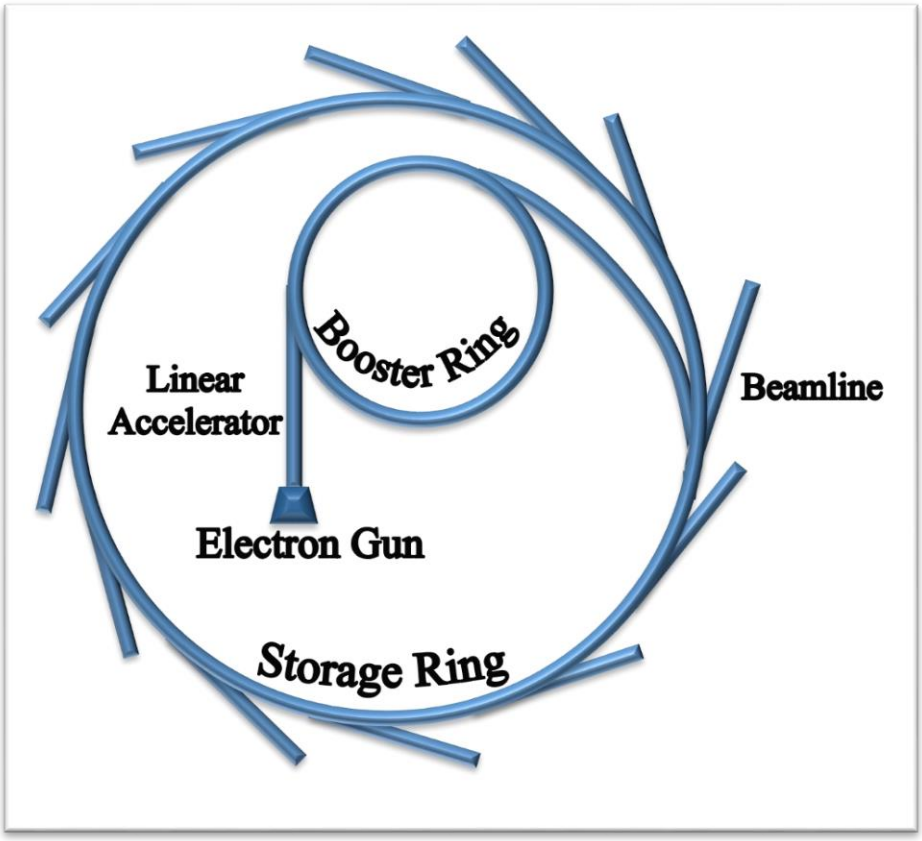

Figure 2.7 Diagram demonstrating the major components of a synchrotron. Adapted from Margaritondo (1988).

The setup for micro-CT scanning at a beamline endstation is similar to that of a desktop micro-CT. With the detector and source in fixed positions, the sample on its stage rotates within the beam. In this case the source is the synchrotron radiation beam. Common configurations include a detector, based on a CCD camera with a scintillator layer to convert the x-rays into visible light (Fig. 2.8).

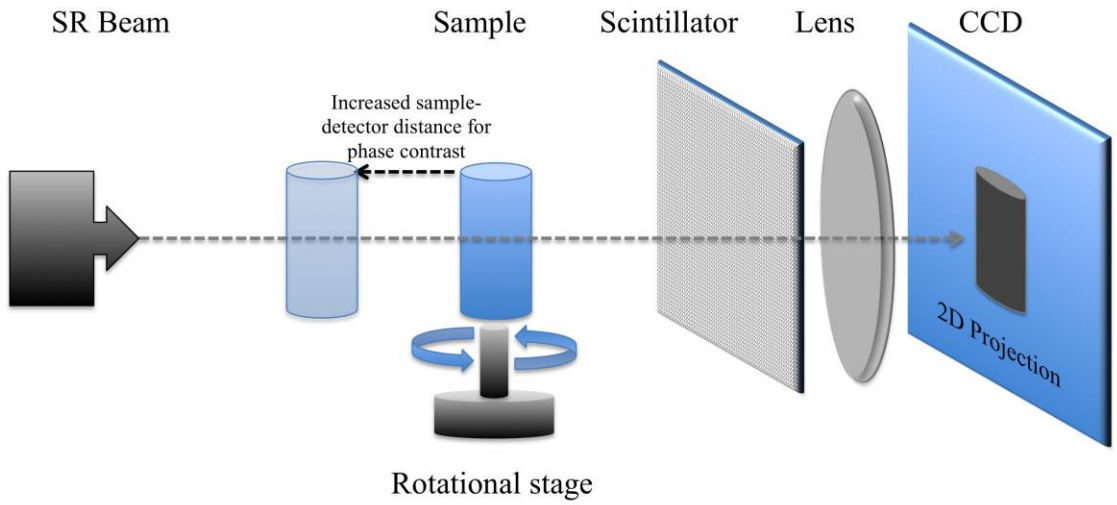

Figure 2.8 Diagram demonstrating the major components of the SR micro-CT setup. Adapted from Margaritondo (1988) and BMIT setup.

SR micro-CT is currently considered the ideal standard for *ex vivo* bone imaging in 3D [125]. Scans are able to be acquired over a shorter timeframe and provide more accurate quantitative data than a similar micro-CT setup utilizing a non-synchrotron source [129]. SR micro-CT also has the benefit of requiring little or no sample preparation and is relatively non-destructive. SR micro-CT has been successfully applied to studies of osteocyte lacunar parameters in 3D in animal models [126, 130] and humans [19, 80, 131].

There are four major limitations to resolving small structures utilizing SR micro-CT. These include: resolution as discussed above, partial volume averaging (PVA), sample movement, and phase contrast [95]. The grey-scale representation of each individual voxel is determined by averaging the attenuation of the materials occupying the volume space to produce a single greyscale value. In areas where contrasting materials, such as the air/bone interfaces,

occupy the same voxel then the greyscale number is a combination of these represented materials, limiting resolution, so small structures such as the lacunar edges and canalicular connections are poorly visualized [96]. PVA also leads to complications in the thresholding process that will be discussed in the methodology sections of subsequent chapters. Artifacts caused by movement can cause extensive problems. At high-resolution movement of a sample by only a few microns can cause interuptions in the scan that will only be noticed after a projection series has been reconstructed (Fig. 2.9). This must be taken into account when designing experiments and sample holders.

Additionally phase contrast must be taken into account. As photons pass through the sample they scatter, producing a refractive index-based source of contrast known as propagation phase contrast [132, 133]. The effect is such that bright and dark halo-like fringes highlight interfaces between materials of different x-ray attenuation. Typically to overcome this, the sample is placed as close to the detector as possible to minimize x-ray interference and distortion; however, phase contrast also provides an excellent mechanism for increasing contrast at bone/air interfaces which can help to enhance and detect structure boundaries. Phase contrast enhanced micro-CT has demonstrated potential for imaging bone microstructure including the osteocyte lacunae [134] and has been used successfully to image individual osteons [135-137]. The optimal phase distance required to effectively delineate lacunar boundaries while preserving accurate geometric dimensions, will need to be determined and will depend both the optical resolution and photon energy used. The use of phase propagation to increase contrast in the sample does have some drawbacks, particularly the detection of soft tissue remnants within the vascular porosity, [136] which can complicate the thresholding process. In short, SR micro-CT offers an excellent balance between resolution and volume of interest that allows for the characterization of the density and morphology of tens of thousands of lacunae in a single scan.

Figure 2.9 Micro-CT scans of human bone showing artifacts caused by movement; note the streaks around the lacunar edges. The white halos around the edges of the canals and lacunae are the result of phase propagation. Taken at the Advanced Photon Source 1.47um pixel size.

2.3 Conclusion

This chapter provides an overview of the current techniques available for visualizing osteocyte lacunae. While the ultimate goal for bone biology would be the use of *in vivo* techniques, this is not possible given the current technology. In Chapter 3 the suitable *ex vivo* x-ray based techniques discussed here will be tested to determine which has the best capabilities for my research requirements, balancing the need for high resolution and large volume of interest.

CHAPTER 3: PRELIMINARY IMAGING EXPERIMENTS

3.1 Introduction

As discussed in Chapter 2 there are a number of x-ray based imaging options for analyzing human bone microstructure. This chapter outlines the preliminary experiments undertaken to establish an imaging protocol to address my research questions with the aim to balance the requirements of large field of view and high resolution. As a control, SR micro-CT scans were taken by collaborators at the Advanced Photon Source, IL, USA (APS) as per established protocols [19, 136]. Two sub-studies were conducted to determine whether measures of osteocyte lacunar density and morphology could be obtained locally, first by comparing the use of desktop source micro-CT and second by comparing the use of the BioMedical Imaging and Therapy (BMIT) bending magnet (BM) beamline at the Canadian Light Source, SK, Canada with APS images.

3.2 The Use of Desktop Micro-CT to Determine Osteocyte Lacunar Density in Human Cortical Bone

3.2.1 Introduction

As outlined in Chapter 2, developments in synchrotron-based imaging have enabled the collection of three-dimensional (3D) data of large osteocyte lacunar counts. SR micro-CT can be considered the standard in bone imaging [129]. Although the preferred method, access to SR-based CT is restrictive with only a small number of micro-CT beamlines in the world, making extensive studies prohibitive.

The purpose of this study was to determine whether more readily accessible desktop micro-CT could be used to accurately determine osteocyte lacunar abundance. Desktop micro-CT offers high spatial resolution of samples with diameters up to a few millimeters, but most importantly overcomes much of the associability issues associated with synchrotron usage.

3.2.2. Specimens

Cortical bone samples were obtained from the femur of a 20 year-old male. The femur forms part of the Melbourne Femur Collection held at the University of Melbourne, Melbourne,

Australia (For a more detailed discussion of the samples see Chapter 4). Previously, a section of the mid-shaft (35 mm long) was removed, parallel to the long axis of the femur and then cut into 10 individual samples with dimensions of approximately 2 mm×2 mm×35 mm.

3.2.3 Comparative Images (SR Micro-CT)

Preliminary SR micro-CT scanning was conducted at the Advanced Photon Source (APS), Argonne National Laboratory IL, USA on beamline 2BM by colleagues at the University of Melbourne, Australia in 2006 [19]. Images were obtained using monochromatic x-rays with a photon energy of 26.4keV and an effective pixel size of 1.47 microns. Images were calculated by standard filtered back-projection from sets of 1440 projection images, with an exposure time of 120 milliseconds per frame and four-frame averaging, to improve the signal-to-noise ratio. The scan time for each sample was approximately 22 minutes. Projection images were reconstructed to create a dataset containing 1280 slices (2048×2048 pixels) (Fig. 3.1.A).

3.2.4 Desktop Micro-computed Tomographic Imaging (Micro-CT)

The samples were subsequently scanned using a desktop micro-CT system, the SkyScan 1172 (Aartselaar, Belgium) x-ray microtomograph (<5 μm x-ray source spot size; 8.83 camera pixel size). The samples were rotated through 360 degrees at a step of 0.05 degrees. The x-ray settings were standardized to 100 kVp and 100 μA, with an exposure time of 660 milliseconds per frame. Four-frame averaging was used to improve the signal-to-noise ratio. A 0.5-mm-thick aluminum filter and a beam hardening correction algorithm were employed to minimize beam-hardening artifacts (SkyScan hardware/software). The scan time for each sample was approximately four and a half hours. Each scan produced 1196 contiguous slices with a nominal resolution of 1.73 μm. (Fig. 3.1.B).

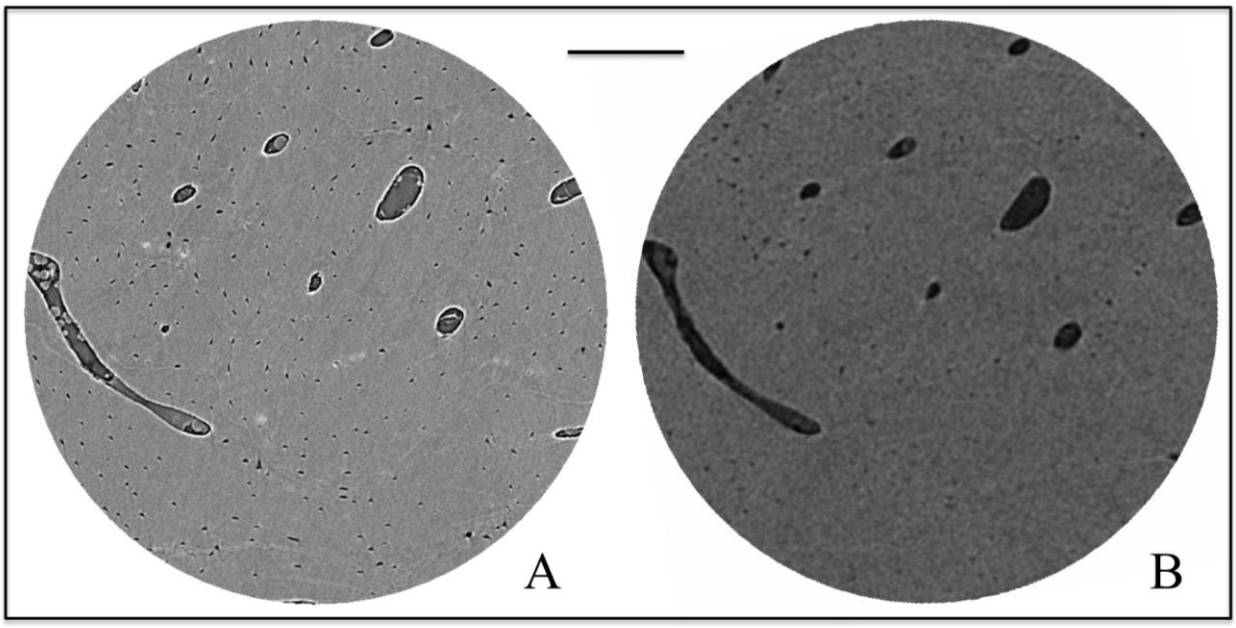

Figure 3.1 Matched micro-CT scan slices of the male femoral specimen taken with a synchrotron (APS) x-ray source (A) and a desktop (SkyScan 1172) source (B). Scale bar = 200μm.

3.2.5 Image Quantification

All scans desktop and SR were analyzed using the same approach. Image stacks were cropped and quantified using CT Analyzer 1.10.9.0 (SkyScan software). A cylindrical region of interest (ROI) with a diameter and height of 1mm and a volume of 0.786mm^3 was defined within each specimen. Lacunae within these ROI's were identified using a standardized global threshold. Following segmentation and removal of elements less than 10μm^3, which were assumed to be noise, lacunar density, volume, and parameters of shape were calculated. The application of this technique on the APS data produced excellent results allowing lacunar parameters including, density, volume, orientation and morphology to be analyzed as well as intermittent visualization of other microstructural features including osteonal borders, lamellae and soft tissue remnants (Fig. 3.2).

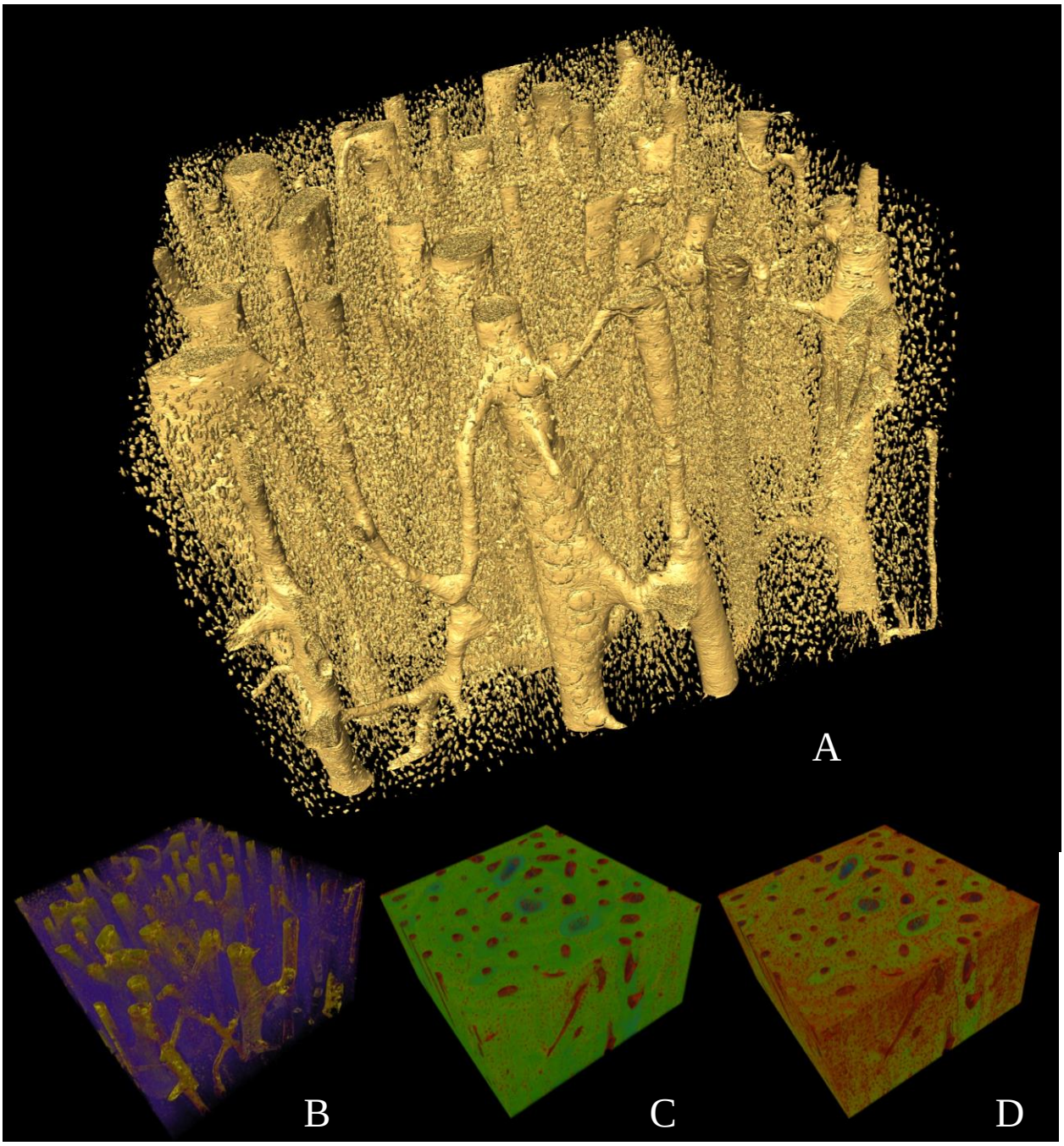

Figure 3.2 False color renders of the APS-acquired scan of a 2x2x1mm region. Micro-CT scan block showing vascular porosity and lacunae in yellow (A) and bone matrix in transparent purple (B), volume render showing canals and their associated lacunae in red (C), and visualization of some microstructural features including osteon boundaries in green (D).

3.2.6 Statistical Methods

Statistical analysis was performed using SPSS 16.0 (SPSS Inc., Chicago, IL, U.S.A.). The results from the two scanning methods were compared in accordance with the approach outlined by Altman and Bland (1983). This method, also known as a Tukey mean-difference plot, focuses on the comparability of the techniques by plotting the difference between the two methods against their means. In our case, the desktop micro-CT results were subtracted from the SR micro-CT results. A paired *t*-test was performed with significance $\alpha < 0.05$ to compare the two methods and provide information on the significance of the differences. This statistical method was chosen because both techniques (SR and desktop micro-CT) are considered to collect measurements with error while producing a single measure of bias, mean difference between the two techniques, and relative error.

3.2.7 Results

Cortical canals and larger lacunae were clearly visualized in the desktop micro-CT slices (Fig. 3.1.B). The average osteocyte lacunar densities from the desktop and SR micro-CT setups were found to be 22179 ±6343 and 25315 ±4230 per mm^3 respectively. Figure 3.3 shows the Bland–Altman plot for lacunar density. The mean difference (positive bias) between the two setups was 3137 ±3022, with the desktop methodology consistently missing lacunae. Additionally high variation in scan quality was evident in the desktop scans with some scans recording 90% of lacunae down to less than 75% in some cases. A paired *t*-test revealed the results from the desktop count was significantly different from those obtained by SR micro-CT ($p = 0.010$).

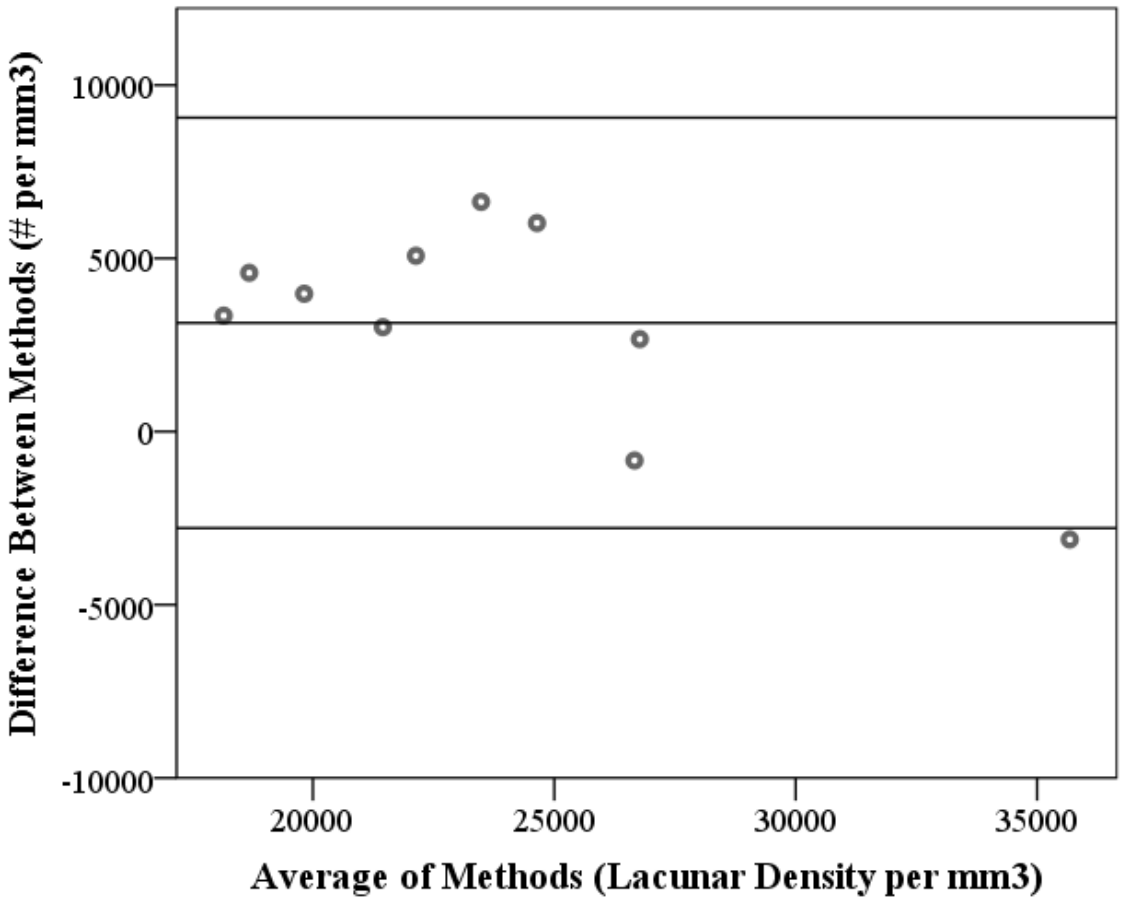

Figure 3.3 Bland-Altman plot of the differences between SR micro-CT and desktop micro-CT for measuring osteocyte lacunar density in human cortical bone. The same 10 specimens were used for both techniques.

3.2.8 Conclusion

Although desktop micro-CT shows promise for large scale more accessible studies of lacunar density, currently the resolution achievable with the 1172's source size of <5μm keeps analysis of the osteocyte lacunae out of reach. Newer higher-resolution commercial machines currently being produced by Xradia and SkyScan may overcome these issues. Additionally, to drive forward questions of the relation between age, sex and osteocyte lacunar parameters, quantification of morphology must be included. With this in mind the SkyScan 1172 desktop micro-CT is not currently capable of thorough analysis of the osteocyte lacunae and SR micro-CT is the only viable option for methodology to answer the questions related to the thesis.

3.3 The Use of Synchrotron Radiation Micro-CT to Determine Osteocyte Lacunar Parameters in Human Cortical Bone

As mentioned above, there currently exist a number of synchrotron facilities that are capable of micro-CT imaging of bone. While preliminary scans using an established protocol from the Advanced Photon Source (APS), Argonne National Laboratory, Il, USA (as detailed above) provided excellent quantitative information, an additional study was undertaken at the Canadian Light Source, Saskatoon, SK, Canada, to determine whether similar quality scans with the capability of measuring osteocyte lacunar density and morphology could be achieved at a more readily accessible facility.

3.3.1 Biomedical Imaging and Therapy BM Beamline (BMIT), Canadian Light Source (CLS), Saskatoon, SK, Canada.

Attempts at the Canadian Light Source, to achieve results comparable to the preliminary SR micro-CT scans conducted at the APS, began with scanning of human and rat bone to visualize and quantify lacunar density and morphology at the BMIT beamline at the Canadian Light Source in June 2010. As noted previously, each synchrotron has different technical specifications and the CLS has a larger source size and shorter beamline distances from the source are achievable. BMIT is not designed for the same level of high resolution imaging as the APS; however, due to its proximity and accessibility it was useful to establish the capabilities of the current setup. Following initial attempts at 4μm isotropic voxel size (Hamamatsu AA40 beam monitor with C9300-124 camera)(Fig. 3.4.B), which were initially plagued by mechanical (rotational) problems, an alternative optical configuration (Nikkor autofocus NIKKOR 24 mm f/2.8) was implemented to reach down to approximately 2μm voxel size. Images were obtained using monochromatic x-rays with photon energy of 24 keV. This configuration was found to be useful in the imaging of lacunar volume and density in rat cortical bone [130]. The application to human bone; however, produced mixed results. The x-ray intensity (flux) limitations and low signal-to-noise ratio were found to be such that reconstructed images allowed for only intermittent visualization of lacunae and other microstructural features and quantification of shape parameters was not possible (Fig. 3.4.C).

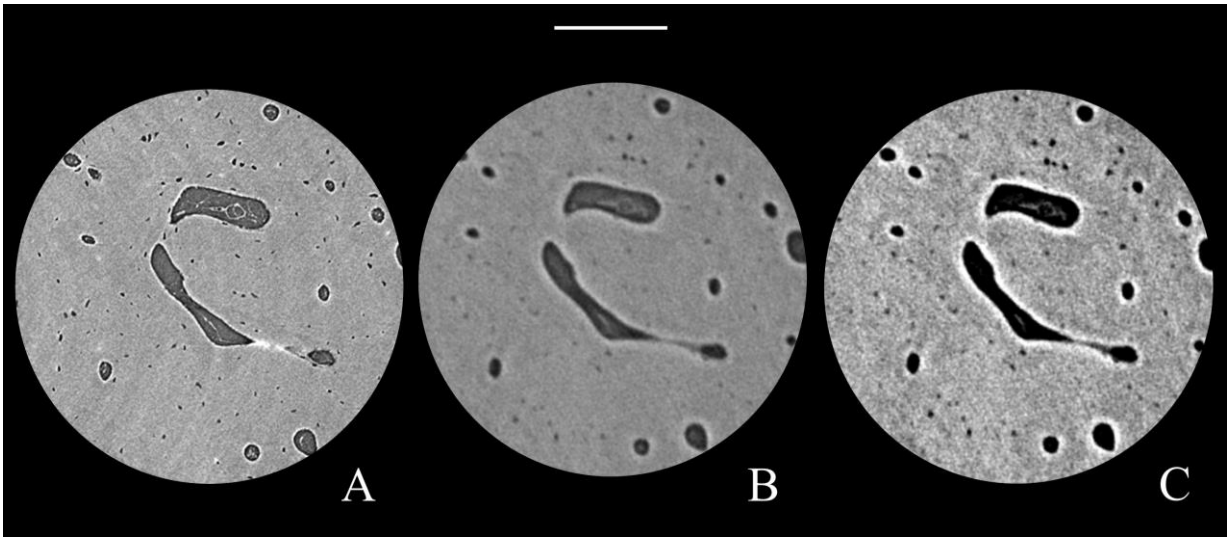

Figure 3.4 Single slice of circular region of interest within a human femoral sample reconstructed from the SR micro-CT scans comparing resolution and noise. APS 1.47μm pixel size (A), CLS 4μm pixel size (B) and CLS 2μm pixel size (C). Scale bar = 150μm.

3.3.2 'Pink beam' Scanning at BMIT

Subsequent imaging experiments at BMIT focused on the use of pink beam in overcoming the current flux limitations to better visualize human microarchitectural features (Fig. 3.5). Most synchrotron imaging utilizes only a portion of the incoming beam filtered with a monochromator in order to provide single peak energy; this filtering; however, reduces flux. 'White beam' refers to the use of the full bandwidth of the incoming beam without the use of a monochromator. For this study, we utilized white beam filtered with aluminum and tin to create a quasi-monochromatic 'pink' beam source. As a pilot, new samples for this study were scanned at the APS and subsequently scanned at BMIT to determine the accuracy of lacunae density counts off the pink beam setup. $2mm^2$ blocks from 6 autopsy derived specimens of women aged 20-81 years were prepared from the anterior region of the proximal femoral shaft, with the same 6 samples being scanned at each facility. The number of samples studied was restricted to 6 due to BMIT beam time restrictions. These blocks were SR micro-CT imaged at the APS with a photon energy of 27.9keV and an effective pixel size of 1.47μm. 1500 frames spanning 180 degrees of rotation were collected with an exposure time of 250 milliseconds per frame, resulting in a scan time of ~17 minutes. The BMIT pink beam setup employed filters of aluminum (6

mm) and tin (0.5 mm) to generate a peak of x-rays in the 25-29 keV energy range with an effective pixel size of 2.08µm. An exposure time of 1 second per frame and two-frame averaging was employed for each of the 1800 frames spanning 180 degrees of rotation resulting in a scan time of approximately 80 minutes. A cylindrical 1.65mm^3 region of interest was analyzed for osteocyte lacunae parameters for each specimen as described above. Statistical comparison of the two techniques was conducted as outline above (section *3.2.5).*

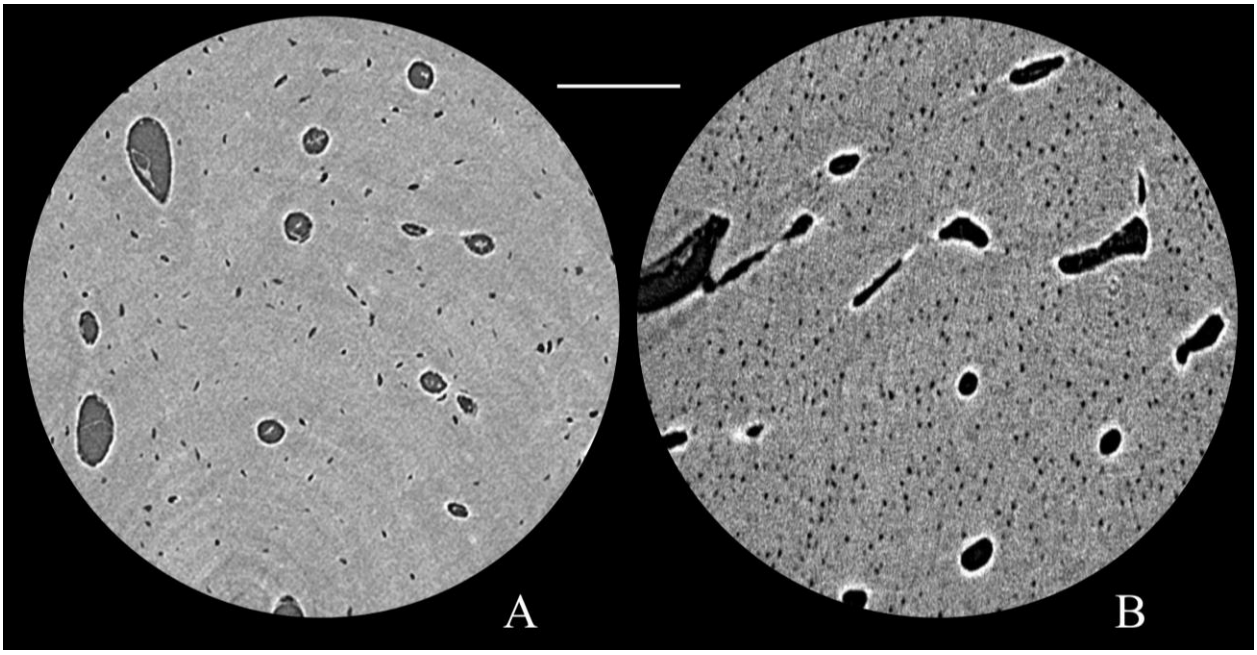

Figure 3.5 Unmatched single slice of circular region of interest within a human femoral specimen reconstructed from the micro-CT scans comparing resolution and noise. APS 1.47µm pixel size (A) and CLS 2µm pixel size utilizing pink beam (B). Note the sphericity of the lacunae in the CLS scan due to resolution limitations. Scale bar = 150µm.

3.3.3 Results

Results showed that compared to APS scans, the BMIT setup accounted for 94.6% of the osteocyte lacunae, but was unable to measure volume or shape parameters. The average osteocyte lacunar densities from the APS and BMIT micro-CT setups were found to be 23662 ±2690 and 22337 ±2567 per mm^3 respectively. Figure 3.6 shows the Bland–Altman plot for lacunar density. The mean difference (bias) between the two setups was 1324 ±1687;

additionally high variation in scan quality was evident with the lowest BMIT scans recording only 82% of lacunae, and one scan over-counting. A paired *t*-test revealed the results from the BMIT 'pink beam' count was not significantly different from those obtained by the APS SR micro-CT setup (p= 0.113). Attempts to measure lacunar parameters beyond abundance, including morphology and orientation failed on the BMIT data.

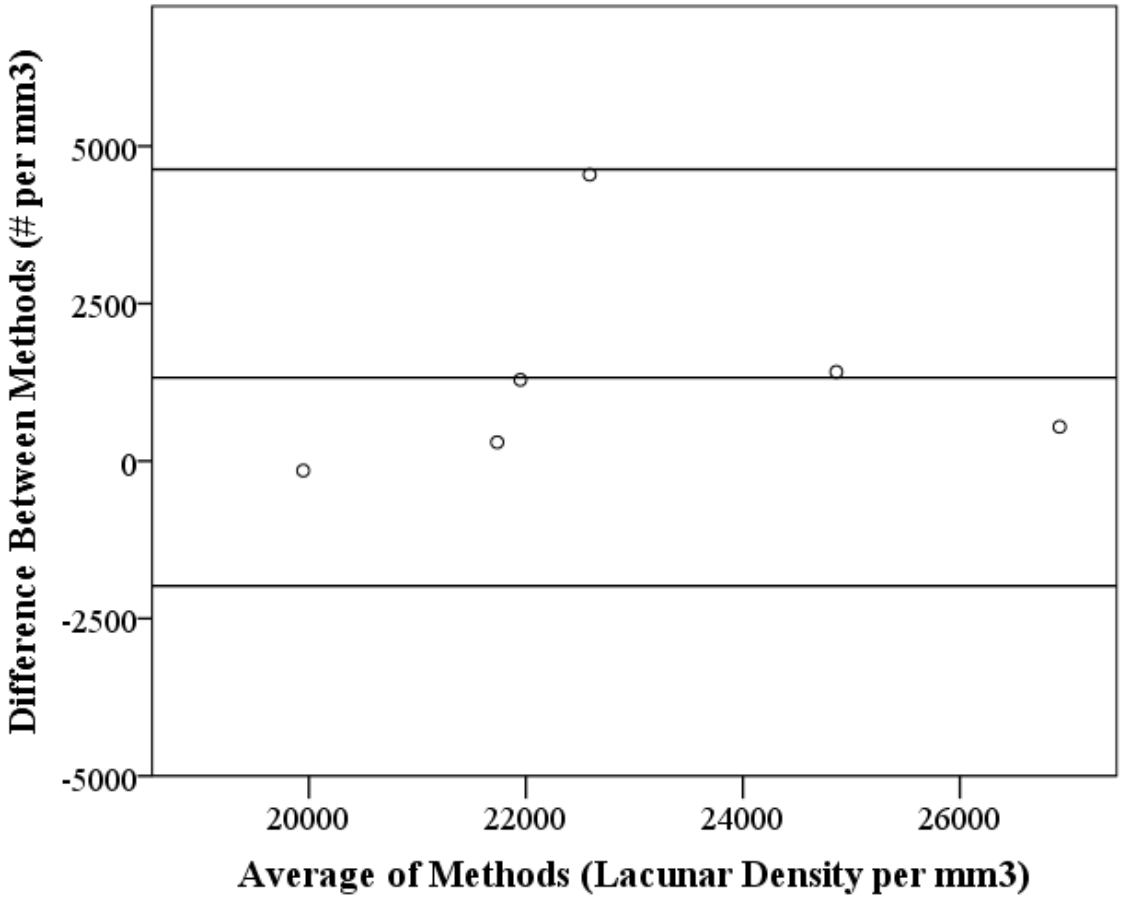

Figure 3.6 Bland-Altman plot of the differences between APS and BMIT SR micro-CT for measuring osteocyte lacunar density in human cortical bone.

3.3.4 Future Directions for BMIT

A new system custom built by SkyScan with a submicron voxel size was commissioned at BMIT in 2012/2013; preliminary scans suggested that, in combination with the pink beam, it may afford the opportunity to achieve human lacunar geometric analysis of density and morphology (Fig. 3.7). Additionally the BMIT beamline is currently commissioning a new, more powerful insertion device ID line. This beamline will have higher flux and allow for shorter scan times with higher signal-to-noise ratios than currently possible at the Canadian Light Source.

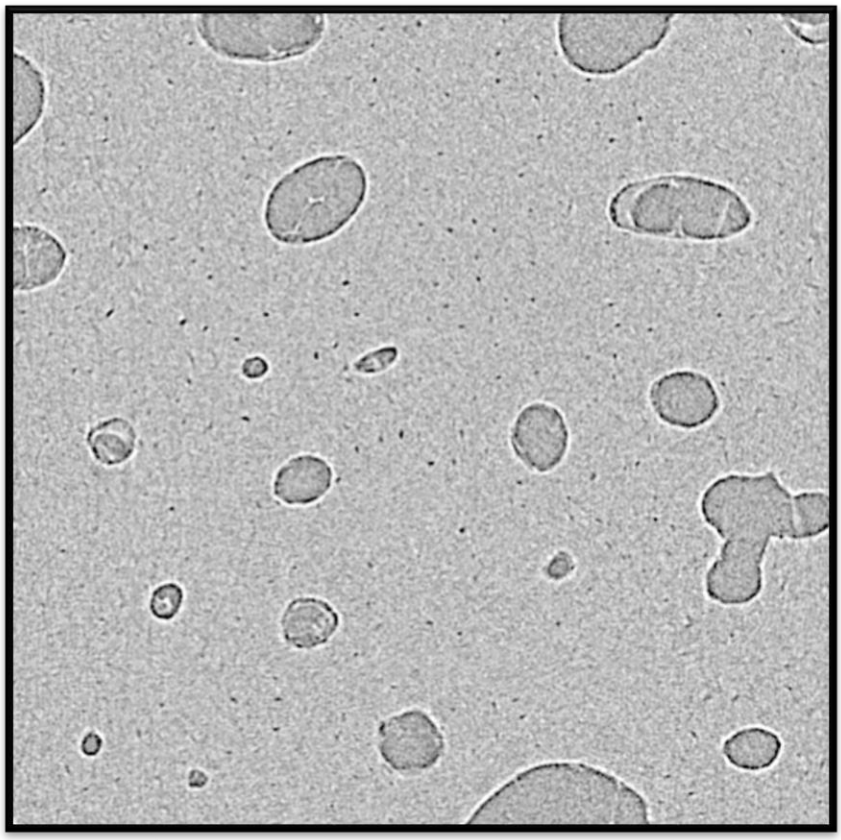

Figure 3.7 Single slice of cortical bone, reconstructed from the SkyScan BMIT micro-CT setup 1.44um resolution.

3.4 Conclusion

The unsuccessful results of the multiple attempts to replicate the quality of the preliminary APS scans on the SkyScan 1172 Desktop micro-CT system and at BMIT necessitated that all scanning required for this thesis was performed at the APS, Argonne

National Laboratory, Il, USA. Due to higher flux, scans acquired at the APS were shorter in duration, with higher signal-to-noise ratios and allowed for quantification of lacunar morphological parameters in addition to density, as required for the previously outlined hypotheses.

CHAPTER 4: VARIATION IN OSTEOCYTE LACUNAR MORPHOLOGY AND DENSITY IN THE HUMAN FEMUR — A SYNCHROTRON RADIATION MICRO-CT STUDY

This chapter has previously been published as: Carter Y, Thomas CD, Clement JG, Peele AG, Hannah K, and Cooper DM. Variation in osteocyte lacunar morphology and density in the human femur--a synchrotron radiation micro-CT study. *BONE* 2013;52: 126-32.

4.1 Introduction

The basic microstructural components of bone, including Haversian systems and the lacuno-canalicular network, exist in a similar form among vertebrates [1] suggesting a strong adaptive relevance; however, a complete understanding of this system remains elusive. Osteocytes are believed to be the primary mechanosensing cells of bone and thus there is great interest in how their shape and density, as reflected by their lacunae, may be related to aging, adaptation and disease. Osteocytes, the most abundant bone cells, are derived from osteoblasts that become trapped within the bone matrix as it forms, occupying spaces known as lacunae. Preservation and visualization of the cells themselves using conventional histological processing methods is difficult; therefore the lacuna is often used as a proxy [63]. While osteocytes can potentially change the morphology of a lacuna over time [138], the spatial density of lacunae is likely more stable. For example, due to the mineralized nature of bone matrix, the local number of lacunae cannot increase unless the bone is remodeled. That said, early work by Frost [68] demonstrated that lacunae may infill with age, a process termed 'micropetrosis' resulting in a small decline in lacunar density. As such, these two parameters (shape and density) potentially reflect conditions from differing temporal scales.

4.1.1 Variation in Osteocyte Lacunar Density

Variation in osteocyte density has been linked to bone adaptation, disease, and age [45, 63, 73] with contradictory results (see, for example, the excellent discussion by Skedros et al. [1]). Lacunar morphology has not been widely studied, although differences in lacunar properties of murine bone have been linked with functional adaptation. In mice, Vatsa and colleagues [7] found osteocyte lacunae in the fibula, an element experiencing uni-directional loading, were elongated relative to those of the cranial vault, a region undergoing multi-directional loading. A

similar study by van Hove *et al.*, comparing human bone samples afflicted with differing diseases [24], found osteopenic bone had relatively large and round lacunae while osteoarthritic bone had relatively large and elongated lacunae. Conversely osteopetrotic bone had small discoid lacuna. In both of these morphologic studies the authors linked the results to adaptation of the bone matrix due to different external loading conditions.

4.1.2 Previous Imaging Techniques

A limitation common to nearly all studies of osteocyte density and shape is restricted sampling as a consequence of the techniques available. The use of conventional histology, confocal microscopy and Scanning or Back-Scattered Electron Imaging [22, 47, 52, 88] allows for only 2D or limited 3D lacunar analyses. The 3D nature of bone's microstructural network makes using a 3D technique preferable – particularly when considering lacunar shape. Laboratory or 'desktop' micro-CT systems have been used extensively to examine 3D bone microarchitecture spanning from trabeculae to cortical vasculature [9, 122-124]. The resolution of most systems; however, is in the range of 8-10 microns [125] making the cellular-level structure of bone inaccessible [126]. Micro-CT systems with submicron resolutions are now available but they too have only seen limited application to lacunar imaging [17, 24].

4.1.3 Application of SR Micro-CT for Imaging Human Cortical Bone

An alternative approach is the use of Synchrotron Radiation (SR) micro-CT. Synchrotron radiation offers a number of enhancements over conventional x-ray tubes including high spatial resolution and brilliance, small beam divergence and monochromaticity [108]. SR micro-CT can be considered the gold-standard in 3D bone imaging [125], producing faster and more accurate quantitative measurements than a similar desktop x-ray system [129]. All x-ray based techniques are limited in that they can visualize the lacunae but not the osteocytes themselves so it is not yet possible to distinguish between occupied and unoccupied lacunae.

4.1.4 Study Objectives

We propose that advantages in the scale of 3D sampling of osteocyte lacunar density and quantification of morphology are needed to better elucidate the functional significance of these parameters. Critically, more work is needed to characterize normal variation– to serve as a foundation for better understanding alterations induced by pathological and adaptive processes. As such, the purpose of this study was to characterize regional variation in lacunar density and

morphology about the proximal diaphysis of femoral samples derived from a young male with no history of disease. SR micro-CT was employed to enable a scale of analysis not previously reported– direct counts and measures of tens of thousands of lacunae, without destruction of the sample.

4.2 Materials and Methods

4.2.1 Specimens

Cortical bone samples were obtained from the femur of a 20 year-old male who had no known conditions that may have affected his bones. The femur forms part of the Melbourne Femur Collection held at the University of Melbourne, Melbourne, Australia and was collected with the informed consent of the donor's next-of-kin. The study was conducted with ethical approval from the Victorian Institute of Forensic Medicine (EC26/2000), the University of Melbourne (HREC 980139) and the University of Saskatchewan (Bio # 08-46). Individual samples with dimensions of approximately 2 x 2 x 35 mm were cut from four regions of the proximal femoral shaft and an adjacent section. Thirteen of these 'match-stick' sized samples were examined for this paper. Three were taken from the anterior, three from the posterior, three from the medial and four from the lateral aspect of the bone (Fig. 3.1). The femoral shaft represents an ideal site of analysis as it is has been the subject of extensive investigation including regional variation in porosity [139] and material density [140]. This area is habitually loaded in bending during common activity such as walking; this bending pattern leads to compression in the medial region and tension laterally [141].

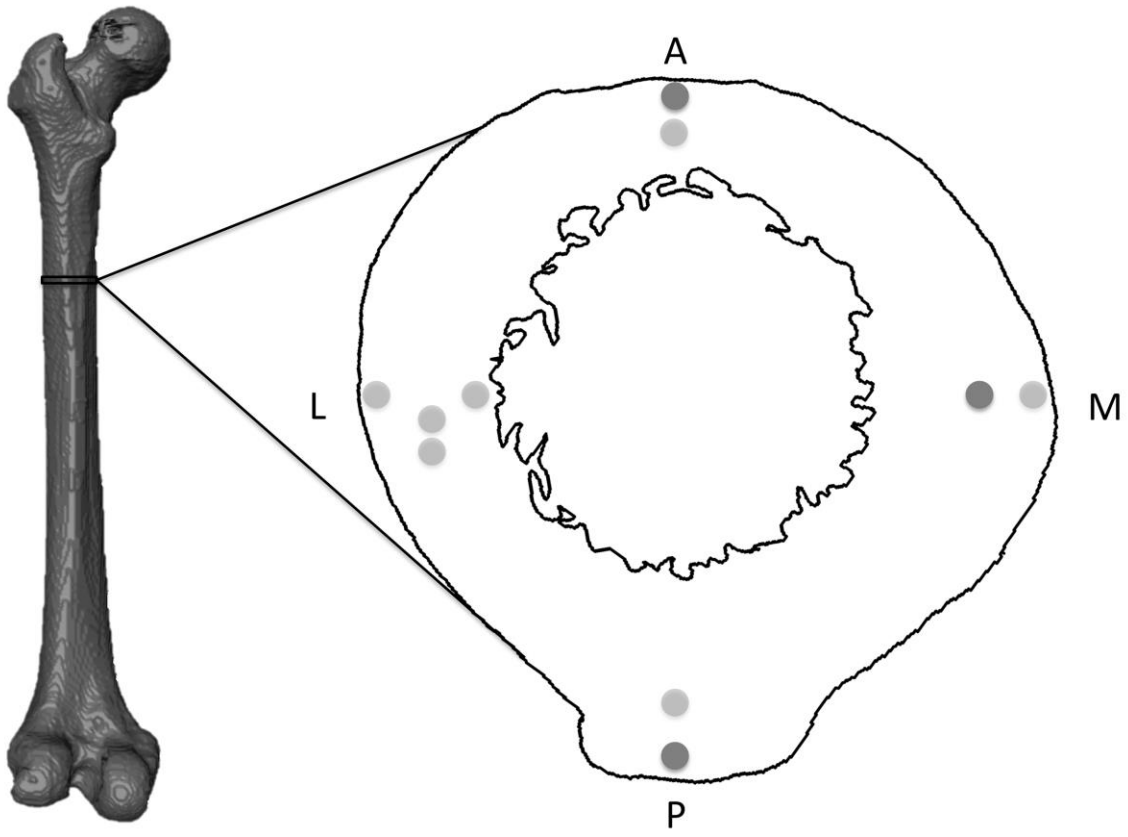

Figure 4.1 Locations of cylindrical regions of interest. Light grey circles represent samples cut from the distal block, dark grey circles represent one sample from each of the proximal and distal blocks.

4.2.2 Synchrotron Radiation Micro-computed Tomographic Imaging (SR Micro-CT)

Synchrotron radiation micro-CT scanning was conducted at the Advanced Photon Source (APS), Argonne National Laboratory on beamline 2BM. Images were obtained using monochromatic x-rays with a photon energy of 26.4keV and an effective pixel size of 1.47μm as described previously by Hannah and colleagues [19]. An exposure time of 120 milliseconds per frame and four-frame averaging was employed for each of the 1140 frames spanning 180 degrees of rotation resulting in a scan time of approximately 22 minutes. This is the same imaging protocol used in Chapter 3. The projection images were reconstructed to create a dataset

containing 1280 slices (2048×2048 pixels). Image stacks were cropped and quantified using CT Analyzer 1.10.9.0 (SkyScan software). A cylindrical region of interest (ROI) with a diameter and height of 1 mm and a volume of 0.786 mm^3 was defined within each specimen (Fig. 3.2.A). Lacunae and canals within these ROI's were identified using a standardized global threshold, which separated the higher density bone from the air-filled lacunar and canal spaces; the same threshold was used for all specimens. Following segmentation, 'despeckling' was conducted of elements less than 10 μm^3, which were assumed to be noise, and elements above 2000 μm^3, which were assumed to be canals, the rest were assumed to be lacunae. These volume limits were based on confocal microscopy measurements of osteocyte volumes which found them to be between 500 – 1300 μm^3 [90]. Lacunar abundance (density) (N.Lc/BV) and volume (Lc.V) as well as average canal diameter (Ca.Dm) were calculated using individual object analysis, which calculates the 3D parameters of each discreet object within the volume of interest after segmentation. Subsequently, 3D renders of the lacunae and bone microstructure were created. Canal diameter [97] was calculated, using CT Analyzer 1.10.9.0, to account for possible effects of vascular porosity on lacunar properties. Shape analysis of the lacunae was conducted utilizing AMIRA 5.4.1 (Visage Imaging, Fuerth Germany). Ellipsoids were fitted to each individual object and filtered for size to remove canals and noise from the analysis as previously described (Fig. 3.2.B); from these, shape parameters were then computed for each ellipsoid based upon the resulting three eigenvalues (EV). The **orientation** (Lc.Φ) of each lacuna was measured as the absolute value of the angular deviation (-90º to 90º) of the axis of the first EV (longest lacunar axis) from the horizontal axis of the sample. An orientation value of 0º represents a transverse (radial or circumferential) orientation and values approaching 90º are increasingly in longitudinal orientation. To describe the shape of the lacunae, three ratios of the eigenvalues were modified from studies of particle shape [142] in order to define the degree of difference. Figure 4.3 demonstrates the importance of all three ratios in describing shape differences. The **Degree of Equancy** (Lc.Eq)(converse of 'degree of anisotropy' in AMIRA 5.4.1) was calculated as the

ratio of the third (shortest) to the first (longest) EV (EV3:EV1)[1]. **Degree of Elongation** (Lc.El) for each lacuna was calculated by one minus the ratio of the second (intermediate) and the first EV (1- EV2:EV1). **Degree of Flatness** (Lc.Fl) was calculated as one minus the ratio of the third and second EV (1- EV3:EV2).

[1] An error in the original publication had this as "The Degree of Equancy ('degree of anisotropy' in AMIRA 5.4.1) was calculated as one minus the ratio of the third (shortest) to the first (longest) EV (1−EV3:EV1)". A correction was published under Y. Carter *et al.* (2013) Corrigendum to "Variation in osteocyte lacunar morphology and density in the human femur — a synchrotron radiation micro-CT study [Bone 52:126–132]'.

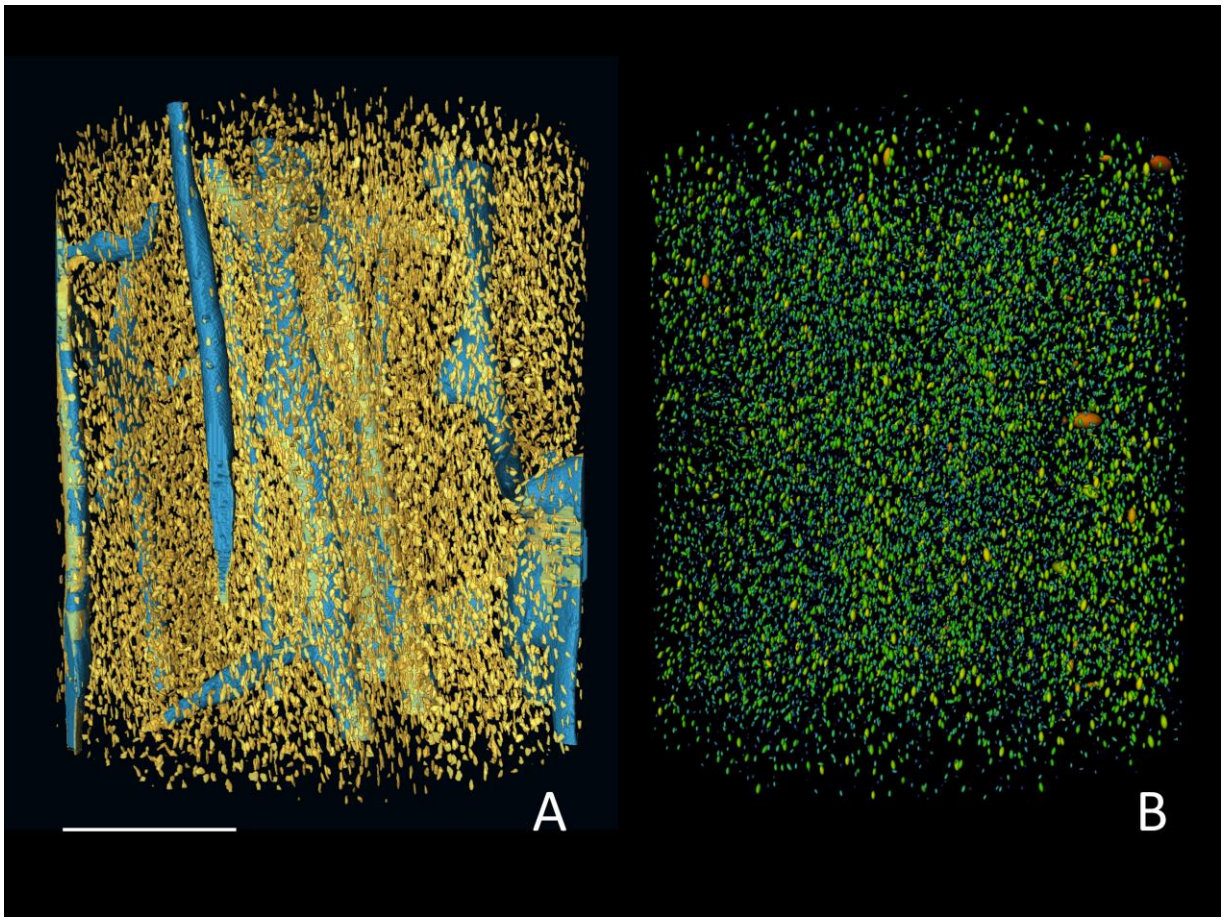

Figure 4.2 A. 3D render of single anterior region of interest 1 x 1 mm showing 19,140 lacunae in gold with the vascular canals in blue. B. Same region of interest with ellipse fit colored for the degree of equancy with red being most equant and blue least. Scale bar = 300 um.

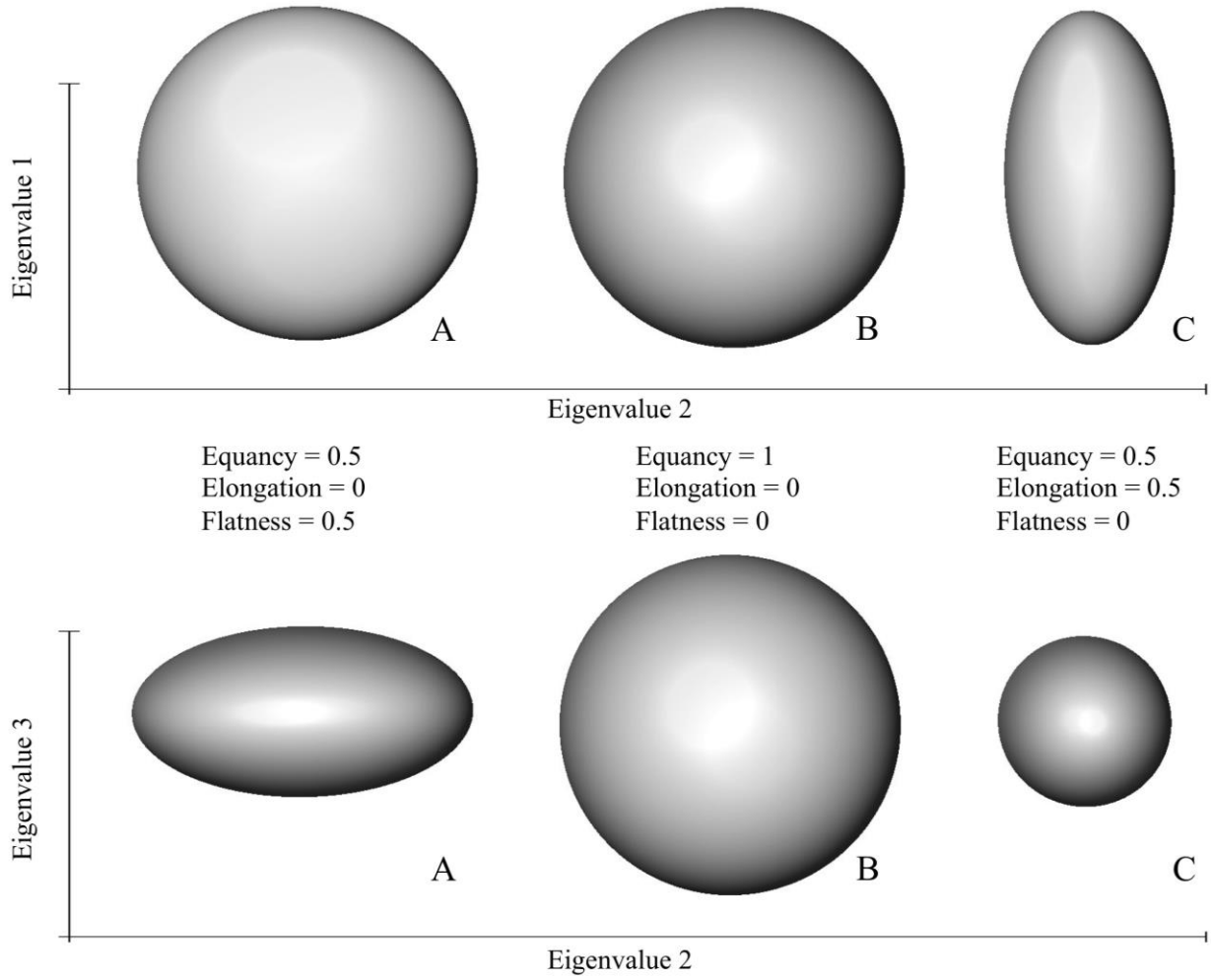

Figure 4.3 Representative examples of ellipsoid shapes. The center ellipsoid (B) has an equancy of 1 with all three eigenvalues being equal (EV1=EV2=EV3) creating a spherical shape. The ellipsoid on the left (A) is flatter with its first two eigenvalues being equal and the third being smaller (EV1=EV2>EV3) resulting in a discoid shape. The ellipsoid on the right (C) is more elongate in shape with the first eigenvalue exceeding the second and third which are equal (EV1>EV2=EV3).

4.2.3 Statistical Analyses

Statistical analysis was performed using SPSS 16.0 (SPSS Inc., Chicago, IL, U.S.A.). Values for lacunae density per mm^3, volume, orientation and shape parameters were averaged from each sample and these results were then grouped according to region (anterior, posterior, medial and lateral). Average canal diameter for each region was compared and used as a covariate (ANCOVA) to determine if there was a relationship with the density values. Since no significance was found, Analysis of Variance (ANOVA) with post-hoc Bonferroni adjustment were performed with significance $\alpha < 0.05$ to compare the regions.

4.3 Results

The density and morphological results are summarized in Table 4.1. Average lacunar density values were different between the medial and both the anterior and posterior regions (p=0.001) (Fig. 4.4). The density of the combined anterior and posterior regions was also lower (p=0.001) than the combined density of the medial and lateral regions. There were no differences between mean lacunar volumes (p=0.862); nor were there differences in average canal diameter for each region (p=0.815). No differences were apparent in either lacunar orientation or equancy. The anterior and posterior regions had more elongated (p=0.004) and flattened (p=0.045) lacunae, than those of the medial and lateral regions. Average EV1 was significantly different between the posterior and lateral regions (p=0.045). There were no differences in either EV2 or EV3 for each region. The mean EV1 of the combined anterior and posterior regions was also higher (p=0.004) than the combined value of the medial and lateral regions. The mean EV2 of the combined anterior and posterior regions was also lower (p=0.045) than the combined value of the medial and lateral regions. There were no differences (p=0.181) between mean combined EV3 (Fig. 4.5).

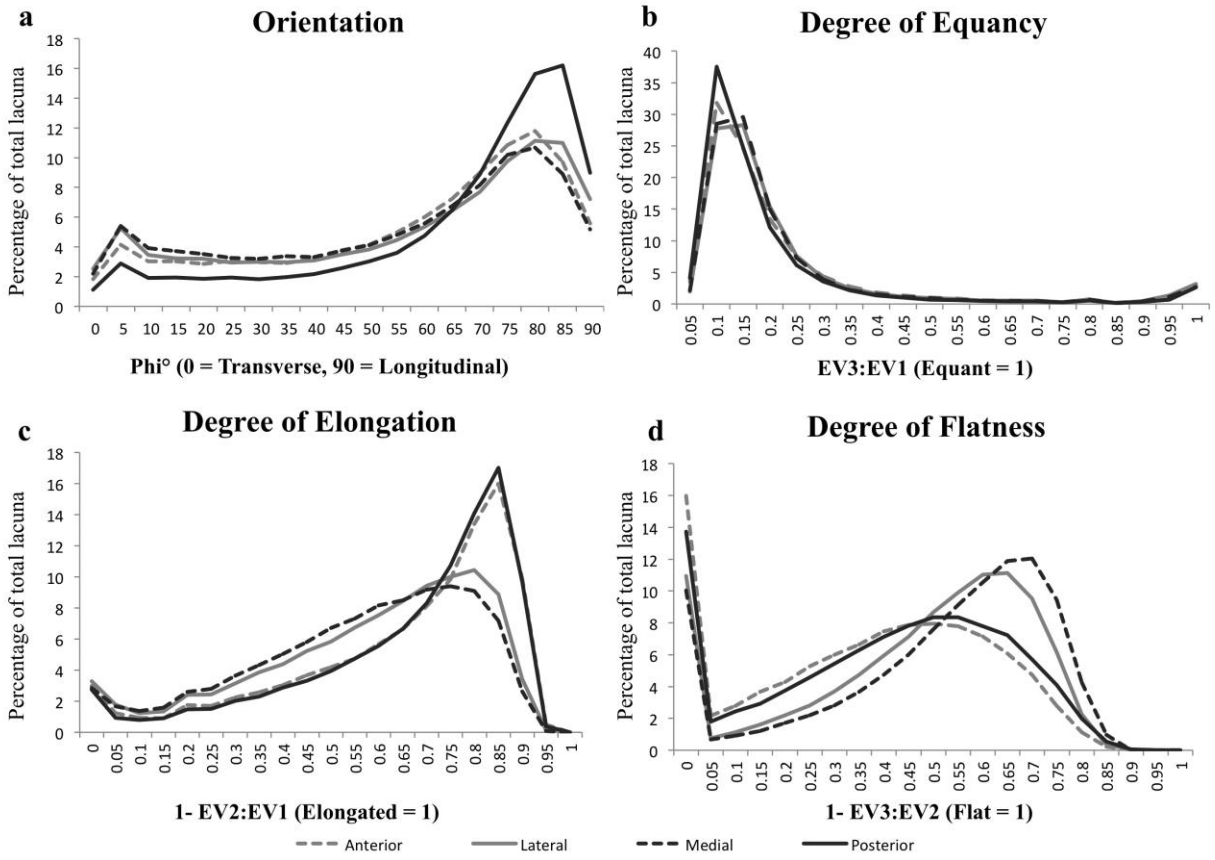

Figure 4.4 Line graphs representing percentage of total lacunar density average for each region and angle of orientation with respect to the horizontal axis of the bone (a), and degree of equancy (b), and degree of elongation (c), and degree of flatness (d). EV1, eigenvalue 1; EV2, eigenvalue 2; EV3, eigenvalue 3. The spike at 1 in the flatness measurement represents the resolution limitation of the technique where eigenvalue 1 and eigenvalue 3 equal one voxel.

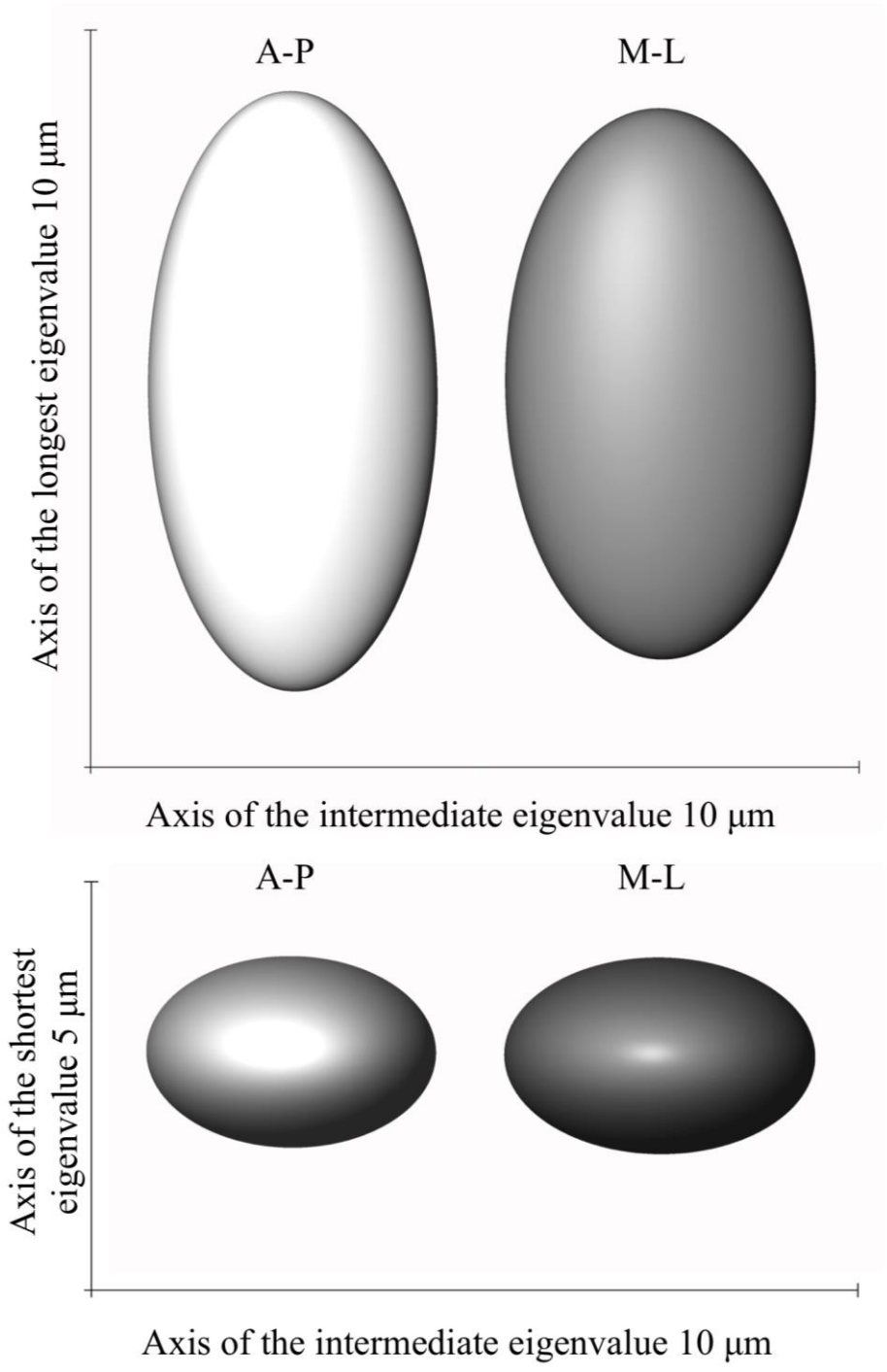

Figure 4.5 3D model of the average shape for the combined anterior-posterior versus the medial-lateral regions.

Table 4.1 Averages of the morphological parameters of osteocyte lacunae from multiple regions of the human femoral proximal shaft. *p<0.05 versus both anterior and posterior regions. ^{Ŧ}p<0.05 versus lateral region. $^{\#}p$<0.05 versus combined medial and lateral regions. N/B: Abbreviations are included for consistency and clarity, although not original to the publication they were used subsequently.

Region	*n*	Lacunar Density (N.Lc/BV) (mm^{-3} ± sd)	Lacunar Volume (Lc.V) (μm^3 ± sd)	Canal Diameter (Ca.Dm) (µm ± sd)	Orientation (Lc.Φ) (° ± sd)	Equancy (Lc.Eq) (± sd)	Elongation (Lc.El) (± sd)	Flatness (Lc.Fl) (± sd)	EV 1 (± sd)	EV 2 (± sd)	EV 3 (± sd)
Anterior	3	27,169 ±1,935	378 ±50	43.61 ±8.73	54.96 ±3.98	0.18 ±0.02	0.77 ±0.02	0.54 ±0.01	16.12 ±0.93	3.74 ±0.33	1.71 ±0.68
Posterior	3	26,343 ±1,262	400 ±32	29.19 ±3.77	62.65 ±1.80	0.15 ±0.01	0.77 ±0.03	0.57 ±0.01	17.37 ±1.26^{Ŧ}	3.99 ±0.91	1.70 ±0.43
Medial	3	37,521 ±6,416*	409 ±45	36.71 ±4.42	52.00 ±5.49	0.20 ±0.02	0.67 ±0.02	0.62 ±0.02	14.17 ±0.78	4.68 ±0.48	1.78 ±0.16
Lateral	4	33,972 ±2,513	408 ±66	39.17 ±9.61	53.99 ±4.12	0.21 ±0.05	0.69 ±0.03	0.58 ±0.01	14.10 ±1.83	4.29 ±0.68	1.80 ±0.16
Combined Ant + Post	6	26,756 ±1,529$^{\#}$	389 ±40	36.40 ±9.92	58.81 ±5.04	0.17 ±0.18	0.77 ±0.4$^{\#}$	0.56 ±0.03$^{\#}$	16.75 ±1.21$^{\#}$	3.87 ±0.26$^{\#}$	1.70 ±0.51
Combined Med + Lat	7	35,493 ±4,525	408 ±53	38.12 ±7.38	53.13 ±4.43	0.21 ±0.04	0.68 ±0.07	0.60 ±0.02	14.13 ±1.37	4.46 ±0.59	1.78 ±0.14

4.4 Discussion

To our knowledge this paper represents the first examination of variation in lacunar density and morphology in 3D between regions of a single cross-section of an individual human skeletal element. The use of synchrotron radiation-based micro-CT enabled a scale of analysis not previously reported and revealed significant variation in lacunar density and shape.

Quantification of lacunar density and shape parameters has traditionally been conducted using 2D histologic techniques, coupled with bright-field, phase contrast or epiflorescence microscopy [21, 53, 57, 63, 65, 69, 73, 82, 83]. More recent developments have enabled the collection of 3D data using conventional techniques. Confocal microscopy, for example, allows for a change in the depth of the focal plane resulting in a stack of 2D images, which are then stitched together to form a 3D data volume [39]. Confocal Laser Scanning Microscopy (CLSM) [17, 24] and Scanning or Back-Scattered Electron Imaging [22, 47, 52, 88, 89] have been used to improve resolution limits and examine the nanostructure of osteocytes and their lacunae. The major disadvantage of these approaches is that they are either essentially 2D or have a limited penetration depth. These techniques have been successful at quantifying osteocyte lacunar density. The methodology used in this study; however, has additional benefits, including limiting destruction of the samples, analysis of larger volumes of interest, and concurrent quantification of morphological parameters. Comprehensive studies of lacunar density and morphology require sufficient numbers to be counted which in turn requires a larger volume of interest. This paper demonstrates the usefulness of SR micro-CT not only in determining lacunar density but also shape and orientation parameters.

Studies of lacunar density in bone have mostly been restricted to counts acquired in the pursuit of primary hypotheses regarding disease, aging and biomechanics. The majority of those studies that have produced values for lacunar densities have extrapolated from a small 2D count to a high number per millimeter^3 creating the potential for a large margin of error. For example, Bromage *et al.* [86] determined a lacunar density of 23,333 mm^{-3} for the *Australopithecus afarensis* specimen known as “Lucy” extrapolated from an original count of 63 lacunae. The range of values for lacunar density recorded in normal human bone is high and largely dependent on location, tissue type and analytical technique. Sissons *et al.* [14] found human cortical bone to

have between 13,900 and 19,400 lacunae mm^{-3} depending on the sectioning technique used. Hobdell and Howe [15] recorded lacunar densities of 13,000 mm^{-3} using traditional histology techniques for cancellous bone. Conversions of previous studies' area counts (mm^{-2}) to volume counts (mm^{-3}) conducted by Metz *et al*. [16] found an average of 46,400 mm^{-3} for women of various ages and 70,000 mm^{-3} for elderly women. The large differences in density were attributed to inter-element and individual changes. The total lacunar densities reported in the current study, ~26,000 to 37,000 mm^{-3} are high compared to the results of earlier studies [14, 15] but agree well with those values of reported in Metz *et al.* [16]. This difference is likely related to the improved sampling of the 3D method we utilized, allowing a larger region of interest to be examined and much larger numbers of lacunae to be counted rather than the earlier reliance on extrapolation from small 2D counts.

Currently intra-element analyses of human cortical lacunar density have been restricted to two studies with differing results. Power *et al.* [143] reported significant variation in regional lacunar density of the femoral neck between and within hip-fractured and control elderly women. The inferior region showed more lacunae than the superior, however this was a 2D study analyzing only around 500 lacunae mm^{-2}. In contrast, Jordan *et al.* [144] reported no intra-element femoral neck differences in lacunar density in men or women both with and without osteoporotic fracture or osteoarthritis. Studies of trabecular bone [53, 63, 65] determined significant differences exist between superficial trabecular (<25 μm from the surface) and deep trabecular bone (>45 μm) of the iliac crest, with superficial bone containing higher densities of osteocytes.

The regional variation within the femoral cortex we observed was high, with the anterior and posterior having the least lacunae and the medial and lateral having the most. The medial sample contained 26.7% more lacunae per mm^3 than the anterior and 29.8% more than the posterior (Fig. 4.4). Ultimately, the likely cause of this variation in osteocyte lacunar density is the mechanical environment during formation (primary growth and/or secondary remodeling); however, the proximate causes remain unclear. Possible mechanisms for this intra-element variation in density include differences in the formation rates across the diaphysis [67], differential remodeling of these areas [65] and differences in the local strain environment [17]. Micropetrosis, another possible source of variation in density, is more likely to be a significant

factor in senescent or diseased bone [68], and not in a young individual such as the one used in this study.

The greatest source of stress on the proximal femoral shaft comes from bending; however, experimental strain gauge studies have demonstrated that strains in the anterior and posterior regions are substantially less than those of the medial and lateral [145]. When experiencing forces from bending due to motions such as walking or single leg stances, a neutral axis exists which passes through the center of gravity where there is no tensile or compressive stress. This axis is along the sagittal plane of the femur in an anteroposterior direction [146]; however, it has been demonstrated that this region experiences a strain environment with the peak tensile and compressive strains occurring close to the medial and lateral aspects of the neutral axis [147]. Further research is required to determine whether the patterns observed in this study are related to the reduced strain directly associated with the neutral axis or with the strain gradients associated with the outer neutral zones. Thomas and colleagues [139] observed increased vascular porosity in the anterolateral and posterior regions that became more pronounced with age. We report a decrease in lacunar density across these areas. Thomas and colleagues' observed pattern was consistent with progressive bone loss occurring along the neutral axis of the cortex where loading stress is at its lowest and our study demonstrates lower lacunar density in the same region. The significance of a reduced density to mechanotransduction and initiation of remodeling and repair remains unclear; however, the potential links between these two results are intriguing and require further study. Calcanei from a number of cloven-hoof species and horses demonstrate significantly increased lacunar densities in areas of the cortex under compression compared to those under tension [148, 149]. Equine third metacarpals; however, show decreased lacunar density in compression [1] suggesting that a model based on strain mode is insufficient to explain the high variation demonstrated in this study. It has been suggested that regional variations in mean lacuna volume may reflect differences in habitual loading conditions [17, 22]. If this hypothesis is correct then differences in lacunar volume should be evident within regions of cortical bone in the same bone but exposed to differing loads; however, this study found similar lacunar volumes in all regions.

It is widely reported that lacunar density declines with age in males and females [57, 64-66], the rate of this decline; however, is still debated. The state of lacunae populations in

osteoporosis is an area of interest for researchers but results have been inconclusive to date. A number of studies report lacunar density to be increased in women with osteoporosis ranging from 15-30% [58, 64, 73]. In contrast to this, a more recent study by Mullender *et al.* [45] found reduced lacunar density (~14%) in osteoporotic patients. This later finding is consistent with results by Mori *et al.* [57] and Qiu *et al.* [63] who report an average of 30% lower lacunar densities in patients with a history of osteoporotic fracture. The results of our study indicated that variation in lacunar density, even within a single bone of a single individual, can be considerable, up to 30% between regions. This large site-specific variation in lacunae densities brings into question any ability to extrapolate from those studies above. This, in turn, makes inferences regarding bone disease based on far smaller differences potentially problematic.

Although no strong regional patterns were observed in either the orientation or equancy of lacunar shape, the anterior and posterior regions had significantly more elongated lacunae than those of the medial and lateral regions. The anterior and posterior regions also had significantly more flattened lacunae (Fig. 4.5). Conversely, a 3D study of unidirectional versus multi-directional loaded murine bone [17] found more elongated lacunae in the more unidirectionally loaded fibula than compared to the calvarium. Our seemingly contrary finding of more elongate and flattened lacunae in the area of the neutral axis suggest that correlation between shape and functional mechanics may be more complex than initially expected. Osteocyte orientation has been demonstrated to change with differing collagen fiber orientation within specific osteonal morphotypes [83, 89]. It is possible that inter-osteon differences in osteocyte lacunae shape parameters would be obscured in a large-scale analysis such as this; however, the techniques described here could be used to test hypotheses focused on variations in specific subsets of bone. The scale of analyses supported by the techniques applied here will enable tens of thousands of lacunae able to be analyzed for shape differences. This will allow many of the current hypotheses regarding changes in lacunar parameters related to biomechanics to be investigated further.

Clearly the current study is limited by its focus on a single individual. Despite this limitation, this research highlights the possible variances in lacunae populations within human cortical bone, an area of research currently experiencing a resurgence due to increasing access to emerging high-resolution imaging modalities. The underlying functional significance of the observed variation in lacunar density and morphology likely relates to localized variations in the

loading environment. Patterns in both the density and morphology of the lacunae coincide with the approximated axes of mechanical loading, with lower lacunar densities being observed along the neutral axis, an area of reduced strain. Our findings demonstrate that current functional and pathological interpretations, which are increasingly being drawn from high resolution imaging of lacunae [17, 24], need to be better situated within the broader context of baseline variation, including that which occurs within a single skeletal element. Further exploration of the variations in lacunar density and their interactions with aspects of bone material and structure, using a larger sample representing the adult life span, will allow for a better understanding of the relation of osteocyte populations to bone's biomechanical properties and adaptation.

4.5 Conclusion

This chapter has outlined the importance of normal variation, serving as a foundation for a more complete understanding of alterations induced by pathological and adaptive processes. Additionally this research provides a novel method of visualizing and quantification of lacunar density and shape parameters. The finding of high variation in osteocyte lacunar density (up to 30%) between anatomical regions with associated lacunar shape change is intriguing and requires further analysis to determine whether this exists as a part of normal variation. The next chapter of this thesis looks at this intra-element variation in a larger sample of healthy young individuals. Chapters 6 and 7 apply this technique to the quantification of osteocyte lacunae in men and women over the human lifespan.

CHAPTER 5: NORMAL VARIATION IN CORTICAL OSTEOCYTE LACUNAR PARAMETERS IN HEALTHY YOUNG MALES

This chapter is published as: Carter Y, Suchorab JL, Thomas CDL, Clement JG, and Cooper DML. Normal Variation in Cortical Osteocyte Lacunar Parameters in Healthy Young Males. *Journal of Anatomy*. 225(3); 328-36

5.1 Introduction

Osteocytes are the most abundant cell in bone; they become individually enveloped by the extracellular matrix during bone production within spaces known as lacunae. These cells and their lacunae form an interconnected system upon which the regulation of normal healthy bone relies [150]. Although the complete nature of the role of osteocytes has yet to be defined they are generally accepted to play a part in the sensing of load and the initiation of damage repair. Once bone reaches maturity, the twinned processes of bone formation and bone removal are kept in delicate balance by the information supplied to and through the osteocyte lacunar network. Acting as mechanosensors and transducers, biological input is interpreted and disseminated by a healthy and regular network [26]. As the cells themselves are difficult to study *in situ* in sufficient quantities, their lacunae are commonly used as substitutes. Although all lacunae contain a viable osteocyte during formation, the degree of occupancy can decline over time through cell death. That said, the percentage of empty cellular spaces is very low in the young and healthy [151] and thus the number of lacunae should be a close reflection of the number of osteocytes present within young bone.

A number of studies have focused on differences in osteocyte lacunar density with regard to age, loading and disease with contradictory results [1, 17, 24, 45, 53, 64, 65, 73, 126, 152-156]; however, very little is known regarding normal variation in human osteocyte lacunar density and morphology. The variation in the range of lacunar abundance values in normal human bone is high and depends on location, tissue type and analytical technique. Commonly referenced as a baseline, Hobdell and Howe, [15] using traditional histology techniques, recorded lacunar densities in human cancellous bone of ~13,000 mm^{-3}. Much higher values were calculated by Metz *et al*. [16], by converting previously published area counts (mm^{-2}) to volume counts (mm^{-3}) and found an average of 46,400 mm^{-3} for women of various ages and 70,000 mm^{-3}

for elderly women. These differences in lacunar density are not related to methodology alone. In Chapter 4 we reported values of 26,000-37,000 mm^{-3} in differing regions of a femoral shaft from a young male [80]. Hannah and colleagues determined within individual osteons of healthy males, osteocyte densities varied from 40,000 mm^{-3} close to the Haversian canals to about 90,000 mm^{-3} at the periphery of the osteon [19]. While the values from these recent studies are high compared to that of earlier studies, this difference is likely related to the improved methodologies and techniques available; however, they do suggestion caution when comparing samples taken from different regions or elements.

The small size of the lacunae and their location deep within the bone matrix has restricted studies characterizing lacunar parameters outside of density. High-resolution imaging techniques can overcome this issue, the gold-standard being synchrotron radiation-based imaging [39, 81, 125, 131, 134, 157]. Measures of lacunar shape are of particular interest because external application of mechanical forces on cells has been shown to influence cytoskeletal structure and thus cell shape. This implies that the shape and long axes of osteocytes, and therefore their lacunae, should align parallel to the principal mechanical loading direction [43]. It is then possible to extrapolate that differences in osteocyte lacunar morphology may indicate differences in osteocyte mechanical environment at the time of their burial from an actively growing bone surface. Studies of uni-directional versus multi-directional loaded murine bone support this with the finding of elongated lacunae in the more unidirectionally loaded fibula than calvarium [17]. A study of women over the age span showed a tendency towards smaller more spherical lacunae with age and a presumptive reduction in loading [81]. McCreadie *et al*. [23] found no difference in size or shape, limited to measures of anisotropy, in lacunae of older women with and without osteoporotic fracture. Nano-CT studies comparing osteopenic, osteopetrotic and osteoarthritic tibial samples found osteopenic lacunae were relatively large and round while osteopetrotic lacunae were small and discoid shaped, and osteoarthritic were large and elongated [24], although we note this study was restricted by its lack of a control sample.

The study described in Chapter 4 [80] identified high intra-element variation in osteocyte lacunar density of up to 30%. The lacunar density in the combined anterior and posterior regions was significantly lower than that of the combined medial and lateral regions. The anterior and posterior regions were also found to exhibit more elongated and flattened lacunae. We suggested

that the functional significance of the observed variation was related to localized variations in loading conditions [80]. That study; however, was limited to a single individual; therefore the aim of the current study was to determine whether this pattern of intra-element variation in lacunar parameters consistently occurs in a number of individuals of restricted age and sex. Our previous work proposed a differential biomechanical mechanism for the observed differences. If normal differential loading in the cross section of the femora causes variation in the osteocyte lacunae, we would expect to see this pattern recurring in normal individuals.

5.2 Materials and Methods

5.2.1 Specimens

Cortical bone samples were obtained from the femora of 10 deceased men between the ages of 20 and 35, with no known medical conditions that may have affected their bones, only 7 of which made it into the study. These femora form part of the Melbourne Femur Collection held at the University of Melbourne, Melbourne, Australia and were collected at autopsy with the informed consent of the donor's next-of-kin. The study was conducted with ethical approval from the Victorian Institute of Forensic Medicine (EC26/2000), the University of Melbourne (HREC 980139) and the University of Saskatchewan (Bio # 08-46). In order to investigate intra-element variation within the femoral shaft, individual samples with dimensions of approximately 2 x 2 x 5 mm were cut from four mid-cortical regions of a cross-section of the proximal femoral shaft: anterior, posterior, medial and lateral.

5.2.2 Synchrotron Radiation Micro-computed Tomographic Imaging (SR Micro-CT)

SR micro-CT scanning was conducted at the Advanced Photon Source (APS), Argonne National Laboratory on beamline 2BM. Images were obtained using monochromatic x-rays with a photon energy of 27.9keV and an effective pixel size of 1.47μm. An exposure time of 100 milliseconds per frame was employed for each of the 1800 frames spanning 180 degrees of rotation resulting in a scan time of approximately 9 minutes. The projection images were reconstructed to create a dataset containing 1841 slices (2016×900 pixels each). This protocol is different than that used to obtain the images in Chapters 3 and 4, due to a change in the setup available at the beamline. While the energy is similar a shorter exposure time and a continuous

rotating frame collection allowed for a shorter scan duration with only a small reduction in scan height.

5.3.3 3D Quantitative Morphometry

A cylindrical region of interest (ROI) was defined within each specimen, with a diameter of 1.0 mm and height of 1.25 mm (volume = 0.98 mm^3). As per our previous protocol outlined in Chapter 4, [80] lacunae and canals within the ROI were segmented using a standardized global threshold, which separated the higher density bone from the low-density air-filled canal and lacunar spaces, the same threshold was used for all specimens. Following this, based on confocal microscopy measurements of osteocyte volume [23], elements less than 10 μm^3 were assumed to be noise and removed, and elements above 2000 μm^3 were assumed to be canals. All remaining elements were analyzed as lacunae.

SR micro-CT image stacks were cropped and analysis of the canals was conducted with CT Analyzer 1.10.9.0 (SkyScan, Kontich, Belgium), while AMIRA 5.4.1 (Visage Imaging, Fuerth Germany) was used for analysis of the lacunae. Standard nomenclatures for canal [97] and lacunar [80, 126] indices measured included: total ROI volume (TV), total canal volume for ROI (Ca.V), Average canal diameter (Ca.Dm), total number of lacunae (N.Lc) and lacunar volume (Lc.V). In order to determine lacunar density per mm^3 (N.Lc/BV), bone volume (BV) was calculated as TV - Ca.V.

Ellipsoids were fitted (AMIRA 5.4.1, Microscopy Module) to each individual lacuna; from these, shape parameters were computed for each based upon the resulting three eigenvalues (EV) of the covariance matrix. The length of each axis was approximated by two times the EV of the covariance matrix (95% confidence interval)[2]. A simplified model of the obliquity of the biomechanical environment within the proximal femur was used, with the direction of principal mechanical strain being approximated by the longitudinal axis with which it is closely aligned [158]. The actual deviation of the angle of principal strain within the femur is small, as demonstrated by secondary osteons which have been shown to orient obliquely between 0-15°

[2] This statement replaces that in Chapter 4 where the semi-axis lengths were defined as equal to the square-root of the EV.

from the longitudinal axis [159]. The **orientation** (Lc.Φ) of each lacuna was measured as the absolute value of the angular deviation (-90º to 90º) of the axis of the first EV (longest lacunar axis) from the horizontal axis of the sample. An orientation value of 0º represents a transverse (radial or circumferential) orientation and values approaching 90º are increasingly in longitudinal orientation. To describe the shape of the lacunae, three ratios of the EV's were used in order to define the degree of difference [80]. The **Degree of Equancy** (Lc.Eq) was calculated as the ratio of the third (shortest) to the first (longest) EV (EV3:EV1). An Lc.Eq value of one represents an object equal in the shortest and longest dimensions. **Degree of Elongation** (Lc.El) for each lacuna was calculated by one minus the ratio of the second (intermediate) and the first EV (1-EV2:EV1). An Lc.El value of one represents an elongated object. **Degree of Flatness** (Lc.Fl) was calculated as one minus the ratio of the third and second EV (1- EV3:EV2). An Lc.Fl value of one represents a flat object.

5.2.4 Statistical Analyses

Statistical analysis was performed using SPSS 16.0 (SPSS Inc., Chicago, IL, U.S.A.). Values for N.Lc/BV (mm^{-3}) were calculated, and Lc.V (μm^3), Lc.Φ (º) and shape (Lc.Eq, Lc.El, Lc.Fl) were averaged from each sample and, along with the canal measures; these results were then grouped according to region (anterior, posterior, medial and lateral). Analysis of Variance (ANOVA) with repeated measures and post-hoc Bonferroni adjustment was performed with significance $\alpha < 0.05$ to compare the regions. A second analysis was conducted with the regions grouped according to biomechanical 'tension/compression' axes into a combined anterior-posterior group and a combined medial-lateral group. ANOVA tests were performed with significance $\alpha < 0.05$ to compare the two groups.

5.3 Results

Due to issues with scan quality and artifacts, three of the original 10 samples SR micro-CT scanned were removed from the analysis. The lacunar density and morphological analysis results are summarized in Table 5.1. Average N.Lc/BV values were different between the anterior (23,394 mm^{-3}) and both the posterior (30,180 mm^{-3}) (p=0.042) and medial (35,946 mm^{-3}) (p<0.001) regions (Fig. 5.1.A). The density of the combined anterior and posterior regions (26,786 mm^{-3}) was also lower (p=0.006) than the combined density of the medial and lateral

regions (32,812 mm^{-3}). There were no differences between mean Lc.V for the separate regions (p=0.219); however, a trend was noticeable in the combined results (p=0.054), with higher volumes in the combined medial lateral regions. No differences were apparent in average Ca.V or Ca.Dm (p>0.05). Average Lc.Φ was not significantly different between the four regions nor when combined (p>0.05). No differences were apparent in Lc.Eq (p>0.05) (Fig. 5.1.B). The anterior region had more elongated lacunae than those of the medial and lateral regions (Lc.El p=0.001). Lacunae in the posterior region were significantly more elongated than those of the medial (p=0.014) but not lateral regions (p=0.553) (Fig. 5.1.C). The same trend followed for Lc.Fl, which was significantly less flat in the anterior, compared to the medial and lateral (p<0.001) and the posterior to the medial (p=0.019) (Fig. 5.1.D). The combined anterior-posterior lacunae were significantly more elongated and less flat than the combined medial-lateral values (p<0.001). There were no differences in either EV1 or EV3 for each region; however, average EV2 was significantly different between the posterior and medial regions (p=0.009). The eigenvalues of the combined regions followed the same pattern with EV2 higher in the combined medial and lateral region (p=0.001).

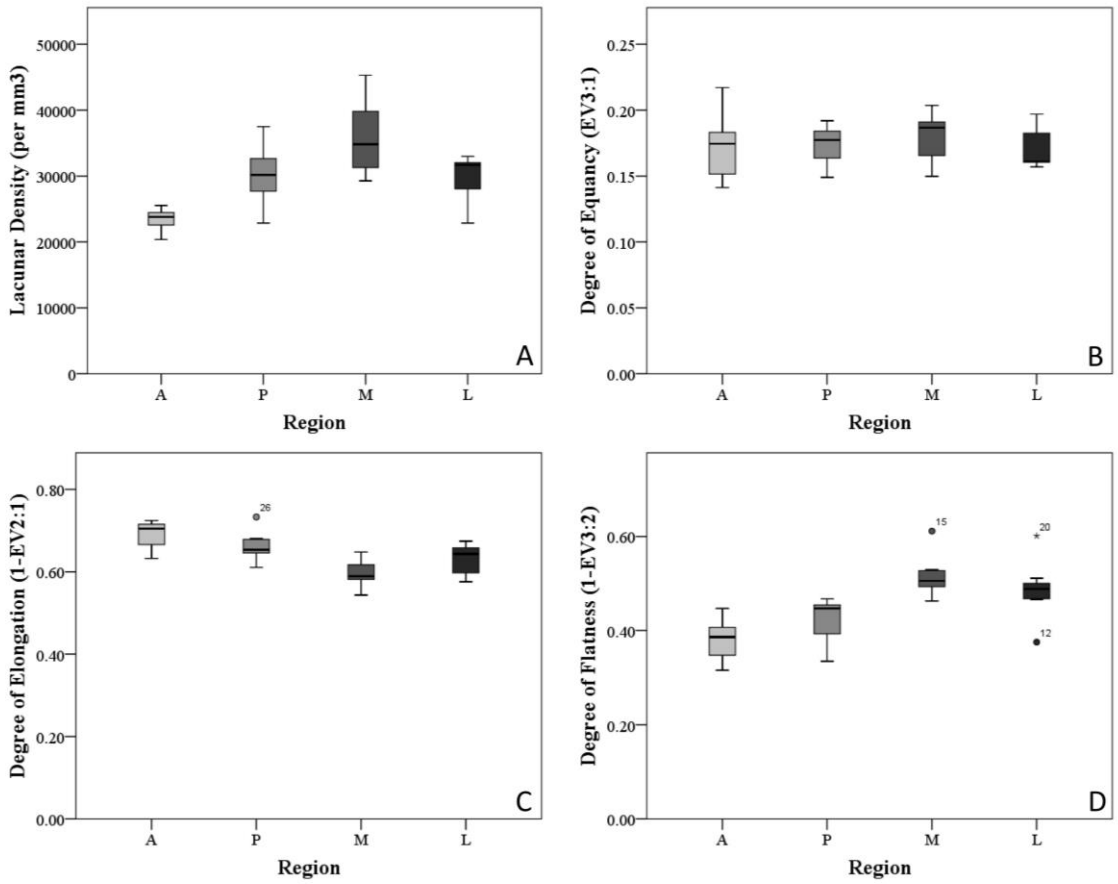

Figure 5.1 Box plots representing the average osteocyte lacunar density for each region (A). Measures of morphology include: degree of equancy (B), degree of elongation (C), and degree of flatness (D).

Table 5.1 Results from the ANOVA of the morphological parameters of osteocyte lacunae. Δp<0.05 versus both posterior and medial regions. §p<0.05 versus both medial and lateral regions. Ħp<0.05 versus medial region. #p<0.05 versus combined medial and lateral .

Region	N.Lc/BV (mm^{-3} ± sd)	Ave Lc.V (μm^3 ± sd)	Ca.Dm (µm ± sd)	Ca.V (mm^3 ± sd)	Ave Lc.Φ (° ± sd)	Ave Lc.Eq (± sd)	Ave Lc.El (± sd)	Ave Lc.Fl (± sd)	Ave EV1 (± sd)	Ave EV2 (± sd)	Ave EV3 (± sd)
Anterior	23,394 ±1,705Δ	242 ±44	52.81 ±13.16	0.04 ±0.01	60.23 ±3.97	0.17 ±0.03	0.69 ±0.04§	0.38 ±0.05§	12.74 ±1.56	3.09 ±0.34	1.56 ±0.06
Posterior	30,180 ±4,860	261 ±49	53.03 ±19.62	0.04 ±0.02	55.90 ±5.41	0.17 ±0.02	0.66 ±0.04Ħ	0.42 ±0.06Ħ	12.46 ±1.55	3.28 ±0.39Ħ	1.59 ±0.07
Medial	35,946 ±5,990	299 ±45	51.01 ±12.94	0.04 ±0.01	53.37 ±4.61	0.18 ±0.02	0.60 ±0.04	0.52 ±0.05	11.68 ±1.38	3.95 ±0.46	1.62 ±0.05
Lateral	29,678 ±6,081	282 ±71	47.79 ±13.78	0.04 ±0.01	56.70 ±3.74	0.17 ±0.02	0.63 ±0.04	0.49 ±0.07	12.24 ±1.49	3.74 ±0.67	1.58 ±0.09
Combined Ant+Post	26,786 ±4,964#	252 ±46	52.92 ±16.05	0.04 ±0.01	58.06 ±5.08	0.17 ±0.02	0.68 ±0.04#	0.40 ±0.06#	12.69 ±1.50	3.19 ±0.37#	1.57 ±0.06
Combined Med+Lat	32,812 ±5,711	291 ±55	49.45 ±12.95	0.04 ±0.01	55.04 ±4.39	0.18 ±0.02	0.61 ±0.04	0.50 ±0.06	11.96 ±1.41	3.85 ±0.56	1.60 ±0.07

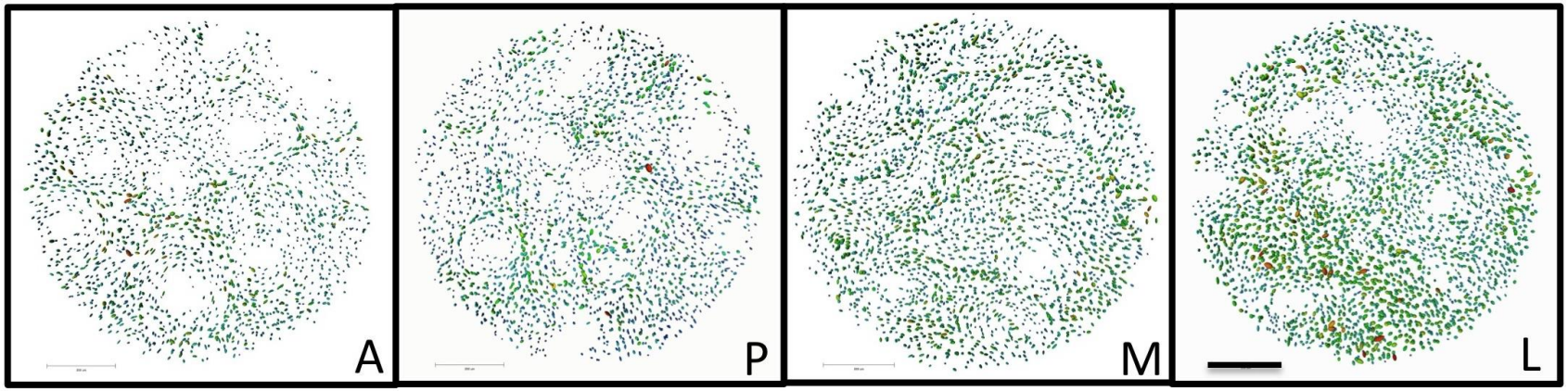

Figure 5.2 Renders of 100 µm thick slice demonstrating the differences in lacunar density. With fitted and colored ellipses scaled for Eigenvalue 2, the major contributor to change in elongation and flatness in the anterior (A), posterior (P), medial (M), and lateral (L) regions. Color gradient from blue to red representing increasing EV2. Scale bar = 200µm.

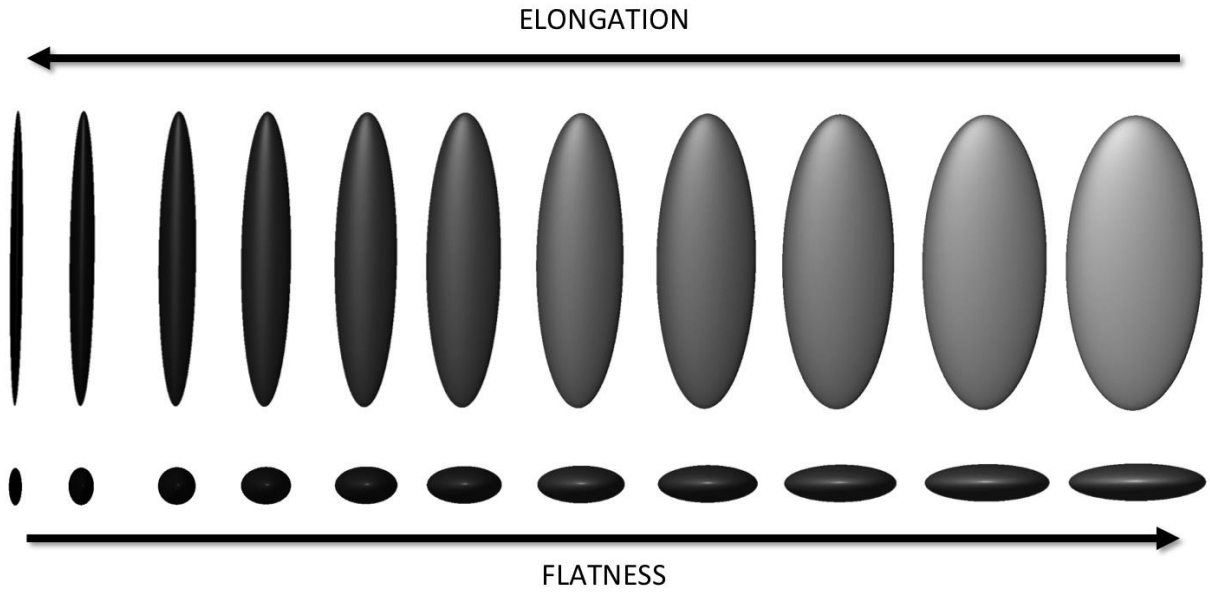

Figure 5.3 3D model demonstrating increasing elongation accompanied by decreased flatness.

5.4 Discussion

The most plentiful cell in bone, osteocytes, form an interconnected system upon which the maintenance of healthy bone relies. The results of this study demonstrate that the variation in osteocyte lacunar density and morphological parameters between regions of a single cross-section of human femoral shaft previously noted in Chapter 4 [80] can be seen in a larger group. As expected, in this larger study, there was a dramatic difference in lacunar density between the medial and anterior region (up to ~54%). Average lacunar densities were significantly different between the anterior and both the medial and posterior regions. The density of the combined anterior and posterior regions was also significantly lower than the density of the combined medial and lateral regions. Although no difference was found in predominant orientation, shape differences were found; with the combined anterior-posterior regions having lacunae that were significantly more elongated and less flat than the combined medial-lateral values. In addition to providing a more definitive picture of normal variation to enable better context for drawing inferences with regard to age, disease and biomechanics, this study provides geometric measures relevant to future computational modeling of the normal osteocyte and its mechanical environment.

Variation in bone microstructural features, such as regional differences in the orientation of secondary femoral osteons, has been linked to the mechanical environment [159, 160]. In this study we found no differences in lacunar orientation, with the long axis of lacunae in all regions oriented essentially parallel to the longitudinal axis of the bone, well aligned with the slightly oblique principal strain axes. A previous study of femoral mid-shaft regional variation in vascular canals have demonstrated increased porosity in the anterolateral and posterior regions [139]. This study revealed no regional differences in any of the canal indices measured. The majority of intra-element variation appears to occur non-uniformly increasing from the periosteal to endosteal surfaces [139, 161, 162] and may not be represented in this study's mid-cortical samples. One possible explanation for regional differences in lacunar parameters and not in the vascular canal system is, even though they are connected, fluid pressures in these systems behave almost independently of each other [163].

The study discussed in Chapter 4 found average lacunar densities to be significantly different between the medial and both the anterior and posterior regions with the anterior and posterior regions combined significantly lower than that of the combined medial and lateral regions [80]. The observed differences in the current study were actually higher than previously demonstrated at ~54%, although the medial region is no longer significantly different from the posterior. The anterior region had significantly fewer osteocytes incorporated than the medial and posterior regions. This differs from our previous study where the medial was much higher than both the anterior and posterior. However, as a trend the lacunar density along the anteroposterior axis declined by approximately 18% compared to the mediolateral axis, which is in keeping with previous results.

Differences can occur in lacunar density via two routes. First, bone is deposited or remodeled incorporating varying numbers of new osteocytes in the osteoid as it is laid down. From this point no new osteocytes can be incorporated, although through a process of cellular apoptosis and consequent long-term infilling, lacunar density can decrease. This second route of change is unlikely to be the driving mechanism for the shift in density demonstrated here as the percentage of viable cells decreases with age from 99% to approximately 58% by the 8th decade of life [151], the young age of the individuals in this study means that apoptosis is likely to have little effect.

As with lacunar density there are two mechanisms by which lacunae can come to differ in size and shape. Firstly, as cells are encysted in the bone matrix during formation, the shape of the lacunae is determined by the osteocyte. Secondly, it has recently been noted that the pericellular environment is capable of modification at an individual lacunar level by the osteocyte [164, 165]. The role of loading in both of these situations has yet to be determined.

Although no differences were evident in equancy, lacunae from the anterior region were more elongated and less flat, than those of the medial and lateral regions. Lacunae in the posterior region were significantly more elongated and less flat than those of the medial but not lateral region. The combined anteroposterior lacunae were significantly more elongated and less flat than the combined mediolateral lacunae (Fig. 5.2). Elongation follows the same trend as reported in Chapter 4 from a single individual; however flatness is now significant in the medial and lateral regions. In the previous study of a single individual [80]. EV1 the long axis of the lacunae was significant between the regions and a trend was seen in EV2. In this larger study, EV1 demonstrates the high inter-individual differences associated with normal variation and EV2 shows the single greatest significance (Fig. 5.3). This pattern fits with that seen in younger women who had flatter lacunae in the anterior region compared to older women in the same region as discussed in Chapter 6 [81].

Ultimately, the likely mechanism for the variation in lacunar parameters described here is related to the local mechanical environment both during deposition of the osteocytes and throughout the cells' lives. Strains generated by activity represent an efficient epigenetic parameter through which bone cells can assess structural efficiency and influence their morphology [166]. Early work on the mechanics of the femoral shaft suggested the greatest source of stress on the human femur comes from bending. When experiencing bending due to motions such as walking or single leg stances, the shaft of the femur is subject to compression on the medial side and tension on the lateral with a neutral axis which passes through the center of gravity where there is no tensile or compressive stress; this axis is along the sagittal plane of the femur in an anteroposterior direction [166, 167]. These studies; however, were based on analytical methods such as simple beam theory, photo-elastic analysis and static analysis, all of which suffer from inherent biases and generally assume a homogenous material. Newer research incorporating finite element modeling and the thigh muscles suggest that stress and strain

patterns in the femoral diaphysis are characterized by combined bending and torsion [168-170]. Although bending force decreases from proximal to distal, the proximal surface is characterized by a relative reduction in torsion [171, 172], making the proximal shaft a simpler biomechanical region than that of the midshaft; however, inter-femur strain variability for cadaveric specimens has been shown to be high [169].

We report a decrease in lacunar density with elongated but less flat spaces across the purported neutral axis where under natural circumstances the strains do not reach high values [173]. The highest density of spaces is found in the medial region where, under bending forces, the shaft would be experiencing the highest compression strains. Although no significant differences in lacunar volume were seen between the regions, a trend was noted in the combined groupings with the anteroposterior regions having slightly smaller (252 μm^3) lacunae than the mediolateral (291 μm^3). This fits the patterns found in studies of extreme differences in loading conditions where lacunae in unloaded rat bone became smaller [130], perhaps representing the decrease in strain along the purported neutral axis. Caution must be noted that the biomechanical environment of the proximal femoral shaft is complex, and drawing direct parallels between lacunar parameters and strain may not be entirely accurate. Above all, the results of this study demonstrate the necessity of further research into the mechanisms governing normal lacunar distribution and morphology, beginning with a simple biomechanical system. This said, localized strain environment is only one of a myriad of factors affecting the microstructure of bone at the individual level: lifestyle, activity levels, diet, health and metabolism also play a role [166]; however, these factors could not be controlled for in this study and therefore their relative influences cannot be determined.

Adequate numbers of osteocytes have been demonstrated as essential to coordinate the removal of bone damage and lacunar density correlates with indices of bone quality [56]; however, as the variation seen here demonstrates, 'adequate' is a relative term. It has been suggested that a reduction in osteocyte abundance can result in the deterioration of matrix fluid flow and a decrease in the ability to detect microdamage that may lead to impaired repair and increased fragility. It has previously been noted that lacunar density and size may cause variation in the apparent stiffness of bone [41]. An increase in microcracking *in vivo* has been associated with reduced lacunar abundance [69, 174]; however, finite element analyses have found

increased lacunar density linked to microcracking, in older individuals, although lacunar occupancy may be a factor here [58].

The effects of lacunae on bone mechanical quality are not limited to abundance and size. Lacunar shape influences the mechanical strain applied to the osteocyte, with different lacunar morphology resulting in differing strain magnitudes in the matrix and cell when subject to the same loads [23]. We can readily see the effects of inclusions such as osteocytes and their lacunae on any solid structure by referring to materials science and structural mechanics models. The primary effect of inclusions within any material is a disruption in the homogeneity of the structure, and their influence on mechanical and other properties can be considerable [175]. The mechanical properties of the bone matrix are significantly degraded by inclusions, because they are not only discontinuities in the parent material, they are also local stress concentrators. During deformation under loading of the primary structural element, inclusions become the focal point for the initiation of micro cracking; as has been demonstrated for lacunae [59]. This study demonstrated a lower number, of more elongated spaces, along the anterolateral axis and an increase in less elongated but flatter lacunae in the tension and compression zones (lateral/medial). Unfortunately we have been unable to visualize the canaliculi, which connect each lacuna and contain the cell processes. These canaliculi represent additional discontinuities that may predispose the bone to crack propagation even more readily. Additionally, this does not take into account the torsional strains that the proximal femur experiences. In simulations, strains are higher in elongated cells compared to those less elongated [23]. It may be that the elongated cells seen in our low strain regions are evidence of amplification, in order to gain the required 'regular' lacunar network. Maximum principle strains occur in the matrix approximately parallel to the long axis of the lacunae; however, relatively larger increases in strain magnitude occur perpendicular to this axis, measured here as EV2 and EV3 [23]. These relative differences in local strain environment might provide a mechanism for the directional specific differences we see in lacunar shape.

Although this study was limited to seven healthy individuals, hundreds of thousands of lacunae were analyzed with consistent results. This work clearly demonstrates that the high variation seen in osteocyte lacunar density as well as other lacunar parameters, noted in a number of biomechanical, age and pathology studies are well within the range of normal variation;

however, the reasons for and consequences of this variation remain unclear. Lacunar parameters including abundance and shape are being increasingly incorporated into computational modeling of bone biology and this paper represents a more comprehensive description of the normal healthy lacunae.

5.5 Conclusion

This chapter has demonstrated that the high regional variation in lacunar parameters noted in Chapter 4 occurs in a larger sample of healthy young men. This is important as it suggests a link between biomechanics and lacunar density and morphology parameters. Additionally it represents a baseline for osteocyte lacunar density and shape parameters in healthy individuals, which is currently lacking in the literature and is vital to controlling future studies of lacunar properties in varying situations of age, sex and pathology. Future research should focus on whether intra-element variation occurs in women and ask how these parameters align with the specific biomechanical environments and change with pathology. Chapter 6 uses the techniques outlined in Chapters 3-5, restricted to a single region to reduce the effect of variance, to examine lacunar parameters in women over the human lifespan.

CHAPTER 6: FEMORAL OSTEOCYTE LACUNAR DENSITY, VOLUME AND MORPHOLOGY IN WOMEN ACROSS THE LIFESPAN

This chapter has previously been published as: Carter Y, Thomas CD, Clement JG, and Cooper DM. Femoral osteocyte lacunar density, volume and morphology in women across the lifespan. Journal of Structural Biology 2013; 183: 519-26

6.1 Introduction

During life, human bone undergoes a constant process of remodeling, in which old bone is removed (resorption) and replaced with new bone (formation). In the young, these twinned processes are balanced; however, with advancing age there comes a net increase in bone resorption and a loss of bone architectural quality leading to fragility and fractures associated with diseases such as osteoporosis [10]. Studies examining the effect of aging at the cellular level have been restricted due to the encasement of the bone cells, osteocytes, deep within the bone matrix. Because the osteocytes themselves cannot be visualized using x-ray based techniques the spaces in which they reside, lacunae, are used as proxy.

6.1.1 Role of the Lacuno-Canalicular Network

Osteocytes are the most ubiquitous cell found in bone and are connected through an extensive network of cell processes which allows for communication and nutrient transportation [4]. Together, the lacunae and the spaces formed around the cell processes, the canaliculi, form a network considered vital to maintaining bone homeostasis. The exact role of the lacuno-canalicular network (LCN) is not yet fully understood. Several functions of the LCN have been proposed including initiation of bone remodeling via ion-sensation and regulation of osteoid matrix maturation and mineralization [5]. Currently a general consensus exists that osteocytes play a role in translating mechanical stimuli into biochemical signals, forming the basis of the mechanosensation and transduction systems [176]. The surface area of the LCN is immense and in the adult male has been calculated to be 400 times larger than that of the Haversian systems and 130 times greater than the surface area of the trabecular rods and plates [6]. The sheer scale of this network of connected spaces and cells suggests that differences in the scale or morphology of the LCN could affect mechanosensation/transduction [39].

6.1.2 Changes in the Lacuno-Canalicular Network with Age

Changes in LCN with age are of particular interest, especially in women since they are more susceptible to the bone loss and fragility associated with senescent diseases such as osteoporosis. Osteocyte density in humans correlates with the biomechanical quality of bone [56], with differing density and volume causing variations in the apparent stiffness of the bone matrix [177]. Several studies have reported that lacunar density (number of lacunae per mm^3 of bone), a reflection of the abundance of lacunae, declines with age in males and females [57, 64-66]; the rate and causes of this decline; however, is debated. Mori and colleagues [57] reported that age-related decline of lacunar density in trabeculae of the human femoral head did not begin until 70 years of age, which was then followed by a sharp decline. More recent studies by Mullender *et al.* [45] reported the decline to be linear while Qiu *et al.* [67] determined the decrease to be exponential.

The state of lacunae populations in osteoporotic patients is an intriguingly complex research area which is currently hotly debated. A number of studies report lacunar density to be increased in women with osteoporosis [58, 64, 73]. In contrast to this, a more recent study by Mullender *et al.* [45] found reduced lacunar density in osteoporotic patients. This is consistent with studies by Mori *et al.* [57] and Qiu *et al.* [63] who report lower lacunar densities in patients with a history of osteoporotic fracture and Zarrinkalam *et al.* [74] who found reduced lacunar density in the lumbar vertebrae of osteoporotic sheep. Previous research has demonstrated that in some individuals destined to experience an osteoporotic fracture, bone is made with fewer osteocytes than normal [63], suggesting that some individuals may be predisposed to developing an osteoporotic fracture.

6.1.3 Study Objectives

The study of cortical microstructure has gained momentum recently due to the increasing availability of high-resolution micro-CT, both desktop and Synchrotron Radiation (SR micro-CT). This technology provides highly accurate 3D images for analysis at micrometer or better resolutions and with much larger volumes of interest. SR micro-CT can be considered the benchmark in 3D bone imaging [125], producing more accurate and faster quantitative measurements than a similar desktop-CT setup [129]. SR micro-CT has been utilized to examine osteocyte lacunar density in 3D in rodents [126, 130] and humans [19, 80, 131]. Quantification

of human osteocyte lacunar morphology in 3D beyond simple measures of orientation has been limited [80], and mostly restricted to nano-scale studies of a few lacunae [17, 24]. The purpose of this study was to test whether differences exist in the osteocyte lacunar density, orientation and morphology in the femoral cortex of adult women spanning the human lifespan using SR micro-CT.

6.2 Materials and Methods

6.2.1 Specimens

Cortical bone samples were obtained from the femora of 30 deceased women between the ages of 20 and 86. These femora form part of the Melbourne Femur Collection held at the University of Melbourne, Melbourne, Australia and were collected at autopsy with the informed consent of the donor's next-of-kin. The study was conducted with ethical approval from the Victorian Institute of Forensic Medicine (EC26/2000), the University of Melbourne (HREC 980139) and the University of Saskatchewan (Bio # 08-46). Individual samples with dimensions of approximately 2 x 2 x 5 mm were cut from the anterior mid-cortical region of the proximal femoral shaft. All samples were removed from the same region of the bone to minimize the effects of intra-individual variation in lacunar properties associated with the biomechanical axes [80]. The proximal femoral shaft represents an ideal site of analysis as it has been the subject of recent investigation including regional variation in porosity [178] and material density [140]. This region is subjected most strongly to compression forces with some incidental tensile forces dependent on bending associated with movement such as walking [146].

6.2.2 Synchrotron Radiation Micro-computed Tomographic Imaging (SR Micro-CT)

SR micro-CT scanning was conducted at the Advanced Photon Source (APS), Argonne National Laboratory on beamline 2BM. Images were obtained using monochromatic x-rays with a photon energy of 27.9keV and an effective pixel size of 1.47μm. An exposure time of 250 milliseconds per frame was employed for each of the 1500 frames spanning 180 degrees of rotation resulting in a scan time of approximately 17 minutes. The projection images were reconstructed to create a dataset containing 1408 slices (2048×2048 pixels). This configuration utilizes the same energy as the experiments outlined in Chapter 5; however, due to beamline specific optic changes in setup, the exposure time was increased and frame number was

decreased. These changes in setup did not affect the quality of the images or the data obtained from them.

6.2.3 3D Quantitative Morphometry

A cylindrical region of interest (ROI) with a diameter and height of 1.5 mm and a volume of 2.65 mm^3 was defined within each specimen (Fig. 6.2). Lacunae and canals within these ROI's were identified using a standardized global threshold, which separated the higher density bone from the air-filled lacunar and canal spaces, the same threshold was used for all specimens. Following segmentation, 'despeckling' was conducted on elements less than 10 μm^3, which were assumed to be noise, and elements above 2000 μm^3, which were assumed to be canals, the rest were assumed to be lacunae. These volume limits were based on confocal microscopy measurements of osteocyte volumes which found the minimums and maximums to be 28–1713 μm^3 [23].

Image stacks were cropped and analysis of the cortical canals were conducted using CT Analyzer 1.10.9.0 (SkyScan, Kontich, Belgium). Morphological analysis of the lacunae was conducted using AMIRA 5.4.1 (Visage Imaging, Fuerth Germany). Standard nomenclatures for canal [97] and lacunar [126] indices were used, for morphological parameters describing lacunar shape descriptions have been created by the authors as discussed in Chapter 4 [80]. The extracted parameters included: total ROI volume (TV), total canal volume for ROI (Ca.V), Average canal diameter (Ca.Dm), total number of lacunae (N.Lc) and lacunar volume (Lc.V). N.Lc and Lc.V were calculated using individual object analysis, which calculates the 3D parameters of each discreet object within the volume of interest after segmentation. In order to determine lacunar density per mm^3 (N.Lc/BV), bone volume (BV) was calculated as TV-Ca.V. Subsequently, 3D renders of the lacunae and canals were created.

To quantitatively assess the morphology of the lacunae, ellipsoids were fitted (AMIRA 5.4.1, Microscopy Module) to each individual object and filtered for size to remove canals and noise from the analysis as previously described; from these, shape parameters were then computed for each ellipsoid based upon the resulting three eigenvalues (EV) of the covariance matrix (Fig. 6.1). The length of each axis was approximated by two times the EV of the covariance matrix (95% confidence interval). Our previous work, incorrectly stated the value of the semi-axis as the square root of the corresponding EV; however, the reported findings remain

unchanged as they were based on ratios reflecting shape, only extrapolated dimensions would be in error [80]. In traditional shape analysis the above statement would be true of the EV's describing an ellipsoid; however, AMIRA uses the Eigenvalues of the covariance matrix. The **orientation** (Lc.Φ) of each lacuna was measured as the absolute value of the angular deviation (-90º to 90º) of the axis of the first EV (longest lacunar axis) from the horizontal axis of the sample. An orientation value of 0º represents a transverse (radial or circumferential) orientation and values approaching 90º are increasingly longitudinal in orientation. To describe the shape of the lacunae, three ratios of the EV's were used in order to define the degree of difference [80]. The **Degree of Equancy** (Lc.Eq) was calculated as the ratio of the third (shortest) to the first (longest) EV (EV3:EV1). An Lc.Eq value of one represents an object equal in the shortest and longest dimensions. **Degree of Elongation** (Lc.El) for each lacuna was calculated by one minus the ratio of the second (intermediate) and the first EV (1- EV2:EV1). An Lc.El value of one represents an elongated object. **Degree of Flatness** (Lc.Fl) was calculated as one minus the ratio of the third and second EV (1- EV3:EV2). An Lc.Fl value of one represents a flat object.

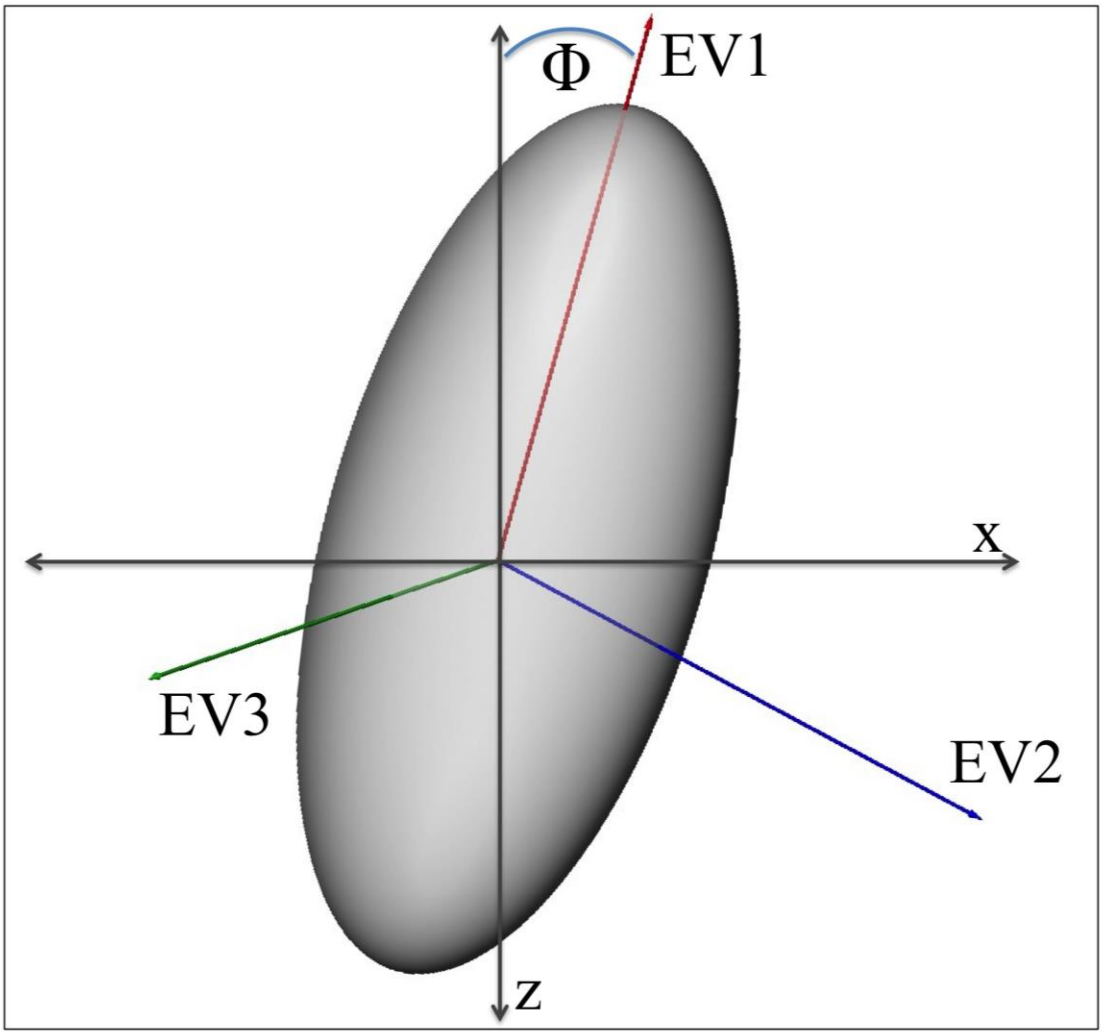

Figure 6.1 Model demonstrating the coordinate system used for morphological analysis.

6.2.4 Statistical Analyses

Statistical analysis was performed using SPSS 16.0 (SPSS Inc., Chicago, IL, U.S.A.). The values for N.Lc/BV (mm^{-3}), the canal measures and average Lc.V (μm^3), Lc.Φ (º) and shape parameters (Lc.Eq, Lc.El, Lc.Fl) were examined for their relationship with age using linear regression. A second analysis was conducted with the samples grouped according to age: under 50 years old at time of death and over 50 years old. One-way ANOVA tests were performed with significance $\alpha < 0.05$ to compare the two groups. As distribution of the results for measures were not normally distributed, as confirmed by Kolmogorov-Smirnov test the median as well as the average for each sample was studied, neither produced statistically different results, except for

EV3 as noted in tables 6.1 and 6.2. The median results are included in tables 6.1 and 6.2, however, for clarity only the average results are discussed in the results.

6.3 Results

The results of the linear regression analysis are presented in Table 6.1. As expected Ca.V increased with age (p=0.04), as did Ca.Dm (p=0.012). N.Lc/BV values were not significantly related to age (p=0.05), although there was a downward trend. Lc.V decreased with age (p<0.001) as reflected by declines in EV1, EV2 and EV3 (all three p<0.001). Lacunae became more equant with age (p<0.001), a change related to lower Lc.Fl with age (p<0.001) but not Lc.El (p=0.836). No relation between Lc.Φ and age was observed (p=0.474).

The results of the density and morphological ANOVA are summarized in Table 6.2. Ca.V increased with age (p<0.001), as did Ca.Dm (p=0.029). N.Lc/BV values were not significantly different between the age groups (p=0.173). Lc.V differed between the younger (298.5μm^3 ±53) and older (211.7 μm^3 ±38) groups (p<0.001). Average EV1, EV2 and EV3 were reduced in the over 50 group (p<0.010). The differences in eigenvalues were strongest in the first and second EVs. EV1 had a change of 21.54% with age while EV2 had a 21.8% shift, with only 2.53% for EV3. Older individuals had more equant lacunae than the younger individuals (p<0.001). The under 50 group demonstrated flatter (p<0.001) lacunae than the over 50 group, but with no difference seen in elongation (Lc.El p>0.05). The grouped data showed the no significant difference in orientation (Lc.Φ p>0.05).

Table 6.1 Average (Ave) and Median (Med) results from the linear regression analysis of the morphological parameters of osteocyte lacunae. *p<0.05.

	Ca.V (mm^3)	Ca.Dm (µm)	N.Lc/BV (mm^{-3})	Ave Lc.V ($µm^3$)	Med Lc.V ($µm^3$)	Ave Lc.Φ (°)	Med Lc.Φ (°)	Ave Lc.Eq	Med Lc.Eq	Ave Lc.El	Med Lc.El	Ave Lc.Fl	Med Lc.Fl	Ave EV1	Med EV1	Ave EV2	Med EV2	Ave EV3	Med EV3
Result (± sd)	0.15 ±0.12	59 ±30	23942 ±2529	252 ±63	239 ±70	59.45 ±3.44	66.69 ±3.82	0.18 ±0.03	0.14 ±0.03	0.66 ±0.04	0.72 ±0.05	0.41 ±0.9	0.44 ±0.11	13.00 ±2.39	11.71 ±2.39	3.33 ±0.63	2.92 ±0.69	1.55 ±0.45	1.47 ±0.00
R^2	0.264	0.203	0.131	0.462	0.427	0.018	0.014	0.395	0.386	0.002	0.000	0.453	0.421	0.417	0.426	0.433	0.425	0.213	-
P value	0.04*	0.012*	0.050	<0.001*	<0.001*	0.474	0.535	<0.001*	<0.001*	0.836	0.919	<0.001*	<0.001*	<0.001*	<0.001*	<0.001*	<0.001*	0.01*	-

Table 6.2 Average (Ave) and Median (Med) results from the ANOVA analysis of the morphological parameters of osteocyte lacunae. *p<0.05 between younger and older group.

Age	*n*	Ca.V (mm^3 ± sd)	Ca.Dm (µm ± sd)	N.Lc/BV (mm^{-3} ± sd)	Ave Lc.V ($µm^3$ ± sd)	Med Lc.V ($µm^3$ ± sd)	Ave Lc.Φ (° ± sd)	Med Lc.Φ (° ±sd)	Ave Lc.Eq (±sd)	Med Lc.Eq (±sd)	Ave Lc.El (±sd)	Med Lc.El (± sd)	Ave Lc.Fl (± sd)	Med Lc.Fl (± sd)	Ave EV1 (± sd)	Med EV1 (± sd)	Ave EV2 (± sd)	Med EV2 (± sd)	Ave EV3 (± sd)	Med EV3 (±sd)
<50	14	0.09 ±0.04 *	47 ±13*	24621 ±2955	298 ±53 *	288 ±67*	60.00 ±4.21	67.14 ±4.77	0.16 ±0.02 *	0.12 ±0.02 *	0.67 ±0.05	0.72 ±0.06	0.47 ±0.09 *	0.51 ±0.11 *	14.72 ±1.96 *	13.35 ±1.89 *	3.76 ±0.63 *	3.39 ±073 *	1.58 ±0.05 *	1.47 ±0.00
>50	16	0.21 ±0.12 *	70 ±36*	23347 ±1998	211 ±38*	195 ±37 *	58.97 ±2.65	66.30 ±2.85	0.20 ±0.03*	0.15 ±0.02 *	0.66 ±0.03	0.72 ±0.04	0.36 ±0.05 *	0.38 ±0.06 *	11.51 ±1.62 *	10.28 ±1.53 *	2.95 ±0.29 *	2.51 ±0.30 *	1.54 ±0.03 *	1.47 ±0.00

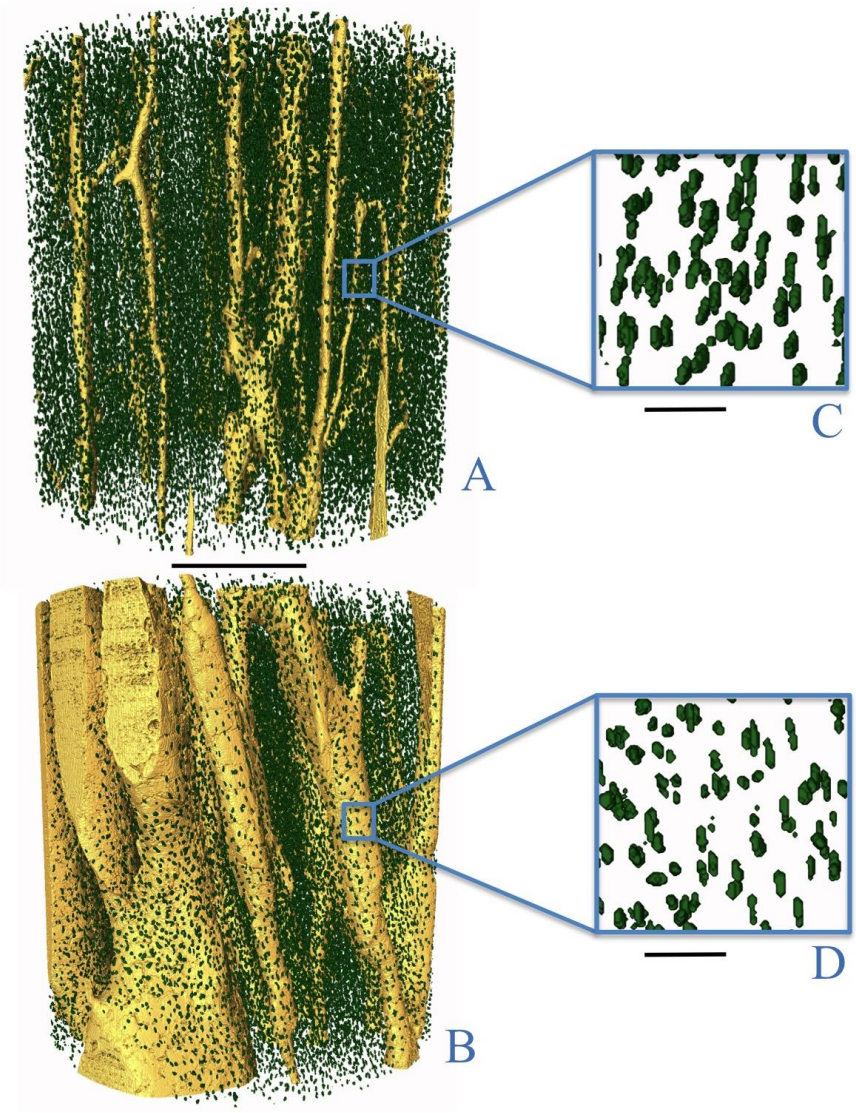

Figure 6.2 Renders demonstrating the differences between the under 50 (A. and C.) and over 50 age groups (B. and D.). A. and B. 3D render of a 1.5x1.5mm section showing lacunae and vascular canals, demonstrating the reduced osteocyte lacunar density and increased porosity in the older group. Scale bar = 500µm. B. and D. Close-ups of same region demonstrating the decrease in volume and shift in morphology. Scale bar = 50µm.

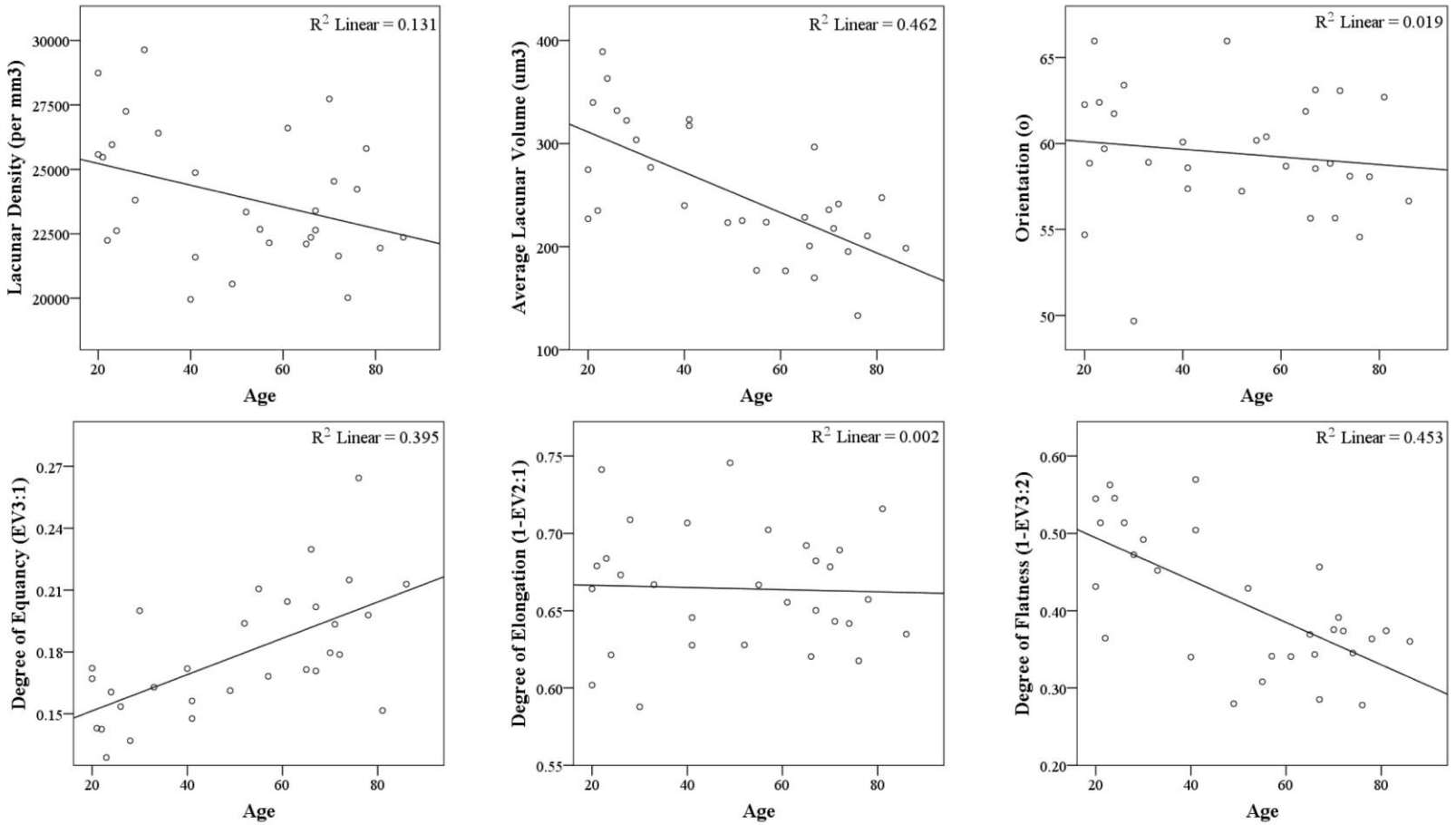

Figure 6.3 Graphs with R^2 values representing the average osteocyte lacunar density for each individual (A), lacunar volume (B) and angle of orientation with respect to the horizontal axis of the bone (C). Measures of morphology include: degree of equancy (D), degree of elongation (E), and degree of flatness (F).

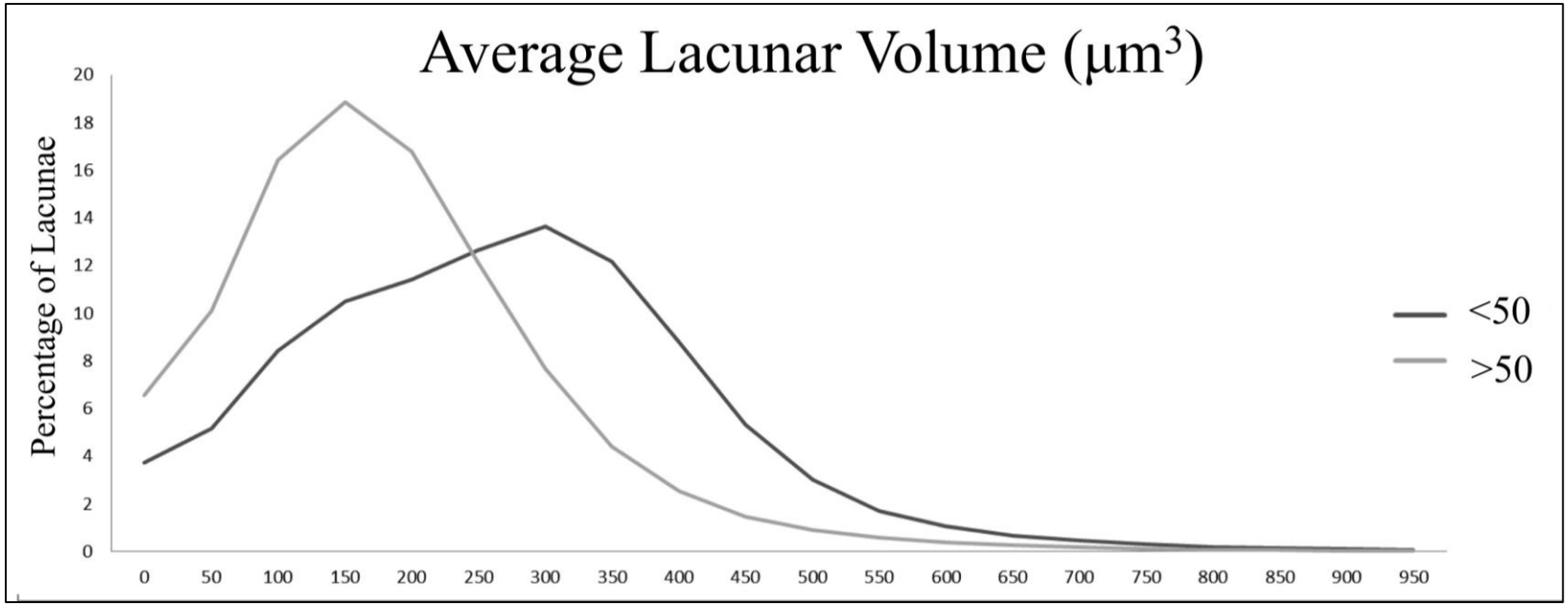

Figure 6.4 Histogram of osteocyte lacunar volumes grouped by age, demonstrating the shift in lacunar density associated with increased age. The graph represents percentage of total lacunar volumes averaged for each of the under and over 50 age groups with lacunae volumes and pooled in 50 μm bins.

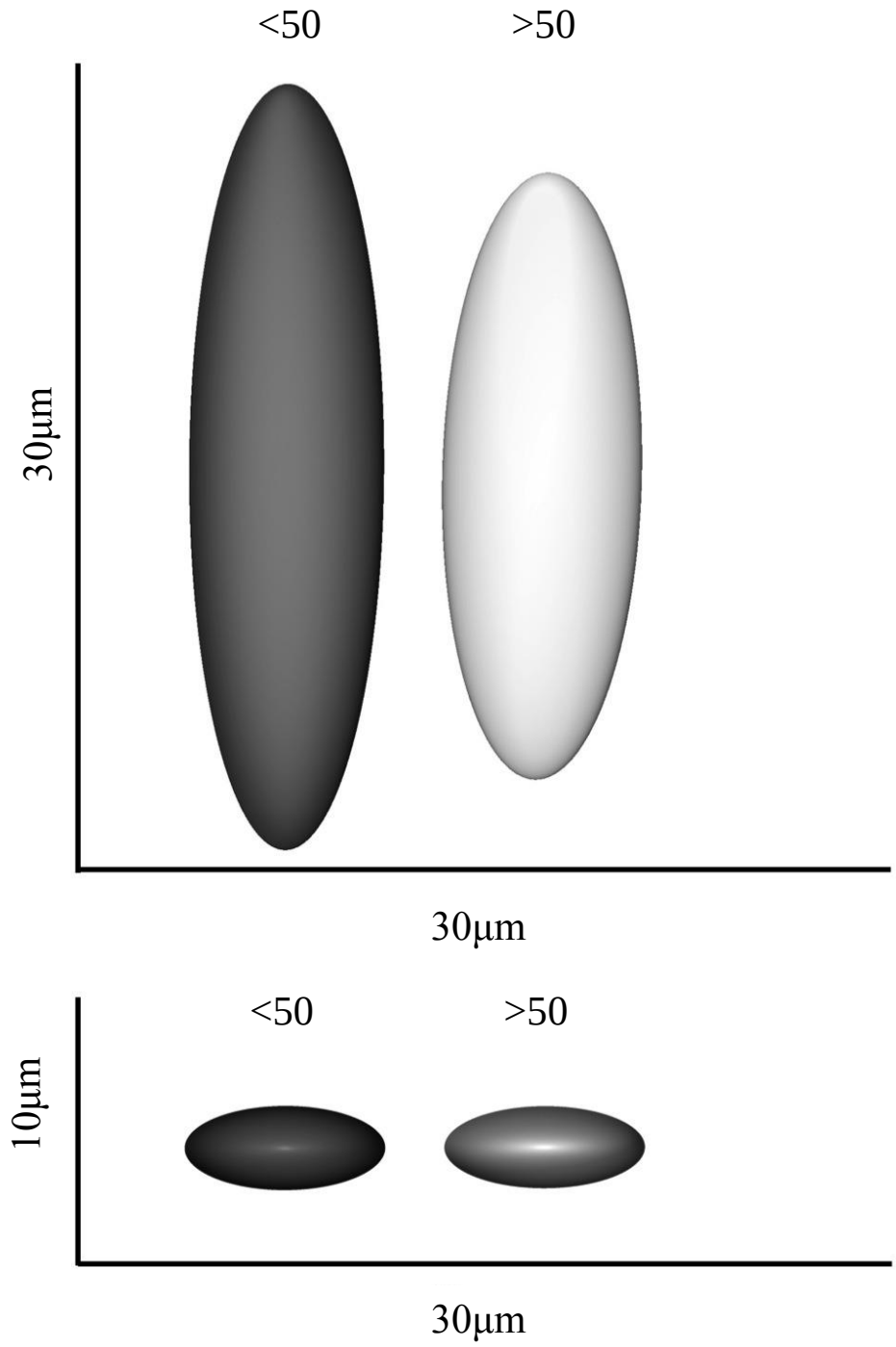

Figure 6.5 3D model of the average lacunar size and shape for the under and over 50 age groups.

6.4 Discussion

Loss of bone mass associated with age is related to skeletal weakening, suggesting that age-related microarchitectural changes are important determinants of bone quality [56]. To our knowledge this paper is the first to report measures of multiple cortical lacunar parameters in 3D in women over the human life span. The use of SR micro-CT extended the scale of analysis and revealed significant relations between age and variation in lacunar size and shape.

Comprehensive analyses of the osteocyte lacunar system have mostly been restricted to near two-dimensional techniques such as traditional light microscopy, scanning electron microscopy (SEM) and transmission electron microscopy (TEM)[39]. Less commonly applied three-dimensional methods include confocal microscopy [21, 63, 65, 67, 69, 73, 82], desktop nano-CT [17, 24], pytchographic CT [92], transmission x-ray microscopy-CT [34], TEM-CT [87], back-scattered electron microscopy (BSE) [88] and serial Focused Ion Beam/SEM [93]. All of these techniques are inherently limited in their applications to the study of lacunae. Most provide excellent resolution down to the nanometer scale but concomitantly survey a limited volume of interest, allowing only a few hundred lacunae to be examined. Additionally, requirements for sample preparation can be time consuming and destructive to the specimen. SR micro-CT utilizes a similar setup to a desktop micro-CT system but instead of a traditional x-ray source, light produced by electrons accelerated within a synchrotron are used. This light offers a number of enhancements over conventional x-ray tubes including a monochromatic beam, high spatial resolution capability, and brightness with smaller beam divergence [108]. Our SR micro-CT configuration provides a balance between resolution sufficient to quantify morphology and a volume of interest scaled to better characterize the state of the osteocyte lacunae in human cortical bone. As noted, because the osteocytes themselves cannot be visualized using x-ray based techniques, the spaces in which they reside, lacunae, are used as proxy; however, not all lacunae contain viable osteocytes. Lacunar abundance has been shown to vary with age with the percentage of unoccupied lacunae varying from 5-40% [64]. Location also plays a role as studies have shown female superficial iliac bone stable at 97% occupancy with age while deep bone fell from 82% to 73% [65]. In older women, the femoral neck cortex demonstrated that substantial losses of osteocytes up to 50% was possible depending on the individual and region [143, 179].

Previous studies of the vascular porosity of the human mid-shaft femur have noted a significant increase in mean canal diameter and overall porosity with age in women [3]. The results of this study confirm this, with larger canals, which seen in the older age group have often coalesced (Fig. 6.2). Such increases in vascularization would reduce localized fluid pressure gradients [180] and have significant implications for fluid-flow based hypotheses of bone mechanosensation.

Although reductions in lacunar density have been associated with factors inherent to the loss of bone quality and quantity, the relative importance of this decline is unknown [63]. Previous studies of women have noted significant declines, between 15 and 30%, in osteocyte lacunar populations with age [4, 57, 64-66]. Our results demonstrate a non-significant downward trend in lacunar density (Fig. 6.2, 6.3.A); however, inter-individual variation was high. One limiting factor of earlier studies is the relatively restricted volume of interest assessed by the techniques, with studies often limited to a few hundred lacunae. In normal bone, osteocyte lacunar density has been shown to vary significantly. Osteocyte lacunar density is 17% lower in interstitial bone than in osteonal bone [174] and intra-element variation can be up to 30% [80]. Bone damage in the form of microcracking has been shown to initiate at lacunae, implying that they act as stress concentrating features although the causative relations between the two have yet to be identified [59, 181]. While this association provides a potential mechanism for the detection of strains and damage [59], the reduced lacunar density trend seen here with age would reduce the capacity of this detection system. Conversely, reduction in the number of lacunae to concentrate stresses may reduce the incidence of cracking. The effects of differences in lacunar morphology are currently unknown, although these factors do contribute towards strain magnification measures [181].

One of the most significant results of this study is the reduction in lacunar volume seen in the older women. Lacunar volume in the over 50 group was reduced by almost a third relative to the under 50 group (Fig. 6.2.B). The osteocyte, encased within its lacuna, is surrounded by an extracellular matrix composed of proteoglycans and other matrix molecules [182]. This pericellular environment is involved in maintenance of the cells and their processes by serving as a buffer zone to maintain patency of the extracellular transport pathway, allowing for delivery of nutrition and removal of waste essential to the cells' survival [176]. This zone also facilitates the

interplay between the osteocytes and the matrix molecules, which play a necessary role in mechanotransduction [150, 183]. In culture, osteocytes have the capacity to modulate their extracellular fluid through the production of proteins [176]. The extent to which osteocytes can alter their environment is debated but they have been suggested to add mineral to their lacunae via the extracellular matrix [39]. Research suggests that osteocytes can best be envisaged as active inhabitants with a symbiotic relationship with their lacunae. While the lacunae provide physical protection and an environment for nutritional supply and communication, the osteocytes actively inhibit the mineralization of the space [150, 183].

Frost [68] first described complete mineralization of the lacunar space as *micropetrosis*. This term is used almost exclusively to describe the completely infilled lacunae found most commonly in the bone of senescent humans. Our x-ray based technique does not differentiate between completely infilled spaces and normal bone matrix; however, according to Frost [68], approximately 15% of lacunae meet this fate. This may explain the downward trend with age seen in our osteocyte lacunar density values. The reduction in lacunar volume demonstrated in this study might more accurately be characterized as partial infilling of the cellular space rather than complete micropetrosis. It is also possible that the reduction in lacunar volume may be due to accrual, during turnover, of osteons which were initially made with smaller lacunae. This is unlikely to be the single causative factor; however, as a shift is seen not only in average volume but also in the whole range (Fig. 6.4).

Micropetrosis is usually viewed as a binary state, with lacunae either filled or unfilled and has been linked to apoptosis; however, the reduction reported here may represent an intermediary stage before complete infilling. Cell death has been suggested to "allow" mineralization of the space [4, 183]. Although lacunar occupancy, reflecting loss of osteocytes, declines with age [64, 65, 143, 179] there is little evidence to support cell death on a scale large enough to allow for the infilling of the majority of lacunae reported here. Reports of extensive osteocyte loss are rare, with lacunar occupancy rates of below 30% reported only in interstitial bone from a select few older individuals [143]. We also note, although extensive cell death cannot be ruled out as the driving factor behind the observed infilling, it is unsupported by the lack of decline in osteocyte lacunar density. We therefore suggest the inhibitive properties of the cell are reduced with age allowing small amounts of the extracellular matrix to mineralize the

lacunar walls. Due to limitations in resolution our analysis could not assess if this infilling process extends to the canalicular network and is associated with direct disruption of the canalicular interconnections between the lacunae. This is a hypothesis that warrants further investigation as, if confirmed, it would represent a profound negative impact on the osteocyte network and may provide new clues into age-related bone loss. Some authors report an organic layer lining the lacunae known as the *lamina limitans* [184-188], although it is not seen in all samples, nor all lacunae within a sample [184]. It has been suggested that the *lamina limitans* is not present in osteocytes which are still in the bone formation stage [185] and that its presence points to the cessation of calcification; this phenomenon of a hardening organic layer may share a related mechanism with the age-associated infilling reported here. Further research is required to determine the possible mechanisms for this. Increasing the amount of infilling bone will have an effect on the material properties of bone. Infilling regions make bone more brittle, leading to fatigue damage susceptibility [189]. Reduction of the pericellular space may affect the functioning of the cells without damaging them, as osteocytes are able to expand and contract their cell bodies [190]; however, reduction in lacunar volume has been linked to osteoporosis [152] suggesting a connection to bone loss and, ultimately, fragility.

The shapes of lacunae are commonly accepted as roughly ellipsoid, although animal models have demonstrated changes with age in the morphology of the cells themselves [191, 192]. Lacunar orientation has been linked to the primary collagen fiber orientation of the osteon in which they are situated [83] and this would suggest their orientations are dictated at the time of formation. The reduction in lacunar volume demonstrated in this study was also reflected in a difference in lacunar shape with aging (Fig. 6.5). Under 50 years old, bone is characterized by flatter and less equant lacunae than those of the older group, which are more equal in dimensions (Fig. 6.3.E,F). Elongation does not appear affected in the older group as, although they are significantly smaller through the intermediate axis, the ratios stay stable. Differences in lacunar morphology have been linked to biomechanical environment [17, 80], tissue type [89] and differing disease states [24]; however, the results of this study demonstrate that significant differences in normal lacunar morphology occur with age, possibly due to preferential surface hypermineralization within the extracellular space. This change in morphology may be an adaptive response to the reduction in strain associated with age [65]. Round osteocytes have been

demonstrated to be more sensitive to smaller strains than flat ones [193]; however, a recent study demonstrated flatter and more elongate lacunae in the neutral axis of the proximal femur [80]. Lacunae in both groups were predominately orientated to the long axis of the femur (Fig. 6.3.C).

Our results suggest that decline in lacunar density, and therefore osteocyte number, with age in women may not be as important in the degradation of bone quality associated with aging as much as the reduction in the volume of the lacunae. The viability of the lacunar network and its encysted osteocytes may play a significant role in the maintenance and structural integrity of bone. Reduction in the surface area and volume of this system as well as possible occlusion of the cell connective spaces (canaliculi) will compromise fluid flow and downstream signaling which may negatively affect resistance to failure and possibly impair the mechanotransduction system. Discussions of solute transport and the molecular sieving properties of bone have been demonstrated to depend on the size and structure of both the canal and lacunar level spaces [194]. A reduction in this system would also reduce extracellular fluid flow and decrease the ability to detect microdamage. These may, in turn, lead to insufficient repair and consequent bone loss and fragility [62, 63, 195].

Osteocytes have been shown to inhibit osteoclastic activity [196, 197], hence, a decrease in lacunar density may relate to imperfect bone remodeling, leading to a lack of bone mass and strength, both factors in age-related fragility [45]. Changes in material properties associated with infilling of the cellular spaces in aging bone should also lead to a reduction in the energy absorption and dissipation capacities of the bone, suggesting a possible source of weakness associated with age [183].

Beyond bringing into doubt the widely accepted concept that osteocyte apoptosis is the direct stimulus for lacunar micropetrosis; our findings indicate a reduction in the volume of the lacunar network with age. If indeed the problems associated with the fragility of senescent bone are due to resultant reduction in cell capacity and not cell death, this presents a potential target for intervention initiating remodeling or preventing occlusion.

6.5 Conclusion

This chapter reports differences in osteocyte lacunar parameters seen in the cortical bone of women over the human age span. This includes, a volume reduction of approximately 30%

with concurrent variation in shape. Due to the preferential bias of age-related bone loss and osteoporosis towards women and the current uncertainty in the literate this study is vital to our understanding of the effects of age on bone. The large scale of this analysis – tens of thousands of lacunae in 30 women is unprecedented; however, the middle age range is not as well represented as the older and younger ages, future studies would be benefitted by increased sample numbers from this age range. The next chapter focuses on whether the intriguing age-related changes noted here occur in males.

CHAPTER 7: FEMORAL OSTEOCYTE LACUNAR DENSITY, VOLUME AND MORPHOLOGY IN THE CORTICAL BONE OF MEN ACROSS THE LIFESPAN

7.1 Introduction

As the most abundant cell in bone, osteocytes are ideally placed to sense and react to mechanical loading. Starting life as osteoblasts, they differentiate after becoming embedded in the bone matrix, in spaces known as lacunae. The osteocyte cell bodies are connected via their cellular processes, which pass through small pores connecting the lacunar network, known as canaliculi. Together the connected cells and their spaces form a functional syncytium, known as the lacuno-canalicular network (LCN), which is the increasing focus of research in bone biology. While debate remains, it is generally agreed that the osteocyte syncytium plays a major role in mechanosensation and transduction [198]. While large-scale analyses of the osteocyte system are restricted due to technological visualization limitations, the lacunae are often used as a surrogate from which cell number (spatial density) and cellular morphology can be inferred. Synchrotron radiation micro-computed tomography (SR micro-CT), an x-ray based technique which is capable of detecting lacunae, has proven useful for visualization and quantification of these properties [80, 81, 126, 131, 157, 199].

The processes by which osteocytes embed during bone deposition are not random, and hence the lacunae are representative of the local environment at the time of bone formation [17, 24, 200]. Bone remodeling occurs for three main reasons: to keep the balance of essential minerals and elements, to adapt the skeletal system to the local mechanical environment, and to repair bone damage [200]. While the first aspect does not require spatially-targeted remodeling the other two do. Many models for regulation of remodeling rely upon the osteocytes acting as sensors for strain and microdamage [201-203]. The exact mechanism by which the osteocyte network is able to sense and react to deformation of the bone matrix with mechanical load is currently unknown. Due to recent *in vitro* studies, the focus has been placed on flow of interstitial fluid through the LCN as a potential mechanism [204], acting either to directly activate ionic streaming potentials or o sense fluid shear stress along the cell body [150, 205, 206]. Either mechanism would suggest that the LCN is uniquely arranged in both size and morphology to best conduct this interstitial fluid flow. In mice, the LCN becomes more regular

with growth and it has been suggested that mature bone requires a regular arrangement of the LCN in order to correctly function [192, 200, 207].

Identifying differences in the mechanosensation mechanism, and thus the LCN, between men and women is a vital area of inquiry, particularly when considering aging and the high prevalence of bone loss and fractures associated with osteoporosis that more predominantly plagues women. Measures of bone microstructural properties have been shown to vary between the sexes, with males tending to have greater cortical thickness, bone volume, and tissue volume with lower cortical porosity and canal diameter [161, 162, 208]; however, characterizing differences in lacunar parameters has been less clear-cut. In human bone from multiple regions, osteocyte lacunar density is reportedly higher in healthy females than males [45, 66], although age appears to be a significant factor in determining sex differences. While lacunar density is generally agreed to decline with age in both men and women [57, 64-66], the rate and timing of this decline is debatable. Mullender *et al.* [45] reported the decline in lacunar density to be linear with age while Qiu *et al.* [67] found the decrease to be exponential. Alternatively Mori and colleagues [57], studying trabecular bone from the female femoral head, found that the decrease did not begin until 70 years of age, which was then followed by a sharp decline. Our previous study [81] found a non-significant reduction in lacunar density with age in women, while another study found significant reductions in females but not males [73].

Studies including lacunar descriptors beyond density have only recently begun to be conducted. Lacunar shape has been shown to parallel that of the cell body [209] allowing for description of large-scale morphological differences in the osteocyte lacunae utilizing high-throughput 3D x-ray based techniques. Isolated osteocyte cells in culture have a flexible, stellate morphology [210]; however, upon embedding in the extracellular matrix they are relatively flat ellipsoids parallel to the bone surface [200], with the majority of their cellular processes projecting perpendicular to the long axis of the bone [192]. McCreadie *et al* [23] have demonstrated that the shape of lacunae is an important determinant of the strains experienced by the osteocytes. In unloaded animal models, lacunar volume has been reported to decrease [130, 207]; conversely, lacunar volume increases with increased load [211]. When subjected to increased load, osteocytes become less round and flatter [207] and, similarly, low strain bony elements have smaller more spherical lacunae than high strain ones [17]. These previous studies

support the hypothesis that osteocytes adjust their lacunar morphology in reaction to their localized loading environment, enabling a regular osteocyte lacunar network to be able to efficiently transport fluid and accurately sense mechanical loads, consistent with its suggested role in mechanosensation.

The majority of human cortical and trabecular microarchitectural analyses have focused on women and senescent diseases including as osteoporosis and osteoarthritis [23, 24, 45, 53, 65]. Ideally, baseline information is needed on normal variation over the age-range from both sexes. Chapter 6 provided intriguing results demonstrating difference in osteocyte lacunar morphology, specifically a significant decrease in lacunar volume, associated with advancing age in women [81]. Those results raise the question of whether the same pattern exists in males. As such we set out to test the hypothesis that the differences we previously observed in lacunar parameters from women over the lifespan were sex-specific.

7.2 Materials and Methods

7.2.1 Specimens

Cross-sectional samples of cortical bone were obtained from the femora of 36 deceased men between the ages of 18 and 92, who had no known conditions that may have affected their bones. These femora come from the Melbourne Femur Collection held at the University of Melbourne, Melbourne, Australia and were collected during autopsy with the informed consent of the donor's next-of-kin. The study was conducted with ethical approval from the Victorian Institute of Forensic Medicine (EC26/2000), the University of Melbourne (HREC 980139) and the University of Saskatchewan (Bio # 08-46). Cuboidal sections with dimensions of ~2 x 2 x 5 mm were cut from the anterior mid-cortex of the proximal femoral shaft.

7.2.2 Synchrotron Radiation Micro-computed Tomographic Imaging (SR Micro-CT)

SR micro-CT scanning was conducted at the Advanced Photon Source (APS), Argonne National Laboratory, Il, USA, on beamline 2BM. Projection images were obtained using monochromatic x-rays with a photon energy of 27.9keV and an effective pixel size of 1.47μm. An exposure time of 100 milliseconds per frame was employed for each of 1800 frames spanning 180 degrees of rotation resulting in a scan time of approximately 9 minutes. The projection images were reconstructed to create a dataset containing 1841 slices (2016×900 pixels

each). This protocol differs from that used to obtain the scans for the females due to an optics setup issue at the beamline. While the energy stayed the same for both collections, the shorter exposure time and the use of continuous rotating frame collection for the male samples, allowed for shorter scan duration with a small reduction in scan height. This did not affect the thresholding and subsequent analysis of the scans.

7.2.3 3D Quantitative Morphometry

A cylindrical region of interest (ROI) with a diameter and height of 1.25 x 1.25 mm and a volume of 1.54 mm^3 was defined within each reconstructed image stack; this differs from the previous protocol used for the females whereby the ROI had a diameter and height of 1.5 mm and a volume of 2.65 mm^3 due to the reduction in the field of view. As per the previous protocol [80] lacunae and canals within this ROI were identified using a standardized global threshold for all specimens. Following thresholding, elements <10 μm^3 were assumed to be noise and were removed, additionally elements >2000 μm^3 were assumed to be canals, the rest were labeled as lacunae. These volume limits were based on confocal microscopy studies which determined human osteocyte lacunar volumes to range from 28–1713 μm^3 [23].

ROI's were cropped and analysis of the vascular porosity was conducted utilizing CT Analyzer 1.10.9.0 (SkyScan, Kontich, Belgium). Quantitative assessment of lacunar morphology was conducted using AMIRA 5.4.1 (Visage Imaging, Fuerth Germany) as previously described [80]. Standard nomenclatures for canal [97] and lacunar [81, 126] indices were used. The extracted parameters included: total canal volume for the ROI (Ca.V), canal volume fraction (Ca.V/TV) average canal diameter (Ca.Dm), total number of lacunae (N.Lc) and lacunar volume (Lc.V). In order to determine lacunar density per mm^3 (N.Lc/BV), bone volume (BV) was calculated as TV-Ca.V.

For morphology, the length of each lacunar axis was approximated by two times the EV of the covariance matrix (95% confidence interval). **Orientation** (Lc.Φ) of lacuna was measured by the absolute value of the angular deviation (-90º to 90º) of the axis of the first EV (longest) from the long axis of the sample. (0º = transverse; 90º = longitudinal). As previously described, three EV ratios were used to describe the degree of shape difference [80]. The **Degree of Equancy** (Lc.Eq) was defined by the ratio EV3:EV1 with one representing an object equal in the shortest and longest dimensions (e.g spherical). **Degree of Elongation** (Lc.El) was calculated

using 1- EV2:EV1, with one represents an elongated object. **Degree of Flatness** (Lc.Fl) was calculated as 1- EV3:EV2, where one represents a flat object.

7.2.4 Statistical Analyses

Statistical analysis was performed using SPSS 21.0.0 (SPSS Inc., Chicago, IL, U.S.A.). The individual values for N.Lc/BV and canal measures, along with averaged morphology parameters for Lc.V, Lc.Φ and shape (Lc.Eq, Lc.El, Lc.Fl) were examined in relation to age with linear regression. A comparison of the men grouped according to age: <50 and >50 years old was conducted with one-way ANOVA, with significance $\alpha < 0.05$. All of the measures were not normally distributed, as confirmed by Kolmogorov-Smirnov tests, thus the median as well as the average for each sample was calculated; while median results are included in the tables, for clarity only the average results are discussed unless the inclusion of median data changed the significance. A secondary analysis was conducted by including previously published data from Chapter 6 which utilizes the same region in women across the lifespan [81] with one-way ANOVA tests were compare all males and females and age-grouped sexes. Individual outliers were kept in the study, as previous analyses have demonstrated variation is normal and restricted to one or two variables. Additionally, the homogeneity of variance among the age-groups was tested by the application of Levene's test for equality of variances.

7.3 Results

The results of the linear regression analysis of the men over the lifespan are presented in Table 7.1. As expected Ca.V (p=0.001), Ca.V/TV (p=0.001) and Ca.Dm (p=0.004) increased with age. N.Lc/BV was negatively related to age (p=0.001). No difference was observed in Lc.V with age (p=0.650). An increasingly transverse orientation (Lc.Φ) with age noted (p=0.006). No significant relations were seen in EV1 (p=0.417), EV2 (p=0.225), and EV3 (p=0.605); however shape ratio differences were noted with lacunae becoming less elongated with age (p=0.007). A trend related to higher average Lc.Eq with age (p=0.054) was observed, which was significant in the median values (p=0.044). No significant relations were observed for Lc.Fl (p=0.367).

The results of the male age-grouped ANOVA are summarized in Table 7.2. Levene's test for equality of variances found that a number of parameters demonstrated significant variance between the age-groups, violating the underlying assumptions of the ANOVA, including: Ca.V,

Ca.V/TV, Ca.Dm, Ave and Med Lc.Eq and Med EV3; however, even when an assumption of unequal variances *t*-test for these parameters is included, the results were practically indistinguishable, producing no difference in conclusions regarding significance and therefore for simplicity were not included in this study. Again, Ca.V (p=0.002), Ca.V/TV (p=0.002), and Ca.Dm (p=0.012) were higher in the >50 age-group. N.Lc/BV values were significantly lower in the older age-group (p=0.040). Lc.V did not differ between the younger (247μm^3 ±38) and older (239μm^3 ±67) groups (p=0.730). The grouped data showed significant difference in orientation (Lc.Φ p<0.001). Average EV1 (p=0.212), EV2 (p=0.193) and EV3 (p=0.263) were not significantly different between groups, although this did differ for the median EV1 (p=0.048). Older individuals had less elongate (Lc.El p<0.001) and more equant (Lc.Eq p=0.014) lacunae than the younger individuals.

When compared to previously published data for microstructural parameters of the same cortical region for women (Table 7.2) [81], there was no difference in Ca.Dm or Ca.V/TV between the sexes (p=0.583, p=0.314) or matched age-group (<50 group p=0.791, p=0.612; >50 group p=0.716, p=0.428) respectively. No difference in N.Lc/BV was noted between the sexes in the younger group (p=0.272); however, older males had lower osteocyte density than the older female group (p=0.023). Lc.V was significantly larger in younger females than males (p=0.004), a difference not observed in the older aged sex groups (p=0.126) (Fig. 7.1). Lc.Φ demonstrated no sex-associated differences (p>0.05). No significant differences were seen between the sexes across the age groups in any of the lacunar shape parameters (p>0.05); however, when <50 and >50 age-groups were compared for both sexes, Lc.Eq median values demonstrated significant difference between the two younger groups (p=0.021), Lc.El was not significant for either age-grouped sex. Lc.Fl, however, was significantly lower in the younger males than females (p=0.002) and conversely, significantly higher in the >50 males versus females (p=0.011) (Fig. 7.2). While average EV1 was not different for either age-group, median EV1 was higher in the younger females than males. EV2 was greater in younger females versus males (p=0.004) and, in contrast, was reduced in the older female group compared to the age-matched males (p=0.004). Average EV3 was significantly lower in with age females than males (p=0.002) but not in median values (p=0.316). EV3 was not different between the younger sex-groups but was significantly reduced in the >50 females vs. males for the average (p=0.001) but not the median

values (p=0.292). Again, Levene's test for equality of variances found a number of parameters demonstrated significant variance including in the >50 group: Ca.Dm, Ca.V/TV, Med Lc.V, Med Lc.El, Ave and Med Lc.Fl, Ave and Med EV2; and in the >50 group: Ca.V/TV, Med Lc.V, Med Lc.Φ, EV2, Ave and Med EV3. Again, inclusions of an assumption of unequal variances produced no difference in conclusions regarding significance and are not included in this study.

Table 7.1 Average (Ave) and median (Med) results from the linear regression analysis of the morphological parameters of male osteocyte lacunae. *p<0.05.

	Ca.V (mm³)	Ca. V/TV (% ± sd)	a.Dm (µm)	N.Lc/BV (mm⁻³)	Ave Lc.V (µm³)	Med Lc.V (µm³)	Ave Lc.Φ (°)	Med Lc.Φ (°)	Ave Lc.Eq	Med Lc.Eq	Ave Lc.El	Med Lc.El	Ave Lc.Fl	Med Lc.Fl	Ave EV1	Med EV1	Ave EV2	Med EV2	Ave EV3	Med EV3
Result (± sd)	0.08 0.04	.622 3.06	6.96 22.79	22487 ±2816	244 ±54	233 ±62	59.49 ±4.30	66.72 ±4.98	0.17 ±0.03	0.14 ±0.03	0.67 ±0.04	0.72 ±0.05	0.40 ±0.06	0.43 ±0.07	13.14 ±2.18	11.26 ±2.09	3.30 ±0.45	2.83 ±0.44	1.61 ±0.07	1.48 ±0.07
R^2	.290	.289	.214	0.279	0.006	0.10	0.205	0.174	0.105	0.114	0.197	0.193	0.024	0.024	0.019	0.065	0.043	0.020	0.008	0.005
***P* alue**	001*	001*	.004*	0.001*	0.650	0.563	0.006*	0.011*	0.054	0.044*	0.007*	0.007*	0.367	0.372	0.417	0.134	0.225	0.406	0.605	0.686

Table 7.2 Average (Ave) and median (Med) results from the two-way ANOVA analysis of the morphological parameters of osteocyte lacunae grouped according to age and sex. *p<0.05

Group	*n*	Ca.V/TV (% ± sd)	Ca.Dm (µm ± sd)	N.Lc/BV (mm^{-3} ± sd)	Ave Lc.V (μm^3 ± sd)	Med Lc.V (μm^3 ± sd)	Ave Lc.Φ (° ± sd)	Med Lc.Φ (° ± sd)	Ave Lc.Eq (± sd)	Med Lc.Eq (± sd)	Ave Lc.El (± sd)	Med Lc.El (± sd)	Ave Lc.Fl (± sd)	Med Lc.Fl (± sd)	Ave EV1 (± sd)	Med EV1 (± sd)	Ave EV2 (± sd)	Med EV2 (± sd)	Ave EV3 (± sd)	Med EV3 (± sd)
Males <50	18	4.11 ±0.97	47.68 ±7.08	23443 ±2948	247 ±38*	237 ±47*	61.90 ±3.05	69.21 ±3.26	0.16 ±0.02	0.13 ±0.02*	0.69 ±0.03	0.75 ±0.04	0.39 ±0.05*	0.42 ±0.06*	13.60 ±1.90	11.95 ±1.57*	3.21 ±0.37*	2.74 ±0.35*	1.59 ±0.07	1.47 ±0.00
Females <50	14	3.86 ±1.82	46.70 ±13	24621 ±2955	298 ±53*	288 ±67*	60.00 ±4.21	67.14 ±4.77	0.16 ±0.02	0.12 ±0.02*	0.67 ±0.05	0.72 ±0.06	0.47 ±0.09*	0.51 ±0.11*	14.72 ±1.96	13.35 ±1.89*	3.76 ±0.63*	3.39 ±073*	1.58 ±0.05	1.47 ±0.00
***P* value**		0.612	0.791	0.272	0.004*	0.016*	0.150	0.155	0.329	0.021*	0.68	0.115	0.002*	0.004*	0.112	0.029*	0.004*	0.002*	0.599	1.00
Males >50	18	7.13 ±3.68	66.24 ±28.93	21531 ±2387*	241 ±67	229 ±75	57.08 ±4.06	64.23 ±5.23	0.19 ±0.03	0.15 ±0.03	0.65 ±0.04	0.70 ±0.05	0.41 ±0.06*	0.44 ±0.07*	12.68 ±2.39	10.58 ±2.34	3.40 ±0.50*	2.91 ±0.51*	1.62 ±0.07*	1.50 ±0.10
Females >50	16	9.19 ±6.32	70.35 ±36	23347 ±1998*	211 ±38	195 ±37	58.97 ±2.65	66.30 ±2.85	0.20 ±0.03	0.15 ±0.02	0.66 ±0.03	0.72 ±0.04	0.36 ±0.05*	0.38 ±0.06*	11.51 ±1.62	10.28 ±1.53	2.95 ±0.29*	2.51 ±0.30*	1.54 ±0.03*	1.47 ±0.00
***P* value**		0.428	0.716	0.023*	0.126	0.118	0.127	0.168	0.256	0.761	0.424	0.204	0.011*	0.016*	0.110	0.671	0.004*	0.009*	<0.001*	0.292

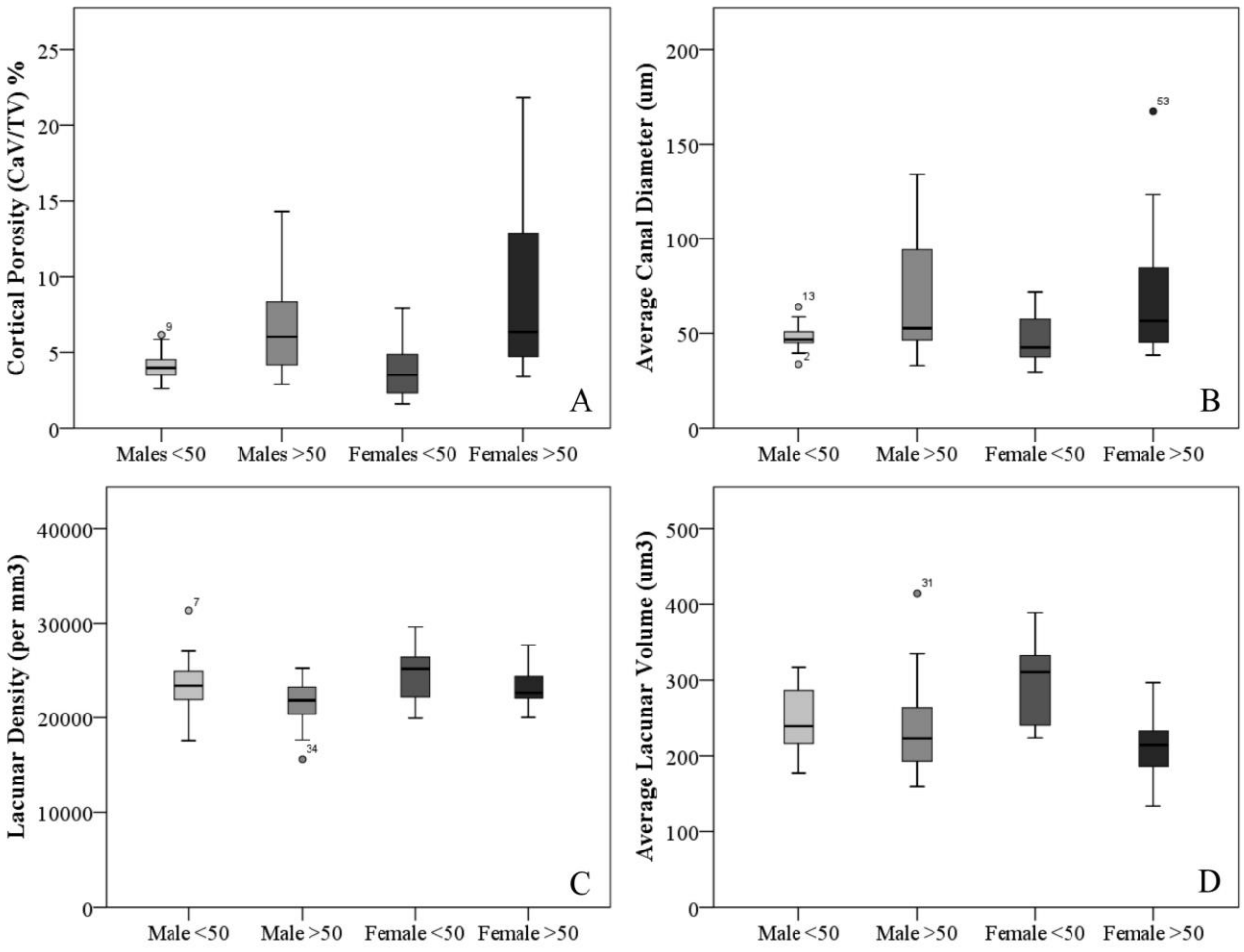

Figure 7.1 Box and whisker plots with values representing the percentage of canal volume per ROI for each individual grouped according to sex and age (A), average canal diameter (μm)(B) average osteocyte lacunar density per mm^3 (C) and average lacunar volume (μm^3)(D).

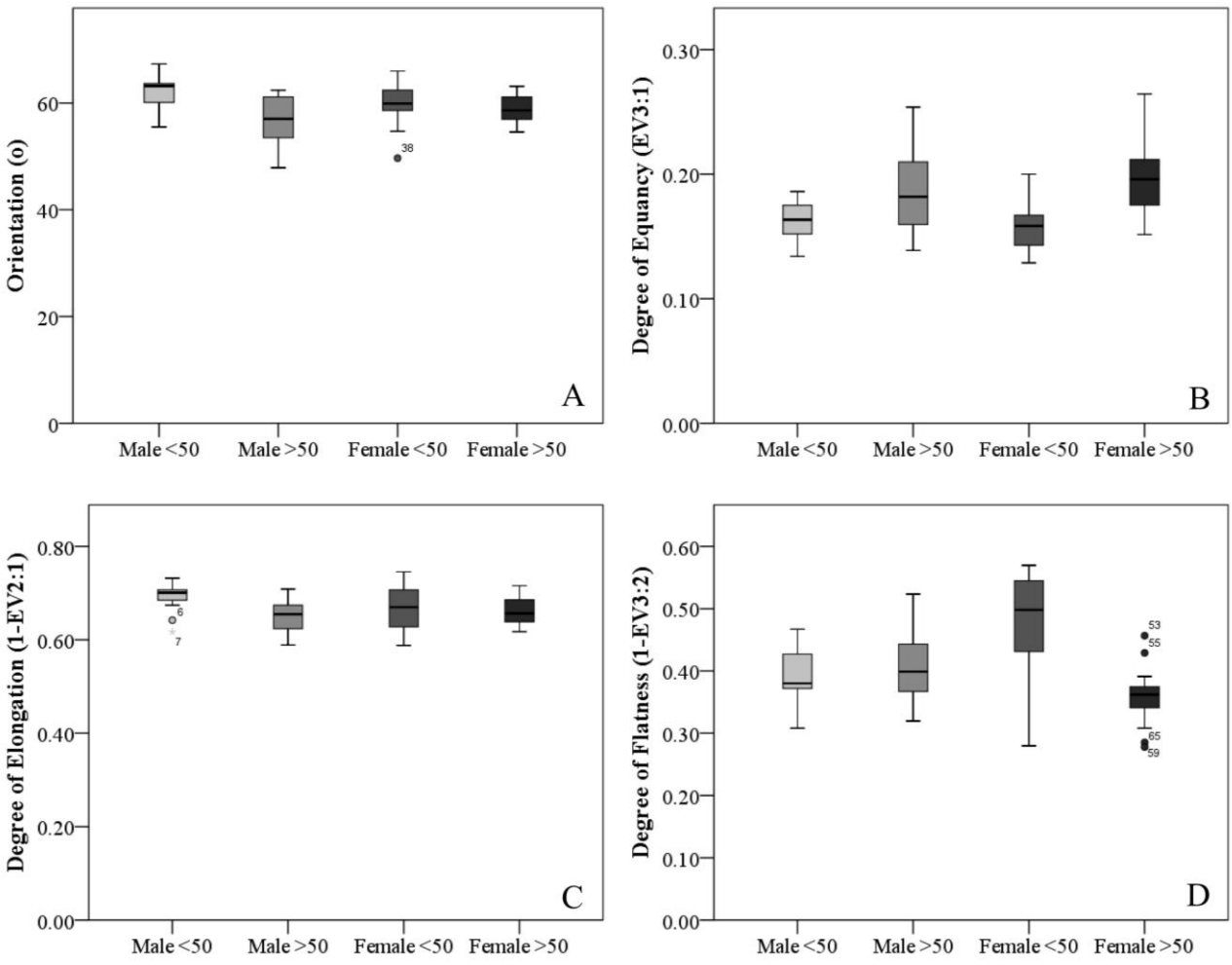

Figure 7.2 Box and whisker plots with values representing the average osteocyte shape for each individual. Measures of morphology include: orientation with respect to long axis of the sample (°)(A), degree of equancy (B), degree of elongation (C) and degree of flatness (D).

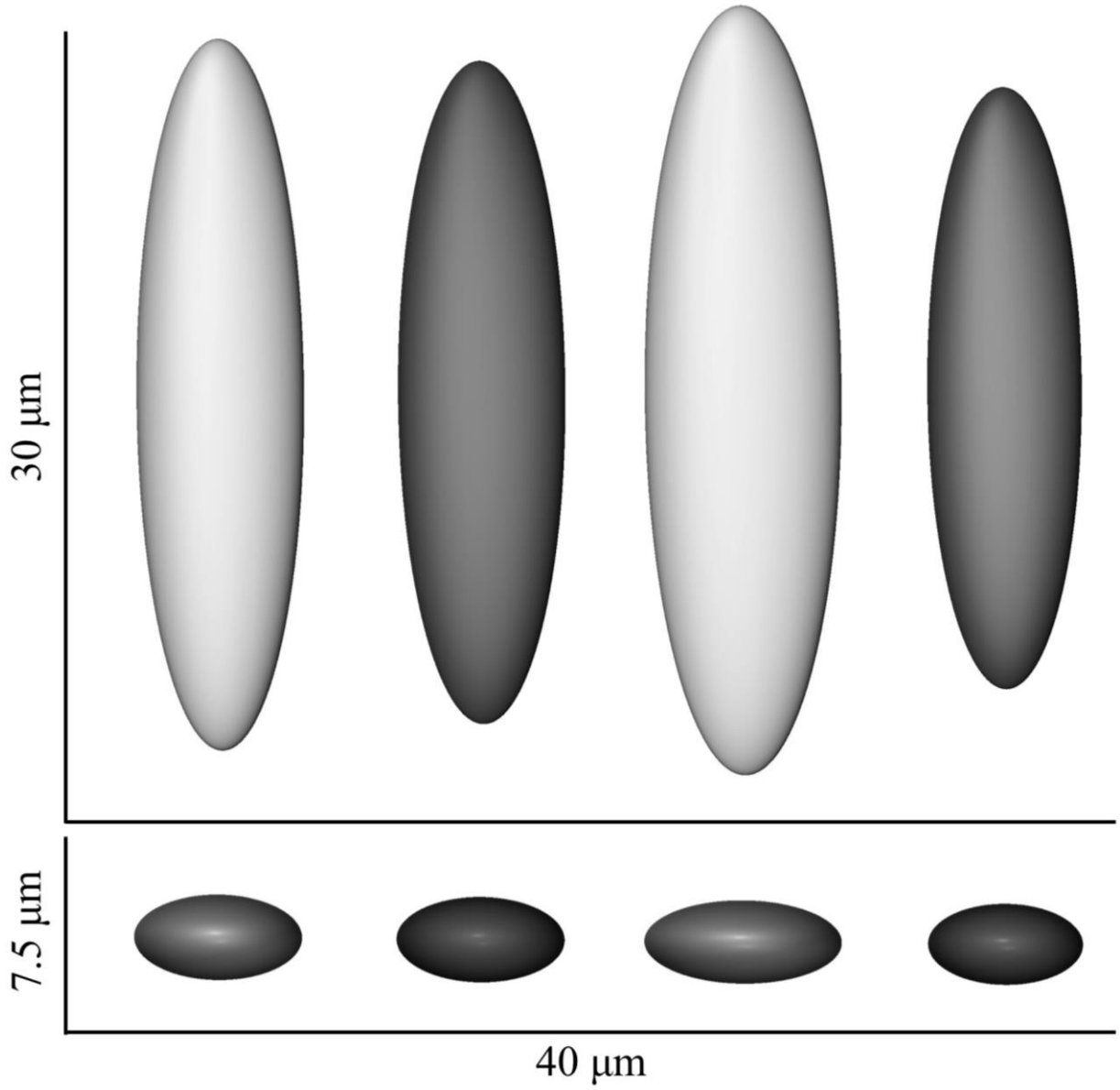

Figure 7.3 3D model of the average lacunar size and shape for the under and over 50 age groups of both sexes.

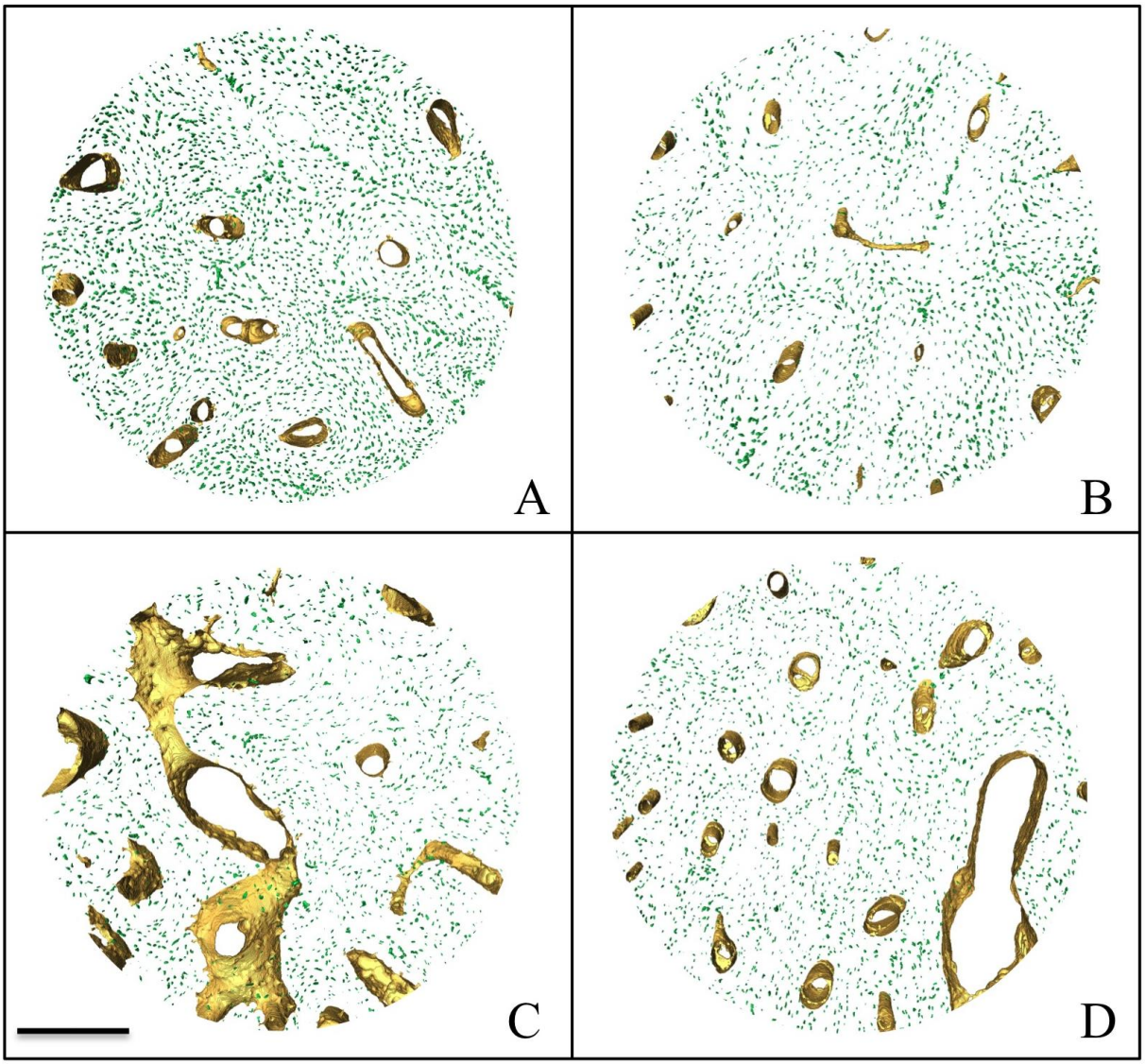

Figure 7.4 Renders demonstrating the sex-based differences in lacunar morphology, the reduced osteocyte lacunar density and increased porosity with age. A. 3D render of a 100µm section from a 20-year-old male. B. 3D render of a 100µm section from a 22-year-old female. C. 3D render of a 100µm section from an 87-year-old male. D. 3D render of a 100µm section from an 86-year-old female Scale bar = 300µm.

7.4 Discussion

Investigation of bone microstructure from healthy individuals over the human lifespan is vital to understanding the differential skeletal reactions to aging between men and women. To our knowledge this paper is the first to report differences in multiple lacunar parameters in 3D in male cortical bone with age. Previously reported reductions in lacunar volume associated with age in women [81], were not observed in males, although both sexes have a tendency towards more equant (spherical) lacunae as they age (Fig. 7.3). In addition this study provides a more definitive picture of normal variation in men over the human lifespan.

The human femoral shaft undergoes macro-morphological changes in response to the functional and postural changes associated with age, becoming larger and more circular with a slight shift to the anterior [161]. While most researchers agree that vascular porosity increases with age, the extent and timing of this increase is debated and evidently closely related to sex, with older women generally having greater porosity [3, 139, 162, 208, 212, 213]. The current results agree with these previous studies, in that men demonstrate canal diameter and vascular porosity increases with age (Fig. 7.4); however, when compared to the previously reported values for women from the same bone region, this phenomenon appears no less pronounced, which is unexpected and may be compounded by the limitations of the methodology used here. In order to gain resolution sufficient to examine the morphology of the lacunae, the region of interest examined was limited to ~2mm^3 taken from the mid-cortical region. Additionally, this study was restricted to the anterior mid-cortex, an area which consistently exhibits high porosity and bone loss in both sexes [139, 161]. These factors, coupled with overall cortical thinning in the older individuals, results in the field of view being positioned closer to the periosteum. Canal diameter in older women with high vascular porosity has been shown to be characterized by 'giant' canals often with diameters >385 μm [212] which coalesce on the endosteal surface, a region which is more likely to be captured in a larger field of view. Also a potential confounder, we note the beam height here was shorter than that used previously, resulting in a smaller field of view

This study showed that men demonstrate a significant decrease in lacunar density with age, which concurs with the literature [64, 66, 73]. Interestingly no significant difference was

noted in lacunar volume with age or between age-groups. The males studied here demonstrate differences in lacunar orientation becoming less longitudinal with age. In our previous study of the same region in females, no significant difference in lacunar orientation was seen [81]. Previous studies have reported change in the orientation of cells *in vitro* in response to differential mechanical stress [214, 215], and Currey [216] suggested that the stress concentrations noted in osteocyte lacunae are in part relieved by their specific orientation. What effect changes in lacunar orientation might have on the mechanical environment for the encased cell has not been studied. The orientation difference noted here may represent sex-based differences in mechanical loading or posture with age. Alternatively it may suggest a breakdown in the adaptive mechanosensation process with age.

External mechanical forces have been shown to influence osteocyte cytoskeletal structure and therefor lacunar shape [43]. Differential lacunar morphology can occur during initial embedding of the cell in bone and over the life of the cell through adaptation of the lacunar lining. In all bone tissue types, the lacuna is lined with a thick layer of loosely arranged collagen fibres known as the perilacunar matrix [217]. Normally this non-mineralized zone allows for strain-derived interstitial fluid flow over the cell's surface and provides a pathway for the nutrient supply and waste removal essential to the cell's metabolic survival [4]. Recent studies have shown that the osteocyte is able to adapt this pericellular region according to its requirements, both mechanical and physiological [165, 200, 218].

As seen here, the lacunae of males become more equant and less elongated with age. These shape differences are due to a decrease along the largest and intermediate axes; additionally, as lacunar density decreases, the lacunae become more spherical. Conversely, studies in mice have shown that as osteocytes mature they develop a flatter more 'spindle' like shape [43, 192]. Finite element models have shown higher strains in elongated lacunae [23], such as those seen in the younger males, and longer thinner cells have higher maximum strains [219]. This suggests that elongated cells are better adapted for reacting to and surviving higher strain forces such as those experienced by younger individuals. *In vitro* studies have shown that rounder osteocytes are more sensitive to weak mechanical stresses [193] and are able to maintain their physiological functions under lower loading conditions [17].

Changes in osteocyte lacunar size and shape have been linked to the differing mechanical environments experienced with disease [24]. In a recent study, Carriero *et al.* [220] suggest that the similar pattern of more equant and less elongated lacunae seen in osteogenesis imperfecta mice models are related to high rates of bone turnover, rather than strict mechanical environment. This high bone turnover would then reduce the opportunity for osteocytes to align along the principal axis of loading. Metz and colleagues [16] postulate that osteocytes actively inhibit refilling of their lacunae and such differential mineralisation on the boundaries could be caused by osteocyte dysfunction or, alternatively, may be an adaptation strategy of the cell to accommodate the changes in mechanical loading which accompany age.

The surface area of the osteocyte lacunar network is several orders of magnitude greater than that of the vascular porosity [198], thus removal or addition of a small amount of mineral surface area per lacuna could have significant effects on circulating systemic ion levels, interstitial fluid flow pressures, bone stiffness and strength [41]. This may provide a mechanism whereby the osteocyte can fine-tune its environment to remain within optimal functional parameters for local bone tissue strains and may act to control the signal sensed by the osteocyte. Whether the shapes of lacunae are passive by-products of the biomechanical environment or active response will require studies of animal models allowing the analysis of longitudinal changes in lacunar parameters.

Variations in the size, shape and number of lacunae will lead to non-uniform strain distributions [221]. Experiments by McCreadie et al. [23] demonstrate that lacunar shape is vital in determining deformation of the cell body related to questions of fluid flow, shear stress and streaming potentials. Predictive models generally use idealized lacunar size, shape and regular spatial density, which leads to underestimation of stresses [222]. Local differences in perilacunar tissue stiffness results in significant differences in predicted perilacunar strains [221]. Local hypermineralization makes bone more brittle [189] allowing it to crack more easily. In addition lacunae act as stress risers with microcracks initiating at their surfaces [59]. Together these factors can be expected to make bone more susceptible to fatigue damage and eventually failure in the form of fracture [189]. Colopy *et al.* [223] suggest that the number of dendritic cell processes that experience load may determine osteocyte response and influence targeted remodeling; therefore, differences in osteocyte lacunar shape can be expected to result in

differing strain magnitudes in the osteocyte body and bone matrix under the same mechanical loads.

Much of the research regarding sex differences in bone microstructural properties has focused on women, in large part due to the higher prevalence of certain senescent diseases, particularly osteoporosis. By incorporating data on the lacunar parameters of women over the age span previously published by this group [81], a number of sex-based differences in the lacunae of human cortical bone are noted. In the current study, males demonstrate a significant decrease in lacunar density with advancing age, although no difference in lacunar volume, with the volumes of the younger and older males more closely resembling those of the older females. Previous studies have reported lacunar density to be higher in healthy females than males [45, 66], with an age-related decline in both sexes [57, 64-66]. The results of this study showed that younger males and females had similar osteocyte densities; which were significantly lowered with age in males, resulting in older females having higher osteocyte lacunar densities than males. The females; however, did demonstrate a trend towards lower lacunar density with age and the inclusion of more samples representing middle age may have strengthened these findings. As previously reported, the lacunae of younger women were approximately 30% larger in volume, and were flatter and less equant than their older counterparts [81]. Lacunar volume of young females was larger than that of both male age-groups. EV2 was larger in younger females versus males and, in contrast, was greatly reduced in the older female group. This lead to a shape difference exhibited in younger males having flatter lacunae than females and conversely, significantly less flat lacunae in the over 50 males versus females. Interestingly, a recent study by Dong *et al.* [199] found more anisotropic (equivalent to less equant) lacunae with longer principal axis ratio to smallest in high porosity regions of female bone. Also of note here is the greater variation seen with age in both sexes, as evidenced by the results of the Levene's test for equality of variances. Although variation is natural, it must be taken into account and becomes even more important when discussing age and pathologically related changes.

One of the major questions raised by the results presented here, is why the lacunae of the younger men and women are dissimilar? In males we saw no significant difference in volume with age; however, osteocyte lacunae in young males were smaller than those of young females so that the observed reduction in osteocyte lacunar volume in older women results in the older

ages of both sexes having approximately the same volumes. This suggests that osteocytes are embedded in the bones of young women in a larger osteocyte network with the same number of osteocytes but with a much greater surface area, which we suggest may be better optimized for the mineral requirements of child bearing and lactation. As previously noted, osteocytes are capable of adapting their perilacunar environment. After parathyroid hormone (PTH) injection, osteocytes enlarged their lacunae [200] while in microgravity environments osteocyte lacunae can become infilled with collagen fibres extensions [218]. In mice, the perilacunar matrix is removed in pregnant animals during lactation and replaced post weaning [165], suggesting that the osteocyte lacunar network can act as a nutrient storage center when needed and plays a role in bone mineral homeostasis. This is particularly relevant for women who have the increased metabolic requirements of childbearing and breastfeeding. It may be this adaptation of the LCN that explains the sex-based differences seen in lacunar volume demonstrated here.

While we suggest that some new osteocytes deposited in remodeled bone of women as they age must be incorporating smaller lacunae, a concurrent process must be reducing the volume of existing lacunae. We previously proposed perilacunar hypermineralization or 'infilling' as a potential mechanism for reducing previously embedded osteocyte spaces. Intriguingly, this hypothesis is supported by a recent study by Milovanovic and colleagues [224], which provides evidence for reduction of the LCN; they noted a 30% reduction in canaliculi numbers with tissue age in human cortex specimens of unspecified sex. Moreover, utilizing energy dispersive x-ray microanalysis of osteon specific Ca/P ratio, reflecting tissue age, demonstrated canaliculi number was inversely related to osteon age. While they were unable to measure canalicular volume or morphology, this suggests that a reduction or infilling of the LCN occurs with age in humans, which would affect the integrity of the system and diminish the pathways for fluid flow and their respective nutrition/waste transportation. The sex bias of this mechanism may be related to the larger initial lacunar space found in young women versus young men; however, the exact cause of this loss of connectivity and its impact on the health of the cell and its capacity for mechanosensation are, as yet, unknown. Even if mechanical loading was to remain static across both sexes with aging, the diminished lacunar populations, coupled with potential reductions in lacunar network capacity, could be responsible for a reduction in mechanosensation and transduction vital to bone maintenance. The sex-based differences in the

LCN identified here for the first time may be key to understanding the differential effects of age-related bone loss and fractures which inequitably affect women. It must be noted; however, that due to the cross-sectional nature of this study we are limited in that we can only infer and not demonstrate that infilling of the osteocyte lacunar network is a process which occurs gradually with age.

Revealing the lacunar density and morphological parameters of normal healthy aging human bone is essential for an accurate understanding of bone microstructure and age-based pathology susceptibility. While lacunar density alone may describe the expanse of bone's cellular network, without inclusion of morphological descriptors this remains an incomplete picture of the function and integrity of the system on which to base future studies of physical and pharmaceutical interventions as well as biomechanical modeling. Additionally, lacunar morphology reflects aspects of bone's properties as a material structure. Although much research has focused on relating osteocyte lacunar density to determining quality of bone [45, 56, 67], several recent studies have questioned whether lacunar density truly correlates with parameters of balanced bone modeling and remodeling [1, 44, 225]. This study is the first to demonstrate major differences in lacunar parameters of men over the age span. Either by direct effect on mechanical properties or by modifying mechanosensitvity control of remodeling (i.e. [41, 59, 204, 226], differences in lacunar morphology, abundance and connectivity could have important implications for the osteocyte network's ability to receive and respond to localized loading information which is the mechanism by which bone deposition and removal are regulated [221]. Whether due to lower loading experienced naturally as a physiological function of age or to the decreased signal from reduction in lacunar density, it would seem the osteocyte lacunae for males undergoes large-scale modification with age.

7.5 Conclusion

This chapter presents the results of the visualization and quantification of osteocyte lacunar density and morphology in the proximal shaft cortical bone of human males over the age span and compares them to the results generated in Chapter 6 from the same region in women. Due to the preferential bias of bone loss against women it is important to define potential sex-differences in bone microstructure. This chapter has shown that the osteocyte lacunar system of

young men and women are significantly different from each other but become more similar with age, identifying for the first time, differences between the bones of men and women at a cellular level.

CHAPTER 8: CONCLUSION

8.1 Introduction

The goal of this dissertation was to contribute a greater understanding of the sex and age-based differences in the lacunae of human cortical bone. Relative to the vascular porosity, little is known regarding the abundance and morphology of the osteocyte lacunae; this area is currently seeing a surge in interest regarding how cellular properties potentially relate to adaptation, disease and aging. This focus has, at least in part, arisen from the availability of increasingly high-resolution imaging modalities which for the first time allow visualization and quantification of lacunae in three-dimensions. By utilizing SR micro-CT and novel morphometric techniques, the studies here have been able to quantify not only normal variation but also for the first time identify age-based difference between the cortical microarchitecture of men and women.

8.2 Overview

In Chapter 1 the rationale for the dissertation was laid out and examined within the context of the literature. Chapter 2 examined the current methodology in use for imaging and quantifying the lacunar network. Chapter 3 discussed preliminary experiments which determined that SR micro-CT was more successful than a desktop source for visualizing lacunae. Additionally, not all synchrotrons and their beamlines are equal and it was determined that, for the purposes of this research, the 2BM beamline at the Advanced Photon Source, Il, USA (APS), was best suited to our imaging requirements.

Chapter 4 presented a new technique for quantifying osteocyte lacunar density, morphology and orientation in 3D, on an unprecedented scale and applied this to multiple bone samples from a single healthy young individual. This study found intra-element variation in lacunar density of up to 30% with lower density associated with the anterior and posterior regions. Additionally, a varied pattern in lacunar morphology was noted, with more elongate shapes also associated with the anterior and posterior aspects. The underlying functional significance of the observed variation was suggested to relate to localized variations in loading conditions as the pattern corresponds well with mechanical axes. This chapter has been

previously published in *BONE* [80] and has been reprinted with the permission of Elsevier, Inc. (see appendix C).

Based on the results of Chapter 4, Chapter 5 tested the hypothesis that lacunar parameters are different in normal healthy humans dependent on the anatomical region from which they are examined. While providing a more robust baseline for descriptions of normal anatomy in healthy young males, the findings also again demonstrated high variation in lacunar properties dependent on region. These findings are vital to future examinations of human bone microstructure, providing the context of normal variation for the functional and pathological interpretations drawn from these. This chapter has been previously published in the *Journal of Anatomy* and has been reprinted with the permission of Wiley & Sons. (see appendix C).

Chapter 6 examined the effect of aging on the human lacunar properties in the proximal shaft femoral cortical bone of 30 women over the age span. Changes in lacunae with age are of particular interest in women since they are more susceptible to bone loss and fragility associated with senescent diseases including osteoporosis. Intriguingly, while only a non-significant relation between lacunar density and age was detected, a significant reduction in lacunar volume with age was observed. Concomitantly, younger women were demonstrated to have flatter and less equant (spherical) lacunae. To my knowledge the observation of lacunar volume and morphology differences over the human lifespan is novel, potentially resulting from preferential surface infilling within the extracellular space. The functional impact of this infilling is unclear but such a change in scale likely impacts the mechanosensing function of the osteocyte network. The content of this chapter has been previously published in the *Journal of Structural Biology* [81] and has been reprinted with the permission of Elsevier, Inc (see appendix C).

Following the unanticipated results of Chapter 6, Chapter 7 undertook a large-scale study of samples from 36 men to determine if the males exhibited the same age-related changes in microstructure. A secondary analysis incorporating the previously published female data was conducted in order to examine the extent of sex-based differences. The males, in contrary to the females, did have significant osteocyte lacunar density decline with age; however, no difference was found in lacunar volume. Interestingly, osteocyte lacunae in young males are smaller than those of young females so that the observed reduction in osteocyte lacunar volume in older women results in the older ages of both sexes having approximately the same volumes. This

suggests that osteocytes are embedded in the bones of young women in a larger lacunar network possibly incorporating more canaliculi.

8.3 Future Directions

The alternative imaging modalities experimented with in Chapter 3 showed promise and deserve future analysis. Desktop-based micro-CT has obvious potential for analyzing lacunae. Although primarily limited by resolution, some images were clear while others were plagued with artifacts and low signal-to-noise ratio, limiting the visible structures. A major benefit of desktop systems is their availability, which leads to greater potential for larger studies. Future work should focus on determining the causes of the high variation seen among individual scans. It is interesting to note that the changes in lacunar volume among the samples demonstrated here (i.e. the effect of sex and age) may provide a possible issue contributing to this variability. Additionally, higher resolution systems including so-called nano-CT should be explored.

SR micro-CT at the BMIT beamline of the Canadian Light Source still needs to be optimized in order to attain the resolution and signal necessary to allow clear visualization of the morphology of the lacunae. A new system custom built by SkyScan with a submicron voxel size has been commissioned at BMIT; preliminary scans suggest that, used in combination with the pink beam, it may afford the opportunity to achieve human lacunar analysis in density and morphology at a facility within Canada (see Fig 3.7), reducing the issues and costs associated with traveling with samples of human remains. Additionally, future development at BMIT includes the opening of the insertion device (ID) beamline for user access. The energy range on this beamline is 20-100 keV, perfect for bone samples, and will allow higher-flux imaging in less time; however resolution is still limited and experimentation will be required to determine if imaging is possible with the current configuration or will require additional optics.

The novel techniques developed for visualizing and measuring lacunae utilizing SR micro-CT could be used for additional projects studying human lacunar parameters, particularly with regard to questions of biomechanics and pathology. Additionally, terrestrial animals, including many models of human health, generally have similar sized lacunae and this setup could be adapted to multispecies analyses. The technique utilized in this dissertation has excellent potential for use in preclinical studies of pharmaceutical interventions such as human

parathyroid hormone (PTH), estrogens, bisphosphonates, and other drugs which are known to affect bone structure and mass [227]. Studies utilizing animal models, allowing for direct testing of the effects of these drugs on cortical bone and the remodeling processes they elicit, will help to elucidate the mechanisms by which these drugs act. This is particularly timely due to growing concerns over side-effects linked to bisphosphonate treatment of osteoporosis and experimental evidence linking these drugs to a negative impact on the LCN [228, 229].

One of the greatest challenges for the studies described here was the restricted access to human specimens and synchrotron beamtime. The discovery of intra-element variation in lacunar parameters in healthy young men is intriguing and its ties to mechanical and functional axes deserve further exploration. It is important to include samples from the bones of women as this study has clearly demonstrated differences in cortical microarchitecture between the sexes. In order to accurately map these variations a dedicated project would be required with a large number of multiregional human samples and sufficient beamtime. Additionally it may be easier to answer questions regarding the links between variation in osteocyte lacunar parameters and biomechanical environment if models of the biomechanics in the human proximal shaft were included and perhaps even mechanical testing of the same specimens.

While this dissertation was able to demonstrate differences in lacunar density and morphological parameters it was only able to do so on the scale of a single region of interest. Also valuable would be an analysis of the spatial geography of lacunar abundance and shape parameters in relation to each other and other microstructural features including; osteonal borders, vascular canals and lamellae. Of particular interest are the functional units of remodeling, the Basic Multicellular Units (BMU's), providing the mechanism for the removal and embedding of osteocytes. Description of lacunar parameters in situ around BMU's, at the front lines of bone maintenance as it were, may help to answer questions regarding the relation between remodeling and the mechanosensation/transduction systems.

This dissertation, by providing a more definitive picture of normal variation in lacunar geometric measures between men and women over the human age span, enables better context for drawing inferences with regard to age, disease and biomechanics and is highly relevant to future computational modeling of the normal osteocyte and its mechanical environment. Future work should focus on removing the concept of the 'idealized" lacunae from mathematical

modeling and integrating the novel microstructural data noted here into a multiscale model of the bone porosity, applicable to studies of fluid-flow mechanics and loading environment.

This dissertation provided the most robust evidence available for sex and age-based differences in the cellular organization of human bone. To my knowledge the observation that lacunar volume and morphology change over the human lifespan is novel, potentially resulting from preferential surface infilling within the pericellular space. The functional impact of the suggested infilling is unclear but such a change in scale likely impacts the mechanosensing and transduction function of the osteocyte network.

Future studies should focus on expanding the current study with more samples representing the middle age of both sexes in order to better identify the scale and timing of the sex differences discovered. Studies should specifically focus on the timing of the lacunar infilling, as a sharp decline later in life for females would suggest a possible link to menopause whereas a continuous decline over the lifespan would suggest other mechanisms are at play.

One major limitation of the technique described in this thesis is the ratio of field of view to image resolution. In order to visualize a sufficient number of lacunae to be biologically and statistically relevant some resolution was sacrificed. Therefore, the canaliculi connecting the lacunar network were unable to be visualized. As such, we could not determine if this process of infilling by mineralization was associated with occlusion of canaliculi. This hypothesis warrants further investigation as, if confirmed, it would represent a profound negative impact on the osteocyte network connectivity and may provide new insights into age-related bone loss and failure.

Due to the technological restrictions, this study was inherently limited to cross-sectional analysis. It is not currently possible to visualize the cellular level microstructure of bone in living organisms. Ideally, studies in the future will be able to move from description of difference to those of change, to characterize the process of lacunar aging, and determine whether the pericellular infilling hypothesized here is occurring with time, where and how. In the end, the increased interest in scientific inquiry regarding the role of the LCN and its impact on bone health can only but be assisted by more and better studies of the lacunar morphology on a large scale and in 3D.

8.4 Conclusion

This dissertation has demonstrated an effective SR μCT protocol for imaging lacunar parameters in cortical bone. It has recognized that the range of normal variation in humans is high, often past that of previous studies of pathology, implying that caution must be taken when inferring the effect of pathology on the cortical bone lacunae and cautioning the importance of strict protocols to restrict the areas sampled between specimens. Given the significance of osteocytes in the maintenance of bone health, it is remarkable that so little is known regarding the osteocyte lacunae. Other than a few largely qualitative studies, virtually nothing is known regarding differences in lacunar parameters between the sexes and across the human lifespan. The most important contribution of this thesis is the identification, for the first time, of differences in osteocyte lacunar parameters with age between men and women. The preferential bias of bone disease such as osteoporosis against women makes the discovery of larger osteocytes being embedded in young women which appear to infill with age, all the more important to explore further.

LIST OF REFERENCES

[1] Skedros JG, Grunander TR, Hamrick MW. Spatial distribution of osteocyte lacunae in equine radii and third metacarpals: considerations for cellular communication, microdamage detection and metabolism. Cells, tissues, organs 2005;180: 215-36.

[2] Currey JD. Bones : structure and mechanics. Princeton, NJ: Princeton University Press; 2002.

[3] Cooper DM, Thomas CD, Clement JG, Turinsky AL, Sensen CW, Hallgrimsson B. Age-dependent change in the 3D structure of cortical porosity at the human femoral midshaft. Bone 2007;40: 957-65.

[4] Busse B, Djonic D, Milovanovic P, Hahn M, Puschel K, Ritchie RO, Djuric M, Amling M. Decrease in the osteocyte lacunar density accompanied by hypermineralized lacunar occlusion reveals failure and delay of remodeling in aged human bone. Aging cell 2010;9: 1065-75.

[5] Kamioka H, Honjo T, Takano-Yamamoto T. A three-dimensional distribution of osteocyte processes revealed by the combination of confocal laser scanning microscopy and differential interference contrast microscopy. Bone 2001;28: 145-9.

[6] Johnson LC. The kinetics of skeletal remodeling in structural organization of the skeleton. Birth Defects 1966: 66–142.

[7] Jowsey J. Studies of Haversian systems in man and some animals. J Anat 1966;100: 857-64.

[8] Frost HM. Bone "mass" and the "mechanostat": a proposal. Anat Rec 1987;219: 1-9.

[9] Cooper DM, Matyas JR, Katzenberg MA, Hallgrimsson B. Comparison of microcomputed tomographic and microradiographic measurements of cortical bone porosity. Calcified tissue international 2004;74: 437-47.

[10] Rodan GA, Martin TJ. Therapeutic approaches to bone diseases. Science 2000;289: 1508-14.

[11] Robling AG, Castillo AB, Turner CH. Biomechanical and molecular regulation of bone remodeling. Annu Rev Biomed Eng 2006;8: 455-98.

[12] Frost HM. Bone remodelling dynamics. Springfield, Ill.,: Thomas; 1963.

[13] Havill LM, Allen MR, Harris JA, Levine SM, Coan HB, Mahaney MC, Nicolella DP. Intracortical bone remodeling variation shows strong genetic effects. Calcif Tissue Int 2013;93: 472-80.

[14] Sissons HA, O'Connor P. Quantitative histology of osteocyte lacunae in normal human cortical bone. Calcif Tissue Res 1977;22 Suppl: 530-3.

[15] Hobdell MH, Howe CE. Variation in bone matrix volume associated with osteocyte lucunae in mammalian and reptilian bone. Isr J Med Sci 1971;7: 492-3.

[16] Metz LN, Martin RB, Turner AS. Histomorphometric analysis of the effects of osteocyte density on osteonal morphology and remodeling. Bone 2003;33: 753-9.

[17] Vatsa A, Breuls RG, Semeins CM, Salmon PL, Smit TH, Klein-Nulend J. Osteocyte morphology in fibula and calvaria --- is there a role for mechanosensing? Bone 2008;43: 452-8.

[18] Bonucci E. The osteocyte: the underestimated conductor of the bone orchestra. Rendiconti Lincei 2009;20: 237-254.

[19] Hannah KM, Thomas CD, Clement JG, De Carlo F, Peele AG. Bimodal distribution of osteocyte lacunar size in the human femoral cortex as revealed by micro-CT. Bone 2010;47: 866-71.

[20] Mullender MG, Huiskes R. Osteocytes and bone lining cells: which are the best candidates for mechano-sensors in cancellous bone? Bone 1997;20: 527-32.

[21] Vashishth D, Gibson G, Kimura J, Schaffler MB, Fyhrie DP. Determination of bone volume by osteocyte population. Anat Rec 2002;267: 292-5.

[22] Skedros JG, Hunt KJ, Hughes PE, Winet H. Ontogenetic and regional morphologic variations in the turkey ulna diaphysis: implications for functional adaptation of cortical bone. The anatomical record. Part A, Discoveries in molecular, cellular, and evolutionary biology 2003;273: 609-29.

[23] McCreadie BR, Hollister SJ, Schaffler MB, Goldstein SA. Osteocyte lacuna size and shape in women with and without osteoporotic fracture. Journal of biomechanics 2004;37: 563-72.

[24] van Hove RP, Nolte PA, Vatsa A, Semeins CM, Salmon PL, Smit TH, Klein-Nulend J. Osteocyte morphology in human tibiae of different bone pathologies with different bone mineral density--is there a role for mechanosensing? Bone 2009;45: 321-9.

[25] Bonewald LF, Johnson ML. Osteocytes, mechanosensing and Wnt signaling. Bone 2008;42: 606-15.

[26] Knothe Tate ML, Adamson JR, Tami AE, Bauer TW. The osteocyte. The international journal of biochemistry & cell biology 2004;36: 1-8.

[27] Duncan RL, Turner CH. Mechanotransduction and the functional response of bone to mechanical strain. Calcif Tissue Int 1995;57: 344-58.

[28] Burger EH, Klein-Nulen J. Responses of bone cells to biomechanical forces in vitro. Adv Dent Res 1999;13: 93-8.

[29] Knothe Tate ML. "Whither flows the fluid in bone?" An osteocyte's perspective. J Biomech 2003;36: 1409-24.

[30] Han Y, Cowin SC, Schaffler MB, Weinbaum S. Mechanotransduction and strain amplification in osteocyte cell processes. Proc Natl Acad Sci U S A 2004;101: 16689-94.

[31] Malone AM, Anderson CT, Stearns T, Jacobs CR. Primary cilia in bone. J Musculoskelet Neuronal Interact 2007;7: 301.

[32] Fritton SP, Weinbaum S. Fluid and Solute Transport in Bone: Flow-Induced Mechanotransduction. Annu Rev Fluid Mech 2009;41: 347-374.

[33] Khosla S, Westendorf JJ, Oursler MJ. Building bone to reverse osteoporosis and repair fractures. J Clin Invest 2008;118: 421-8.

[34] Andrews JC, Almeida E, van der Meulen MC, Alwood JS, Lee C, Liu Y, Chen J, Meirer F, Feser M, Gelb J, Rudati J, Tkachuk A, Yun W, Pianetta P. Nanoscale X-ray microscopic imaging of mammalian mineralized tissue. Microscopy and microanalysis : the official journal of Microscopy Society of America, Microbeam Analysis Society, Microscopical Society of Canada 2010;16: 327-36.

[35] Klein-Nulend J, Nijweide PJ, Burger EH. Osteocyte and bone structure. Curr Osteoporos Rep 2003;1: 5-10.

[36] Bakker AD, Soejima K, Klein-Nulend J, Burger EH. The production of nitric oxide and prostaglandin E(2) by primary bone cells is shear stress dependent. J Biomech 2001;34: 671-7.

[37] Bakker AD, Klein-Nulend J, Burger EH. Mechanotransduction in bone cells proceeds via activation of COX-2, but not COX-1. Biochem Biophys Res Commun 2003;305: 677-83.

[38] Cowin SC, Weinbaum S, Zeng Y. A case for bone canaliculi as the anatomical site of strain generated potentials. J Biomech 1995;28: 1281-97.

[39] Schneider P, Meier M, Wepf R, Muller R. Towards quantitative 3D imaging of the osteocyte lacuno-canalicular network. Bone 2010;47: 848-58.

[40] Martin RB. Porosity and specific surface of bone. Crit Rev Biomed Eng 1984;10: 179-222.

[41] Yeni YN, Vashishth D, Fyhrie DP. Estimation of bone matrix apparent stiffness variation caused by osteocyte lacunar size and density. Journal of biomechanical engineering 2001;123: 10-7.

[42] Fyhrie DP, Vashishth D. Bone stiffness predicts strength similarly for human vertebral cancellous bone in compression and for cortical bone in tension. Bone 2000;26: 169-73.

[43] Sugawara Y, Ando R, Kamioka H, Ishihara Y, Honjo T, Kawanabe N, Kurosaka H, Takano-Yamamoto T, Yamashiro T. The three-dimensional morphometry and cell-cell communication of the osteocyte network in chick and mouse embryonic calvaria. Calcified tissue international 2011;88: 416-24.

[44] Robling AG, Turner CH. Mechanotransduction in bone: genetic effects on mechanosensitivity in mice. Bone 2002;31: 562-9.

[45] Mullender MG, Tan SD, Vico L, Alexandre C, Klein-Nulend J. Differences in osteocyte density and bone histomorphometry between men and women and between healthy and osteoporotic subjects. Calcified tissue international 2005;77: 291-6.

[46] Iwamoto J, Matsumoto H, Takeda T, Sato Y, Yeh JK. Effects of vitamin K2 on cortical and cancellous bone mass, cortical osteocyte and lacunar system, and porosity in sciatic neurectomized rats. Calcif Tissue Int 87: 254-62.

[47] Bonadio J, Jepsen KJ, Mansoura MK, Jaenisch R, Kuhn JL, Goldstein SA. A murine skeletal adaptation that significantly increases cortical bone mechanical properties. Implications for human skeletal fragility. J Clin Invest 1993;92: 1697-705.

[48] Li KC, Zernicke RF, Barnard RJ, Li AF. Differential response of rat limb bones to strenuous exercise. J Appl Physiol 1991;70: 554-60.

[49] Da Costa Gomez TM, Barrett JG, Sample SJ, Radtke CL, Kalscheur VL, Lu Y, Markel MD, Santschi EM, Scollay MC, Muir P. Up-regulation of site-specific remodeling without accumulation of microcracking and loss of osteocytes. Bone 2005;37: 16-24.

[50] Barros RR, Degidi M, Novaes AB, Piattelli A, Shibli JA, Iezzi G. Osteocyte density in the peri-implant bone of immediately loaded and submerged dental implants. J Periodontol 2009;80: 499-504.

[51] Verborgt O, Gibson GJ, Schaffler MB. Loss of osteocyte integrity in association with microdamage and bone remodeling after fatigue in vivo. J Bone Miner Res 2000;15: 60-7.

[52] Skedros JG, Dayton MR, Sybrowsky CL, Bloebaum RD, Bachus KN. The influence of collagen fiber orientation and other histocompositional characteristics on the mechanical properties of equine cortical bone. J Exp Biol 2006;209: 3025-42.

[53] Qiu S, Rao DS, Palnitkar S, Parfitt AM. Differences in osteocyte and lacunar density between Black and White American women. Bone 2006;38: 130-5.

[54] Martin RB. Is all cortical bone remodeling initiated by microdamage? Bone 2002;30: 8-13.

[55] Martin RB. Targeted bone remodeling involves BMU steering as well as activation. Bone 2007;40: 1574-80.

[56] Ma YL, Dai RC, Sheng ZF, Jin Y, Zhang YH, Fang LN, Fan HJ, Liao EY. Quantitative associations between osteocyte density and biomechanics, microcrack and microstructure in OVX rats vertebral trabeculae. Journal of biomechanics 2008;41: 1324-32.

[57] Mori S, Harruff R, Ambrosius W, Burr DB. Trabecular bone volume and microdamage accumulation in the femoral heads of women with and without femoral neck fractures. Bone 1997;21: 521-6.

[58] Soicher MA, Wang X, Zauel RR, Fyhrie DP. Damage initiation sites in osteoporotic and normal human cancellous bone. Bone 2011;48: 663-6.

[59] Reilly GC. Observations of microdamage around osteocyte lacunae in bone. Journal of biomechanics 2000;33: 1131-4.

[60] Voide R, Schneider P, Stauber M, Wyss P, Stampanoni M, Sennhauser U, van Lenthe GH, Muller R. Time-lapsed assessment of microcrack initiation and propagation in murine cortical bone at submicrometer resolution. Bone 2009;45: 164-73.

[61] Schaffler MB, Choi K, Milgrom C. Aging and matrix microdamage accumulation in human compact bone. Bone 1995;17: 521-25.

[62] O'Brien FJ, Brennan O, Kennedy OD, Lee TC. Microcracks in cortical bone: how do they affect bone biology? Current osteoporosis reports 2005;3: 39-45.

[63] Qiu S, Rao DS, Palnitkar S, Parfitt AM. Reduced iliac cancellous osteocyte density in patients with osteoporotic vertebral fracture. Journal of bone and mineral research : the official journal of the American Society for Bone and Mineral Research 2003;18: 1657-63.

[64] Mullender MG, van der Meer DD, Huiskes R, Lips P. Osteocyte density changes in aging and osteoporosis. Bone 1996;18: 109-13.

[65] Qiu S, Rao DS, Palnitkar S, Parfitt AM. Age and distance from the surface but not menopause reduce osteocyte density in human cancellous bone. Bone 2002;31: 313-8.

[66] Torres-Lagares D, Tulasne JF, Pouget C, Llorens A, Saffar JL, Lesclous P. Structure and remodelling of the human parietal bone: an age and gender histomorphometric study. Journal of cranio-maxillo-facial surgery : official publication of the European Association for Cranio-Maxillo-Facial Surgery 2010;38: 325-30.

[67] Qiu S, Rao DS, Palnitkar S, Parfitt AM. Relationships between osteocyte density and bone formation rate in human cancellous bone. Bone 2002;31: 709-11.

[68] Frost HM. Micropetrosis. J Bone Joint Surg Am 1960;42-A: 144-50.

[69] Vashishth D, Verborgt O, Divine G, Schaffler MB, Fyhrie DP. Decline in osteocyte lacunar density in human cortical bone is associated with accumulation of microcracks with age. Bone 2000;26: 375-80.

[70] Shimizu H, Sakamoto M, Sakamoto S. Bone resorption by isolated osteoclasts in living versus devitalized bone: differences in mode and extent and the effects of human recombinant tissue inhibitor of metalloproteinases. Journal of bone and mineral research : the official journal of the American Society for Bone and Mineral Research 1990;5: 411-8.

[71] NIH_Consensus_Panel. Osteoporosis prevention, diagnosis, and therapy. JAMA 2001;285: 785-95.

[72] Tarride JE, Hopkins RB, Leslie WD, Morin S, Adachi JD, Papaioannou A, Bessette L, Brown JP, Goeree R. The burden of illness of osteoporosis in Canada. Osteoporos Int 2012;23: 2591-600.

[73] Vashishth D, Gibson GJ, Fyhrie DP. Sexual dimorphism and age dependence of osteocyte lacunar density for human vertebral cancellous bone. The anatomical record. Part A, Discoveries in molecular, cellular, and evolutionary biology 2005;282: 157-62.

[74] Zarrinkalam MR, Mulaibrahimovic A, Atkins GJ, Moore RJ. Changes in osteocyte density correspond with changes in osteoblast and osteoclast activity in an osteoporotic sheep model. Osteoporosis international : a journal established as result of cooperation between the European Foundation for Osteoporosis and the National Osteoporosis Foundation of the USA 2011.

[75] Santos A, Bakker AD, Klein-Nulend J. The role of osteocytes in bone mechanotransduction. Osteoporos Int 2009;20: 1027-31.

[76] Seeman E. The growth and age-related origins of bone fragility in men. Calcif Tissue Int 2004;75: 100-9.

[77] Eriksen EF. Cellular mechanisms of bone remodeling. Rev Endocr Metab Disord 2010;11: 219-27.

[78] Bonewald LF. The amazing osteocyte. Journal of Bone and Mineral Research 2011;26: 229-238.

[79] Kelkar S. Characterization of the osteocyte lacunocanalicular network in normal and paget's disease bone and study of bone cell resistance to lowered pH. In: Oral Biology: University of Missouri-Kansas City; 2006.

[80] Carter Y, Thomas CD, Clement JG, Peele AG, Hannah K, Cooper DM. Variation in osteocyte lacunar morphology and density in the human femur--a synchrotron radiation micro-CT study. Bone 2013;52: 126-32.

[81] Carter Y, Thomas CD, Clement JG, Cooper DM. Femoral osteocyte lacunar density, volume and morphology in women across the lifespan. Journal of structural biology 2013;183: 519-26.

[82] Qiu S, Fyhrie DP, Palnitkar S, Rao DS. Histomorphometric assessment of Haversian canal and osteocyte lacunae in different-sized osteons in human rib. The anatomical record. Part A, Discoveries in molecular, cellular, and evolutionary biology 2003;272: 520-5.

[83] Marotti G. Osteocyte orientation in human lamellar bone and its relevance to the morphometry of periosteocytic lacunae. Metabolic Bone Disease and Related Research 1979;1: 325-333.

[84] Zehbe R, Haibel A, Riesemeier H, Gross U, Kirkpatrick CJ, Schubert H, Brochhausen C. Going beyond histology. Synchrotron micro-computed tomography as a methodology for biological tissue characterization: from tissue morphology to individual cells. J R Soc Interface 7: 49-59.

[85] Braverman MS, Braverman IM. Three-dimensional reconstructions of objects from serial sections using a microcomputer graphics system. The Journal of investigative dermatology 1986;86: 290-4.

[86] Bromage TG, Goldman HM, McFarlin SC, Perez Ochoa A, Boyde A. Confocal scanning optical microscopy of a 3-million-year-old Australopithecus afarensis femur. Scanning 2009;31: 1-10.

[87] Kamioka H, Murshid SA, Ishihara Y, Kajimura N, Hasegawa T, Ando R, Sugawara Y, Yamashiro T, Takaoka A, Takano-Yamamoto T. A method for observing silver-stained osteocytes in situ in 3-microm sections using ultra-high voltage electron microscopy tomography. Microscopy and microanalysis : the official journal of Microscopy Society of America, Microbeam Analysis Society, Microscopical Society of Canada 2009;15: 377-83.

[88] Boyce TM, Bloebaum RD. Cortical aging differences and fracture implications for the human femoral neck. Bone 1993;14: 769-78.

[89] Marotti G, Muglia MA, Zaffe D. A SEM study of osteocyte orientation in alternately structured osteons. Bone 1985;6: 331-4.

[90] Boyde A. Scanning electron microscopy of bone. Methods Mol Biol 816: 365-400.

[91] Kingsmill VJ, Boyde A. Mineralisation density of human mandibular bone: quantitative backscattered electron image analysis. J Anat 1998;192 (Pt 2): 245-56.

[92] Dierolf M, Menzel A, Thibault P, Schneider P, Kewish CM, Wepf R, Bunk O, Pfeiffer F. Ptychographic X-ray computed tomography at the nanoscale. Nature 2010;467: 436-9.

[93] Schneider P, Meier M, Wepf R, Muller R. Serial FIB/SEM imaging for quantitative 3D assessment of the osteocyte lacuno-canalicular network. Bone 2011;49: 304-11.

[94] Hounsfield GN. Computerized transverse axial scanning (tomography). 1. Description of system. Br J Radiol 1973;46: 1016-22.

[95] Zollikofer CPE, Ponce de León MS. Virtual reconstruction : a primer in computer-assisted paleontology and biomedicine. Hoboken, N.J.: Wiley-Interscience; 2005.

[96] Spoor F, Jeffery N, Zonneveld F. Using diagnostic radiology in human evolutionary studies. J Anat 2000;197 (Pt 1): 61-76.

[97] Cooper DM, Turinsky AL, Sensen CW, Hallgrimsson B. Quantitative 3D analysis of the canal network in cortical bone by micro-computed tomography. Anatomical record. Part B, New anatomist 2003;274: 169-79.

[98] Boutroy S, Bouxsein ML, Munoz F, Delmas PD. In vivo assessment of trabecular bone microarchitecture by high-resolution peripheral quantitative computed tomography. J Clin Endocrinol Metab 2005;90: 6508-15.

[99] Donnelly E. Methods for assessing bone quality: a review. Clin Orthop Relat Res 2011;469: 2128-38.

[100] Burghardt AJ, Buie HR, Laib A, Majumdar S, Boyd SK. Reproducibility of direct quantitative measures of cortical bone microarchitecture of the distal radius and tibia by HR-pQCT. Bone 2010;47: 519-28.

[101] Buie HR, Campbell GM, Klinck RJ, MacNeil JA, Boyd SK. Automatic segmentation of cortical and trabecular compartments based on a dual threshold technique for in vivo micro-CT bone analysis. Bone 2007;41: 505-15.

[102] Burghardt AJ, Kazakia GJ, Ramachandran S, Link TM, Majumdar S. Age- and gender-related differences in the geometric properties and biomechanical significance of intracortical porosity in the distal radius and tibia. J Bone Miner Res 2010;25: 983-93.

[103] Nishiyama KK, Macdonald HM, Buie HR, Hanley DA, Boyd SK. Postmenopausal women with osteopenia have higher cortical porosity and thinner cortices at the distal radius and tibia than women with normal aBMD: an in vivo HR-pQCT study. J Bone Miner Res 2010;25: 882-90.

[104] Macdonald HM, Nishiyama KK, Kang J, Hanley DA, Boyd SK. Age-related patterns of trabecular and cortical bone loss differ between sexes and skeletal sites: a population-based HR-pQCT study. J Bone Miner Res 2011;26: 50-62.

[105] Nicks KM, Amin S, Atkinson EJ, Riggs BL, Melton LJ, 3rd, Khosla S. Relationship of age to bone microstructure independent of areal bone mineral density. J Bone Miner Res 2012;27: 637-44.

[106] Kinney JH, Lane NE, Haupt DL. In vivo, three-dimensional microscopy of trabecular bone. J Bone Miner Res 1995;10: 264-70.

[107] Lane NE, Thompson JM, Haupt D, Kimmel DB, Modin G, Kinney JH. Acute changes in trabecular bone connectivity and osteoclast activity in the ovariectomized rat in vivo. J Bone Miner Res 1998;13: 229-36.

[108] Margaritondo G, Meuli R. Synchrotron radiation in radiology: novel X-ray sources. Eur Radiol 2003;13: 2633-41.

[109] Kinney JH, Lane N, Majumdar S, Marshall SJ, Marshall GW. Noninvasive, 3-Dimensional Histomorphometry Using X-Ray Tomographic Microscopy. Journal of Bone and Mineral Research 1992;7: S136-S136.

[110] Lane NE, Haupt D, Kimmel DB, Modin G, Kinney JH. Early estrogen replacement therapy reverses the rapid loss of trabecular bone volume and prevents further deterioration of connectivity in the rat. J Bone Miner Res 1999;14: 206-14.

[111] Lane NE, Kumer J, Yao W, Breunig T, Wronski T, Modin G, Kinney JH. Basic fibroblast growth factor forms new trabeculae that physically connect with pre-existing trabeculae, and this new bone is maintained with an anti-resorptive agent and enhanced with an anabolic agent in an osteopenic rat model. Osteoporos Int 2003;14: 374-82.

[112] Kinney JH, Ryaby JT, Haupt DL, Lane NE. Three-dimensional in vivo morphometry of trabecular bone in the OVX rat model of osteoporosis. Technol Health Care 1998;6: 339-50.

[113] Bayat S, Apostol L, Boller E, Brochard T, Peyrin F. In vivo imaging of bone micro-architecture in mice with 3D synchrotron radiation micro-tomography. Nuclear Instruments & Methods in Physics Research Section a-Accelerators Spectrometers Detectors and Associated Equipment 2005;548: 247-252.

[114] Coan P, Wagner A, Bravin A, Diemoz PC, Keyrilainen J, Mollenhauer J. In vivo x-ray phase contrast analyzer-based imaging for longitudinal osteoarthritis studies in guinea pigs. Phys Med Biol 2010;55: 7649-7662.

[115] Matsumoto T, Nishikawa K, Tanaka M, Uesugi K. In vivo CT quantification of trabecular bone dynamics in mice after sciatic neurectomy using monochromatic synchrotron radiation. Calcif Tissue Int 2011;88: 432-41.

[116] Pratt I. In vivo imaging of cortical porosity by synchrotron phase contrast micro computed tomography. Unpublished MSc Thesis University of Saskatchewan, Saskatoon, Canada 2013.

[117] Waarsing JH, Day JS, van der Linden JC, Ederveen AG, Spanjers C, De Clerck N, Sasov A, Verhaar JA, Weinans H. Detecting and tracking local changes in the tibiae of individual rats: a novel method to analyse longitudinal in vivo micro-CT data. Bone 2004;34: 163-9.

[118] David V, Laroche N, Boudignon B, Lafage-Proust MH, Alexandre C, Ruegsegger P, Vico L. Noninvasive in vivo monitoring of bone architecture alterations in hindlimb-unloaded female rats using novel three-dimensional microcomputed tomography. J Bone Miner Res 2003;18: 1622-31.

[119] Boyd SK, Moser S, Kuhn M, Klinck RJ, Krauze PL, Musser R, Gasser JS. Evaluation of three-dimensional image registration methodologies for in vivo micro-computed tomography. Annals of Biomedical Engineering 2006;34: 1587-1599.

[120] Schulte FA, Lambers FM, Kuhn G, Muller R. In vivo micro-computed tomography allows direct three-dimensional quantification of both bone formation and bone resorption parameters using time-lapsed imaging. Bone 2011;48: 433-42.

[121] Nebuloni L, Kuhn GA, Vogel J, Muller R. A novel in vivo vascular imaging approach for hierarchical quantification of vasculature using contrast enhanced micro-computed tomography. PLoS One 2014;9: e86562.

[122] Muller R, Van Campenhout H, Van Damme B, Van Der Perre G, Dequeker J, Hildebrand T, Ruegsegger P. Morphometric analysis of human bone biopsies: a quantitative structural comparison of histological sections and micro-computed tomography. Bone 1998;23: 59-66.

[123] Feldkamp LA, Goldstein SA, Parfitt AM, Jesion G, Kleerekoper M. The direct examination of three-dimensional bone architecture in vitro by computed tomography. Journal of bone and mineral research : the official journal of the American Society for Bone and Mineral Research 1989;4: 3-11.

[124] Hildebrand T, Laib A, Muller R, Dequeker J, Ruegsegger P. Direct three-dimensional morphometric analysis of human cancellous bone: microstructural data from spine, femur, iliac crest, and calcaneus. Journal of bone and mineral research : the official journal of the American Society for Bone and Mineral Research 1999;14: 1167-74.

[125] Muller R. Hierarchical microimaging of bone structure and function. Nat Rev Rheumatol 2009;5: 373-81.

[126] Schneider P, Stauber M, Voide R, Stampanoni M, Donahue LR, Muller R. Ultrastructural properties in cortical bone vary greatly in two inbred strains of mice as assessed by synchrotron light based micro- and nano-CT. Journal of bone and mineral research : the official journal of the American Society for Bone and Mineral Research 2007;22: 1557-70.

[127] Mills DM. Third-generation hard x-ray synchrotron radiation sources : source properties, optics, and experimental techniques. New York: Wiley; 2002.

[128] http://www.lightsources.org. In; 2014.

[129] Bernhardt R, Scharnweber D, Muller B, Thurner P, Schliephake H, Wyss P, Beckmann F, Goebbels J, Worch H. Comparison of microfocus- and synchrotron X-ray tomography for the analysis of osteointegration around Ti6Al4V implants. Eur Cell Mater 2004;7: 42-51; discussion 51.

[130] Britz HM, Carter Y, Jokihaara J, Leppanen OV, Jarvinen TL, Belev G, Cooper DM. Prolonged unloading in growing rats reduces cortical osteocyte lacunar density and volume in the distal tibia. Bone 2012;51: 913-9.

[131] Pacureanu A, Langer M, Boller E, Tafforeau P, Peyrin F. Nanoscale imaging of the bone cell network with synchrotron X-ray tomography: optimization of acquisition setup. Medical physics 2012;39: 2229-38.

[132] Zhou SA, Brahme A. Development of phase-contrast X-ray imaging techniques and potential medical applications. Phys Med 2008;24: 129-48.

[133] Snigirev A, Snigireva I, Kohn V, Kuznetsov S, Schelokov I. On the possibilities of x-ray phase contrast microimaging by coherent high-energy synchrotron radiation. Review of Scientific Instruments 1995;66: 5486-5492.

[134] Langer M, Pacureanu A, Suhonen H, Grimal Q, Cloetens P, Peyrin F. X-ray phase nanotomography resolves the 3D human bone ultrastructure. PLoS One 2012;7: e35691.

[135] Sanchez S, Ahlberg PE, Trinajstic KM, Mirone A, Tafforeau P. Three-dimensional synchrotron virtual paleohistology: a new insight into the world of fossil bone microstructures. Microsc Microanal 2012;18: 1095-105.

[136] Cooper DM, Erickson B, Peele AG, Hannah K, Thomas CD, Clement JG. Visualization of 3D osteon morphology by synchrotron radiation micro-CT. J Anat 2011;219: 481-9.

[137] Arhatari BD, Cooper DM, Thomas CD, Clement JG, Peele AG. Imaging the 3D structure of secondary osteons in human cortical bone using phase-retrieval tomography. Phys Med Biol 2011;56: 5265-74.

[138] Belanger LF. Osteocytic osteolysis. Calcif Tissue Res 1969;4: 1-12.

[139] Thomas CD, Feik SA, Clement JG. Regional variation of intracortical porosity in the midshaft of the human femur: age and sex differences. Journal of anatomy 2005;206: 115-25.

[140] Goldman HM, Thomas CD, Clement JG, Bromage TG. Relationships among microstructural properties of bone at the human midshaft femur. J Anat 2005;206: 127-39.

[141] Aamodt A, Lund-Larsen J, Eine J, Andersen E, Benum P, Husby OS. In vivo measurements show tensile axial strain in the proximal lateral aspect of the human femur. Journal of orthopaedic research : official publication of the Orthopaedic Research Society 1997;15: 927-31.

[142] Blott SJ, Pye K. Particle shape: a review and new methods of characterization and classification. Sedimentology 2008;55: 31-63.

[143] Power J, Noble BS, Loveridge N, Bell KL, Rushton N, Reeve J. Osteocyte lacunar occupancy in the femoral neck cortex: an association with cortical remodeling in hip fracture cases and controls. Calcified tissue international 2001;69: 13-9.

[144] Jordan GR, Loveridge N, Power J, Clarke MT, Parker M, Reeve J. The ratio of osteocytic incorporation to bone matrix formation in femoral neck cancellous bone: an enhanced osteoblast work rate in the vicinity of hip osteoarthritis. Calcified tissue international 2003;72: 190-6.

[145] Kim YH, Kim JS, Cho SH. Strain distribution in the proximal human femur. An in vitro comparison in the intact femur and after insertion of reference and experimental femoral stems. J Bone Joint Surg Br 2001;83: 295-301.

[146] Koch JC. The Laws of Bone Architecture. The american journal of anatomy 1917;21: 177-298.

[147] Judex S, Gross TS, Zernicke RF. Strain gradients correlate with sites of exercise-induced bone-forming surfaces in the adult skeleton. Journal of bone and mineral research : the official journal of the American Society for Bone and Mineral Research 1997;12: 1737-45.

[148] Skedros JG, Mason MW, Nelson MC, Bloebaum RD. Evidence of structural and material adaptation to specific strain features in cortical bone. Anat Rec 1996;246: 47-63.

[149] Skedros JG, Su SC, Bloebaum RD. Biomechanical implications of mineral content and microstructural variations in cortical bone of horse, elk, and sheep calcanei. Anat Rec 1997;249: 297-316.

[150] Aarden EM, Burger EH, Nijweide PJ. Function of osteocytes in bone. Journal of cellular biochemistry 1994;55: 287-99.

[151] Tomkinson A, Reeve J, Shaw RW, Noble BS. The death of osteocytes via apoptosis accompanies estrogen withdrawal in human bone. The Journal of clinical endocrinology and metabolism 1997;82: 3128-35.

[152] Mullender MG, Huiskes R, Versleyen H, Buma P. Osteocyte density and histomorphometric parameters in cancellous bone of the proximal femur in five mammalian species. Journal of orthopaedic research : official publication of the Orthopaedic Research Society 1996;14: 972-9.

[153] Skedros JG, Sybrowsky CL, Parry TR, Bloebaum RD. Regional differences in cortical bone organization and microdamage prevalence in Rocky Mountain mule deer. The anatomical record. Part A, Discoveries in molecular, cellular, and evolutionary biology 2003;274: 837-50.

[154] Skedros JG, Sybrowsky CL, Anderson WE, Chow F. Relationships between in vivo microdamage and the remarkable regional material and strain heterogeneity of cortical bone of adult deer, elk, sheep and horse calcanei. Journal of anatomy 2011;219: 722-33.

[155] Skedros JG, Clark GC, Sorenson SM, Taylor KW, Qiu S. Analysis of the Effect of Osteon Diameter on the Potential Relationship of Osteocyte Lacuna Density and Osteon Wall Thickness. Anatomical record 2011.

[156] Skedros JG. Osteocyte lacuna population densities in sheep, elk and horse calcanei. Cells, tissues, organs 2005;181: 23-37.

[157] Mader KS, Schneider P, Muller R, Stampanoni M. A quantitative framework for the 3D characterization of the osteocyte lacunar system. Bone 2013;57: 142-154.

[158] Martin RB, Burr DB. Structure, function, and adaptation of compact bone: Raven Press New York; 1989.

[159] Hert J, Fiala P, Petrtyl M. Osteon orientation of the diaphysis of the long bones in man. Bone 1994;15: 269-77.

[160] Petrtyl M, Hert J, Fiala P. Spatial organization of the haversian bone in man. J Biomech 1996;29: 161-9.

[161] Feik SA, Thomas CD, Bruns R, Clement JG. Regional variations in cortical modeling in the femoral mid-shaft: sex and age differences. American journal of physical anthropology 2000;112: 191-205.

[162] Bousson V, Meunier A, Bergot C, Vicaut E, Rocha MA, Morais MH, Laval-Jeantet AM, Laredo JD. Distribution of intracortical porosity in human midfemoral cortex by age and gender. Journal of bone and mineral research : the official journal of the American Society for Bone and Mineral Research 2001;16: 1308-17.

[163] Cardoso L, Fritton SP, Gailani G, Benalla M, Cowin SC. Advances in assessment of bone porosity, permeability and interstitial fluid flow. Journal of biomechanics 2013;46: 253-65.

[164] Tang SY, Herber RP, Ho SP, Alliston T. Matrix metalloproteinase-13 is required for osteocytic perilacunar remodeling and maintains bone fracture resistance. Journal of bone and mineral research : the official journal of the American Society for Bone and Mineral Research 2012;27: 1936-50.

[165] Qing H, Bonewald LF. Osteocyte remodeling of the perilacunar and pericanalicular matrix. International journal of oral science 2009;1: 59-65.

[166] Rubin CT, McLeod KJ, Bain SD. Functional strains and cortical bone adaptation: epigenetic assurance of skeletal integrity. J Biomech 1990;23 Suppl 1: 43-54.

[167] Pauwels F. Biomechanics of the locomotor apparatus : contributions on the functional anatomy of the locomotor apparatus. Berlin ; New York: Springer-Verlag; 1980.

[168] Cristofolini L, Cappello A, McNamara BP, Viceconti M. A minimal parametric model of the femur to describe axial elastic strain in response to loads. Med Eng Phys 1996;18: 502-14.

[169] Cristofolini L, Viceconti M, Cappello A, Toni A. Mechanical validation of whole bone composite femur models. J Biomech 1996;29: 525-35.

[170] Duda GN, Heller M, Albinger J, Schulz O, Schneider E, Claes L. Influence of muscle forces on femoral strain distribution. J Biomech 1998;31: 841-6.

[171] Oh I, Harris WH. Proximal strain distribution in the loaded femur. An in vitro comparison of the distributions in the intact femur and after insertion of different hip-replacement femoral components. J Bone Joint Surg Am 1978;60: 75-85.

[172] Skedros JG, Baucom SL. Mathematical analysis of trabecular 'trajectories' in apparent trajectorial structures: the unfortunate historical emphasis on the human proximal femur. Journal of theoretical biology 2007;244: 15-45.

[173] Huiskes R. On the modelling of long bones in structural analyses. J Biomech 1982;15: 65-9.

[174] Qiu S, Rao DS, Fyhrie DP, Palnitkar S, Parfitt AM. The morphological association between microcracks and osteocyte lacunae in human cortical bone. Bone 2005;37: 10-5.

[175] Vander Voort GF. Metallography: principles and practices: ASM International; 1984.

[176] Knothe Tate ML, Adamson JR, Tami AE, Bauer TW. The osteocyte. Int J Biochem Cell Biol 2004;36: 1-8.

[177] Yeni YN, Vashishth D, Fyhrie DP. Estimation of bone matrix apparent stiffness variation caused by osteocyte lacunar size and density. J Biomech Eng 2001;123: 10-7.

[178] Thomas CD, Feik SA, Clement JG. Regional variation of intracortical porosity in the midshaft of the human femur: age and sex differences. J Anat 2005;206: 115-25.

[179] Power J, Loveridge N, Rushton N, Parker M, Reeve J. Osteocyte density in aging subjects is enhanced in bone adjacent to remodeling haversian systems. Bone 2002;30: 859-65.

[180] Goulet GC, Cooper DM, Coombe D, Zernicke RF. Influence of cortical canal architecture on lacunocanalicular pore pressure and fluid flow. Computer methods in biomechanics and biomedical engineering 2008;11: 379-87.

[181] Nicolella DP, Bonewald LF, Moravits DE, Lankford J. Measurement of microstructural strain in cortical bone. European journal of morphology 2005;42: 23-9.

[182] Wang L, Wang Y, Han Y, Henderson SC, Majeska RJ, Weinbaum S, Schaffler MB. In situ measurement of solute transport in the bone lacunar-canalicular system. Proceedings of the National Academy of Sciences of the United States of America 2005;102: 11911-6.

[183] Klein-Nulend J, Bonewald LF. The Osteocyte. In: Bilezikian JP, Raisz GL, Martin TJ, editors. Principles of Bone Biology. San Diego: Elsevier; 2008.

[184] Reilly GC, Knapp HF, Stemmer A, Niederer P, Knothe Tate ML. Investigation of the morphology of the lacunocanalicular system of cortical bone using atomic force microscopy. Annals of biomedical engineering 2001;29: 1074-81.

[185] Luk SC, Nopajaroonsri C, Simon GT. The ultrastructure of cortical bone in young adult rabbits. Journal of ultrastructure research 1974;46: 184-205.

[186] Takagi M, Maeno M, Kagami A, Takahashi Y, Otsuka K. Biochemical and immunocytochemical characterization of mineral binding proteoglycans in rat bone. The journal of histochemistry and cytochemistry : official journal of the Histochemistry Society 1991;39: 41-50.

[187] Sauren YM, Mieremet RH, Groot CG, Scherft JP. An electron microscopic study on the presence of proteoglycans in the mineralized matrix of rat and human compact lamellar bone. The Anatomical record 1992;232: 36-44.

[188] Scherft JP. The lamina limitans of the organic bone matrix: formation in vitro. Journal of ultrastructure research 1978;64: 173-81.

[189] Jee WSS. Integrated bone tissue physiology: anatomy and physiology. . In: Cowin SC, editor. Bone Mechanics Handbook. Boca Raton: CRC Press; 2001, p. 1.1–1.68.

[190] Veno PA, Nicolella DP, Sivakumar P, Kalajzic I, Rowe DW, Bonewald LF, al. e. Live imaging of osteocytes within their lacunae reveals cell body and dendrite motions. Journal of bone and mineral research : the official journal of the American Society for Bone and Mineral Research 2006: S38-9.

[191] Okada S, Yoshida S, Ashrafi SH, Schraufnagel DE. The canalicular structure of compact bone in the rat at different ages. Microscopy and microanalysis : the official journal of Microscopy Society of America, Microbeam Analysis Society, Microscopical Society of Canada 2002;8: 104-15.

[192] Hirose S, Li M, Kojima T, de Freitas PH, Ubaidus S, Oda K, Saito C, Amizuka N. A histological assessment on the distribution of the osteocytic lacunar canalicular system using silver staining. Journal of bone and mineral metabolism 2007;25: 374-82.

[193] Bacabac RG, Mizuno D, Schmidt CF, MacKintosh FC, Van Loon JJ, Klein-Nulend J, Smit TH. Round versus flat: bone cell morphology, elasticity, and mechanosensing. Journal of biomechanics 2008;41: 1590-8.

[194] Tami AE, Schaffler MB, Knothe Tate ML. Probing the tissue to subcellular level structure underlying bone's molecular sieving function. Biorheology 2003;40: 577-90.

[195] Burger EH, Klein-Nulend J, Smit TH. Strain-derived canalicular fluid flow regulates osteoclast activity in a remodelling osteon--a proposal. Journal of biomechanics 2003;36: 1453-9.

[196] Tan SD, de Vries TJ, Kuijpers-Jagtman AM, Semeins CM, Everts V, Klein-Nulend J. Osteocytes subjected to fluid flow inhibit osteoclast formation and bone resorption. Bone 2007;41: 745-51.

[197] Heino TJ, Hentunen TA, Vaananen HK. Osteocytes inhibit osteoclastic bone resorption through transforming growth factor-beta: enhancement by estrogen. Journal of cellular biochemistry 2002;85: 185-97.

[198] Bonewald LF. Osteocyte messages from a bony tomb. Cell metabolism 2007;5: 410-1.

[199] Dong P, Haupert S, Hesse B, Langer M, Gouttenoire PJ, Bousson V, Peyrin F. 3D osteocyte lacunar morphometric properties and distributions in human femoral cortical bone using synchrotron radiation micro-CT images. Bone 2013;60C: 172-185.

[200] Sasaki M, Hongo H, Hasegawa T, Suzuki R, Zhusheng L, de Freitas PHL, Yamada T, Oda K, Yamamoto T, Li M. Morphological aspects of the biological function of the osteocytic lacunar canalicular system and of osteocyte-derived factors. Oral Science International 2012;9: 1-8.

[201] Mori S, Burr DB. Increased intracortical remodeling following fatigue damage. Bone 1993;14: 103-9.

[202] Hazenberg JG, Taylor D, Lee TC. The role of osteocytes and bone microstructure in preventing osteoporotic fractures. Osteoporosis international : a journal established as result of cooperation between the European Foundation for Osteoporosis and the National Osteoporosis Foundation of the USA 2007;18: 1-8.

[203] Burr DB, Forwood MR, Fyhrie DP, Martin RB, Schaffler MB, Turner CH. Bone microdamage and skeletal fragility in osteoporotic and stress fractures. Journal of bone and

mineral research : the official journal of the American Society for Bone and Mineral Research 1997;12: 6-15.

[204] Nicolella DP, Moravits DE, Gale AM, Bonewald LF, Lankford J. Osteocyte lacunae tissue strain in cortical bone. Journal of biomechanics 2006;39: 1735-43.

[205] Cowin SC, Moss-Salentijn L, Moss ML. Candidates for the mechanosensory system in bone. Journal of biomechanical engineering 1991;113: 191-7.

[206] Lanyon LE. Osteocytes, strain detection, bone modeling and remodeling. Calcified tissue international 1993;53 Suppl 1: S102-6; discussion S106-7.

[207] Sugawara Y, Kamioka H, Ishihara Y, Fujisawa N, Kawanabe N, Yamashiro T. The early mouse 3D osteocyte network in the presence and absence of mechanical loading. Bone 2013;52: 189-96.

[208] Chen H, Zhou X, Shoumura S, Emura S, Bunai Y. Age- and gender-dependent changes in three-dimensional microstructure of cortical and trabecular bone at the human femoral neck. Osteoporosis international : a journal established as result of cooperation between the European Foundation for Osteoporosis and the National Osteoporosis Foundation of the USA 2010;21: 627-36.

[209] Klein-Nulend J, Bakker AD, Bacabac RG, Vatsa A, Weinbaum S. Mechanosensation and transduction in osteocytes. Bone 2013;54: 182-90.

[210] Klein-Nulend J, Bacabac RG, Bakker AD. Mechanical loading and how it affects bone cells: the role of the osteocyte cytoskeleton in maintaining our skeleton. European cells & materials 2012;24: 278-91.

[211] Bozal CB, Sanchez LM, Mandalunis PM, Ubios AM. Histomorphometric study and three-dimensional reconstruction of the osteocyte lacuno-canalicular network one hour after applying tensile and compressive forces. Cells, tissues, organs 2013;197: 474-83.

[212] Bell KL, Loveridge N, Power J, Garrahan N, Meggitt BF, Reeve J. Regional differences in cortical porosity in the fractured femoral neck. Bone 1999;24: 57-64.

[213] Stein MS, Feik SA, Thomas CD, Clement JG, Wark JD. An automated analysis of intracortical porosity in human femoral bone across age. J Bone Miner Res 1999;14: 624-32.

[214] Wang JH, Goldschmidt-Clermont P, Wille J, Yin FC. Specificity of endothelial cell reorientation in response to cyclic mechanical stretching. Journal of biomechanics 2001;34: 1563-72.

[215] Sakamoto N, Saito N, Han X, Ohashi T, Sato M. Effect of spatial gradient in fluid shear stress on morphological changes in endothelial cells in response to flow. Biochemical and biophysical research communications 2010;395: 264-9.

[216] Currey J. Stress concentrations in bone. Quarterly Journal of Microscopical Science 1962;3: 111-133.

[217] Marotti G. A new theory of bone lamellation. Calcified tissue international 1993;53 Suppl 1: S47-55; discussion S56.

[218] Rodionova NV, Polkovenko OV, Oganov VS. Interactions of cells in zones of bone resorption under microgravity and hypokinesia. Journal of gravitational physiology : a journal of the International Society for Gravitational Physiology 2004;11: P147-51.

[219] McCreadie BR, Hollister SJ. Strain Concentrations Surrounding an Ellipsoid Model of Lacunae and Osteocytes. Computer methods in biomechanics and biomedical engineering 1997;1: 61-68.

[220] Carriero A, Doube M, Vogt M, Busse B, Zustin J, Levchuk A, Schneider P, Muller R, Shefelbine SJ. Altered lacunar and vascular porosity in osteogenesis imperfecta mouse bone as revealed by synchrotron tomography contributes to bone fragility. Bone 2013.

[221] Bonivtch AR, Bonewald LF, Nicolella DP. Tissue strain amplification at the osteocyte lacuna: a microstructural finite element analysis. Journal of biomechanics 2007;40: 2199-206.

[222] Anderson EJ, Knothe Tate ML. Idealization of pericellular fluid space geometry and dimension results in a profound underprediction of nano-microscale stresses imparted by fluid drag on osteocytes. Journal of biomechanics 2008;41: 1736-46.

[223] Colopy SA, Benz-Dean J, Barrett JG, Sample SJ, Lu Y, Danova NA, Kalscheur VL, Vanderby R, Jr., Markel MD, Muir P. Response of the osteocyte syncytium adjacent to and distant from linear microcracks during adaptation to cyclic fatigue loading. Bone 2004;35: 881-91.

[224] Milovanovic P, Zimmermann EA, Hahn M, Djonic D, Puschel K, Djuric M, Amling M, Busse B. Osteocytic Canalicular Networks: Morphological Implications for Altered Mechanosensitivity. ACS Nano 2013.

[225] Hedgecock NL, Hadi T, Chen AA, Curtiss SB, Martin RB, Hazelwood SJ. Quantitative regional associations between remodeling, modeling, and osteocyte apoptosis and density in rabbit tibial midshafts. Bone 2007;40: 627-37.

[226] Nicolella DP, Feng JQ, Moravits DE, Bonivitch AR, Wang Y, Dusecich V, Yao W, Lane N, Bonewald LF. Effects of nanomechanical bone tissue properties on bone tissue strain: implications for osteocyte mechanotransduction. Journal of musculoskeletal & neuronal interactions 2008;8: 330-1.

[227] Hirano T, Burr DB, Turner CH, Sato M, Cain RL, Hock JM. Anabolic effects of human biosynthetic parathyroid hormone fragment (1–34), LY333334, on remodeling and mechanical properties of cortical bone in rabbits. Journal of bone and Mineral Research 1999;14: 536-545.

[228] Allen MR, Burr DB. Mandible matrix necrosis in beagle dogs after 3 years of daily oral bisphosphonate treatment. J Oral Maxillofac Surg 2008;66: 987-94.

[229] Burr DB, Allen MR. Mandibular necrosis in beagle dogs treated with bisphosphonates. Orthod Craniofac Res 2009;12: 221-8.

APPENDIX A: SPECIMENS

Table A.1 Information associated with the specimens utilized from the Melbourne Femur Collection, collected by the Victorian Institute of Forensic Medicine (VIFM).

VIFM Number	Sex	Age	Height (cm)	Weight (Kg)
S5_057	Male	18	1.88	87
S37_032	Male	20	1.74	60
S25_133	Male	26	Unknown	Unknown
S29_089	Male	26	Unknown	Unknown
S13_480	Male	27	1.73	69
S17_037	Male	31	1.74	52
S21_423	Male	35	1.83	97
S45_478	Male	39	1.75	72
S46_463	Male	39	1.71	73
S47_479	Male	40	1.86	87
S48_434	Male	41	1.68	72
S49_447	Male	43	1.67	76
S50_460	Male	46	1.9	88
S51_489	Male	46	1.99	112
S52_030	Male	47	1.78	78
S53_355	Male	47	1.84	110
S59_440	Male	47	1.8	74
S54_487	Male	49	1.76	97
S55_370	Male	53	1.68	62
S56_087	Male	53	1.74	115
S60_462	Male	54	1.7	56
S57_110	Male	55	1.72	50
S61_107	Male	57	1.82	120
S63_484	Male	61	1.74	99
S64_201	Male	61	1.73	79
S65_461	Male	62	1.74	84
S66_067	Male	62	1.84	72
S67_446	Male	64	1.87	87
S69_448	Male	67	1.64	66
S73_490	Male	71	Unknown	Unknown

S74_497	Male	71	1.75	67
S77_451	Male	75	1.69	64
S79_481	Male	76	1.56	52
S86_225	Male	85	1.58	57
S89_148	Male	86	1.72	59
S90_191	Male	92	1.66	60
S1_412	Female	41	1.61	68
S9_81	Female	30	1.64	97
S11_128	Female	33	1.78	64
S15_117	Female	23	1.6	55
S16_406	Female	20	1.63	45
S17_432	Female	49	1.66	92
S18_35	Female	24	1.53	57
S19_188	Female	40	1.59	55
S21_189	Female	20	1.61	105
S22_156	Female	41	1.46	35
S24_172	Female	26	1.52	43
S25_134	Female	28	Unknown	Unknown
S26_126	Female	21	1.74	72
S27_22	Female	22	1.73	68
S2_399	Female	70	1.63	53
S3_426	Female	81	1.84	96
S4_376	Female	67	1.67	72
S5_422	Female	71	1.58	61
S8_109	Female	52	Unknown	Unknown
S10_53	Female	57	1.57	68
S12_56	Female	65	Unknown	Unknown
S13_113	Female	66	Unknown	Unknown
S14_376	Female	67	1.67	72
S20_94	Female	86	1.52	69
S23_127	Female	55	1.72	60
S28_436	Female	74	1.73	65
S30_411	Female	78	1.51	71
S31_439	Female	61	1.7	83
S32_496	Female	76	1.66	64
S33_178	Female	72	1.74	60

APPENDIX B: ETHICS APPROVAL

UNIVERSITY OF SASKATCHEWAN

Biomedical Research Ethics Board (Bio-REB)

Certificate of Approval

PRINCIPAL INVESTIGATOR	DEPARTMENT	Bio #
David M.L. Cooper	Anatomy and Cell Biology	08-46

INSTITUTION(S) WHERE RESEARCH WILL BE CARRIED OUT
University of Saskatchewan
Saskatoon SK

SUB-INVESTIGATOR(S)
Saija Kontulainen

SPONSORING AGENCIES
PENDING

TITLE: A Multi-Level Analysis of Differences Between Normal and Osteoporotic Bone

APPROVAL DATE	EXPIRY DATE	APPROVAL OF
17-Mar-2008	16-Mar-2009	Researcher's summary as submitted

Full Board Meeting ☐

Delegated Review ☒

CERTIFICATION
The study is acceptable on scientific and ethical grounds. The principal investigator has the responsibility for any other administrative or regulatory approvals that may pertain to this research study, and for ensuring that the authorized research is carried out according to governing law. This approval is valid for the specified period provided there is no change to the approved protocol or consent process.

FIRST TIME REVIEW AND CONTINUING APPROVAL
The University of Saskatchewan Biomedical Research Ethics Board reviews above minimal studies at a full-board (face-to-face) meeting. Any research classified as minimal risk is reviewed through the delegated (subcommittee) review process. The initial Certificate of Approval includes the approval period the REB has assigned to a study. The Status Report form must be submitted within one month prior to the assigned expiry date. The researcher shall indicate to the REB any specific requirements of the sponsoring organizations (e.g. requirement for full-board review and approval) for the continuing review process deemed necessary for that project. For more information visit http://www.usask.ca/research/ethics_review/.

REB ATTESTATION
In respect to clinical trials, the University of Saskatchewan Research Ethics Board complies with the membership requirements for Research Ethics Boards defined in Division 5 of the Food and Drug Regulations and carries out its functions in a manner consistent with Good Clinical Practices. This approval and the views of this REB have been documented in writing.

G McKay for
Michel Desautels, Ph.D., Chair
University of Saskatchewan
Biomedical Research Ethics Board

March 19, 2008
Signature Date

Please send all correspondence to:

Ethics Office
University of Saskatchewan
Room 305 Kirk Hall, 117 Science Place
Saskatoon SK S7N 5C8
Telephone: (306) 966-4053 Fax: (306) 966-2069

APPENDIX C: JOURNAL PUBLICATION PERMISSION

Permissions from Elsevier relate to:

Carter Y, Thomas CD, Clement JG, Peele AG, Hannah K, Cooper DM. Variation in osteocyte lacunar morphology and density in the human femur--a synchrotron radiation micro-CT study. *BONE* 2013;52: 126-32

Carter Y, Thomas CD, Clement JG, Cooper DM. Femoral osteocyte lacunar density, volume and morphology in women across the lifespan. *Journal of Structural Biology* 2013;183: 519-26.

Carter Y, Suchorab, JL, Thomas CD, Clement JG, Cooper DM. Normal variation in cortical osteocyte lacunar parameters in healthy young males. *Journal of Anatomy* 2014;225(3): 328-36.

For Authors

Journal authors' home
Author Rights
Ethics
Funding body agreements
Open access
Author services
Journal performance
Early career researchers
Authors' update
Book authors' home

Author Rights

Elsevier supports the need for authors to share, disseminate and maximize the impact of their research. We take our responsibility as stewards of the online record seriously, and work to ensure our policies and procedures help to protect the integrity of scholarly works.

Author's rights to reuse and post their own articles published by Elsevier are defined by Elsevier's copyright policy. For our proprietary titles, the type of copyright agreement used depends on the author's choice of publication:

For subscription articles: These rights are determined by a copyright transfer, where authors retain scholarly rights to post and use their articles.

For open access articles: These rights are determined by an exclusive license agreement, which applies to all our open access content.

In both cases, the fundamental rights needed to publish and distribute an article remain the same and Elsevier authors will be able to use their articles for a wide range of scholarly purposes.

Details on how authors can reuse and post their own articles are provided below.

Help and support
For reuse and posting not detailed below, please see our posting policy, or for authors who would like to:

- Include material from other sources in your work being published by Elsevier, please visit: Permission seeking guidelines for Elsevier authors.
- Obtain permission to re-use material from Elsevier books, journals, databases, or other products, please visit: Obtaining permission to reuse Elsevier material
- Or if you are an Elsevier author and are contacted by a requestor who wishes to re-use all or part of your article or chapter, please also refer them to our Obtaining Permission to Re-Use Elsevier Material page.
- See our FAQ on posting and copyright queries.
- Contact us directly, please email our Permissions Help Desk.

Author Use | Author Posting | Definitions

How authors can use their own journal articles

Authors can use their articles for a wide range of scholarly, non-commercial purposes as outlined below. These rights apply for all Elsevier authors who publish their article as either a subscription article or an open access article.

We require that all Elsevier authors always include a full acknowledgement and, if appropriate, a link to the final published version hosted on Science Direct.

For open access articles these rights are separate from how readers can reuse your article as defined by the author's choice of Creative Commons user license options.

Authors can use either their accepted author manuscript or final published article for:	
✓	Use at a conference, meeting or for teaching purposes
✓	Internal training by their company
✓	Sharing individual articles with colleagues for their research use* (also known as 'scholarly sharing')
✓	Use in a subsequent compilation of the author's works

✓	Inclusion in a thesis or dissertation
✓	Reuse of portions or extracts from the article in other works
✓	Preparation of derivative works (other than for commercial purposes)

*Please note this excludes any systematic or organized distribution of published articles.

JOHN WILEY AND SONS LICENSE TERMS AND CONDITIONS

Aug 06, 2014

This is a License Agreement between Yasmin Carter ("You") and John Wiley and Sons ("John Wiley and Sons") provided by Copyright Clearance Center ("CCC"). The license consists of your order details, the terms and conditions provided by John Wiley and Sons, and the payment terms and conditions.

All payments must be made in full to CCC. For payment instructions, please see information listed at the bottom of this form.

License Number	3443410653264
License date	Aug 06, 2014
Licensed content publisher	John Wiley and Sons
Licensed content publication	Journal of Anatomy
Licensed content title	Normal variation in cortical osteocyte lacunar parameters in healthy young males
Licensed copyright line	© 2014 Anatomical Society
Licensed content author	Yasmin Carter,Jessica L. Suchorab,C. David L. Thomas,John G. Clement,David M. L. Cooper
Licensed content date	Jul 4, 2014
Start page	n/a
End page	n/a
Type of use	Dissertation/Thesis
Requestor type	Author of this Wiley article
Format	Print and electronic
Portion	Full article
Will you be translating?	No
Title of your thesis / dissertation	QUANTITATIVE IMAGING OF SEX AND AGE DIFFERENCES IN HUMAN CORTICAL BONE OSTEOCYTE LACUNAE
Expected completion date	Aug 2014
Expected size (number of pages)	197
Total	0.00 USD
Terms and Conditions	

TERMS AND CONDITIONS

This copyrighted material is owned by or exclusively licensed to John Wiley & Sons, Inc. or one of its group companies (each a"Wiley Company") or handled on behalf of a society with